ANALYZING THE RELATIONSHIP BETWEEN LAND SURFACE TEMPERATURE AND URBAN STRUCTURE TYPES IN BANDUNG, INDONESIA

ROYGER MANIUR SIMANJUNTAK
February, 2017

SUPERVISORS:
Monika Kuffer, M.Sc
Dr. Diana Reckien

ANALYZING THE RELATIONSHIP BETWEEN LAND SURFACE TEMPERATURE AND URBAN STRUCTURE TYPES IN BANDUNG, INDONESIA

ROYGER MANIUR SIMANJUNTAK
Enschede, The Netherlands, February, 2017

Thesis submitted to the Faculty of Geo-Information Science and Earth Observation of the University of Twente in partial fulfilment of the requirements for the degree of Master of Science in Geo-information Science and Earth Observation.
Specialization: Urban Planning and Management

SUPERVISORS:
Monika Kuffer, M.Sc
Dr. Diana Reckien

THESIS ASSESSMENT BOARD:
Prof.dr.ir. M.F.A.M. van Maarseveen (Chair)
Dr. Maik Netzband (External Examiner, Ruhr-Universität Bochum)

ABSTRACT

Urbanization has driven massive land use and land cover changes, and generated urban heat island (UHI) phenomenon around the world. UHI effect refers to difference of thermal conditions between the dense urban areas and suburban or rural areas during daytime or night time. To monitor the UHI effect, land surface temperature (LST) is extracted from thermal imagery to see the behaviour of surface temperature. However, urban areas are not homogenous, densely built-up neighbourhoods might be different affected by UHI compared to lower density neighbourhoods. Thus, different urban structure types (UST) potentially impact LST patterns.

As different configurations of UST can affect the thermal conditions of cities, further spatial details on its types will deepen the understanding of their impact on UHIs. In urban climatology, the concept of local climate zone (LCZ) method has been recently used to address this issue with the aim to interpret the temperature patterns within the urban context by classify the surface form of the local surroundings area. However, the spatial patterns of UST in developing countries are typically very heterogeneous where a mix of residential, commercial and industrial uses is located in one area. Hence, this condition could significantly impact surface temperature patterns. Therefore, a study combining the advantages of very high resolution (VHR) and thermal image can be used to find out the relationships between LST and UST in a complex urban environment of a city in developing countries.

We applied two different methods of image classification to extract the LCZ. First, we used pixel based classification to get LCZ for the entire area of Bandung using a moderate resolution image (Landsat). Random forest algorithm was used due to its capability not only to handle large features but also to gain high accuracy results. Second, we employed object based image analysis (OBIA) using a VHR images (Pleiades and SPOT 6). A rule set was developed using segmentation and classification approach. Two subset areas were selected to ensure the rule set works and the coverage of LCZ are fulfilled. The result showed that the OBIA approach provides higher accuracy compare to the pixel based classification. Pleiades overall accuracies ranged from 86 to 89%, while SPOT6 ranged from 76 to 82%. Landsat overall accuracies are much lower, ranging from 66 to 69%. Furthermore, the OBIA method presents more spatially detailed information about the UST.

Based on the classification results, the effect of composition and configuration patterns of UST were generated using spatial metrics like percentage of landscape (PLAND), aggregation index (AI) and number of patches (NP). As a result, we found not only does the types significantly affect the LST pattern, but so does the composition and configuration patterns. Built-up types like compact low rise and open low rise are found as the highest surface temperature. Meanwhile, vegetation types like dense trees and low plants are seen as the lowest surface temperature. Regarding the composition patterns, high percentage cover of vegetation and water significantly reduces the magnitude of LST while high percentage cover of built-up tends to significantly increase the magnitude of LST. Similar result is also found from configuration patterns where an increase in aggregation index of vegetation and water tend to decrease the value of LST. In contrast, an increase of aggregation index of built-up types leads to an increase of LST value. The study reveals that the spatial arrangement of UST should be considered as the primary factors on mitigating UHI effect.

Keywords: Land surface temperature, Urban structure types, Local climate zone, VHR image, Spatial metrics, Composition and Configuration pattern

ACKNOWLEDGEMENTS

First and foremost I would like to thank God for his guidance and bless all the way through my life. Without his favor and blessings, I would not have made it this far.

I would like to express my sincere gratitude to my supervisors, Monika Kuffer, M.Sc. and Dr. Diana Reckien for your priceless assistance, advice, discussion and critics throughout the research process. Thank you so much.

Immense credit goes to Joint Japan/World Bank Graduate Scholarship Program (JJ/WBGSP) for providing financial support towards my studies in The Netherlands – you made my dream come true.

My sincere gratitude also goes to the European Space Agency (ESA) and Badan Informasi Geospasial (BIG), whom kindly support my research by providing the Pleiades and SPOT6 image. I would like to thank also to my fellow UPM 2015-2017 classmate for your friendship and kindness during our studies here. I wish you all success in your future. Special thanks to all my Indonesian friends who bring home close to me. It was such an honour and unforgettable experiences to be with you guys.

Last but not least, I would like to dedicate this work to my parents and my brothers for their endless love and pray. Finally, my forever grateful goes to my beloved wife, Monika Fenita Samaria for your wonderfully support, patience and encouragement during my study.

Enschede, February 2017

Royger Maniur Simanjuntak

TABLE OF CONTENTS

LIST OF FIGURES

LIST OF TABLES

LIST OF ABBREVIATIONS AND ACRONYMS

AUHI	:	Atmospherics Urban Heat Island
Bappeda	:	Badan Perencanaan Pembangunan Daerah/ Development Planning Board at Provincial Level
BPS	:	Badan Pusat Statistik/ National Statistical Agency
DN	:	Digital Number
ESP	:	Estimation of Scale Parameter
GPS	:	Global Positioning System
GLCM	:	Grey Level Co-occurrence Matrix
IPCC	:	Intergovernmental Panel on Climate Change
LCZ	:	Local Climate Zone
LIDAR	:	Light Detection and Ranging
LULC	:	Land Use Land Cover
LSE	:	Land Surface Emissivity
LST	:	Land Surface Temperature
MLA	:	Machine Learning Algorithm
MLC	:	Maximum Likehood Classifier
NDVI	:	Normalized Difference Vegetation Index
NIR	:	Near Infra-Red
PV	:	Proportion of Vegetation
RF	:	Random Forest
SUHI	:	Surface Urban Heat Island
UHI	:	Urban Heat Island
UST	:	Urban Structure Types
VHR	:	Very High Resolution
WUDAPT	:	World Urban Database and Access Portal Tools

1. INTRODUCTION

This chapter describes the background and justification of the study, followed by the research problem, which presents the role of local climate zones for studying the urban heat islands effect. It also includes the identification of the research objectives, research questions, hypotheses that need to be answered, conceptual framework of this study and an overview of the study area.

1.1. Background and Justification

Nowadays, many developing countries are suffering from rapid urbanization, which can endanger sustainable development of urban areas (Wu, Ye, Shi, & Clarke, 2014). According to the United Nations (2015), around 66% of the world's population will live in urban areas by 2050. At the same time, because more than half of the world's population live in urban areas, cities become highly vulnerable to climate change, as they present concentration not only to people but also to assets and infrastructure (De Gregorio Hurtado, Olazabal, Salvia, Pietrapertosa, Olazabal, Geneletti, D'Alonzo, Si Leo, & Reckien, 2015). As a result, massive changes in land use and land cover occurred in urban areas. Moreover, the effect of city expansion has altered the local climate (Argueso, Evans, Pitman, & Luca, 2015).

One of the major issues of climate change in urban areas is the increase of surface temperature. For example, IPCC (2014) predicted an increase of the global surface temperature over the 21st century. The effects of this phenomenon could lead to periods of heat waves which will impact in particular urban population around the world. Heat waves have triggered increasing mortality rates, reducing the habitats comfort area and elevating the peak energy demand of buildings (Mirzaei, 2015). When studying the effect of different temperature patterns and heat waves, one of the most well-known term in urban climate studies is the Urban Heat Islands (Li, Zhang, & Kainz, 2012). Urban Heat Islands (UHIs) refer to the difference of thermal conditions between the dense urban areas and their suburban/rural surroundings during daytime or night time where the variations depend on rates of warming and cooling that characterize each land cover type and their surface materials (Sismanidis, Keramitsoglou, & Kiranoudis, 2015). The UHI effect is mainly caused by the high heat capacity of urban surfaces, trapping of heat among urban structures/geometry (e.g. urban canyons), as well as due to low wind speeds across the urban areas, and anthropogenic heat generation (Yow, 2007). This phenomenon happens when urban surfaces absorb more solar energy and therefore heats up, compared to others locations such as rural areas with vegetation cover (Sachindra, Ng, Muthukumaran, & Perera, 2016).

According to Wu et al. (2014), there are two methods to assess the UHI effect. First, data can be collected by a ground based survey which is connected to a local weather station (Voogt & Oke, 2003). Second, nowadays researchers use satellite based image technology to analyze this phenomenon with multispectral data and thermal feature bands. For example, Kikon, Singh, Singh, and Vyas (2016) assessed UHIs using multi-temporal satellite data in Noida, India. Furthermore, Sismanidis, Keramitsoglou and Kiranoudis (2015) mentioned that satellite-based systems allow in principle a continuous monitoring of UHIs. However, in most tropical regions the continuous monitoring is limited by frequent cloud cover.

Remote sensing allows also studying phenomena like city growth, land use and land cover changes, and population growth which have important implications on UHIs patterns. For example, Zhang, Qi, Ye, Cai, Ma, and Chen (2013) found that the alteration in Land Use Land Cover (LULC) and population shifts have caused significant variations in spatiotemporal patterns of UHIs. Furthermore, Hu and Jia (2010) mentioned that the behaviour of temperature patterns is mostly influenced by land use and land cover changes. Therefore, information about urban structure types, e.g. the location of densely built-up residential areas, heavy industries and land cover areas such as vegetation, road and water bodies will improve the understanding of UHIs effects. Thus, a study on details of urban structure types which can describe physical and functional properties can be very useful to determine the causes of increasing surface temperature.

Additionally, so far only few studies analysed the variety of urban structure types and their influence on surface temperature patterns. For instances, Connors, Galletti, and Chow (2013) assessed the relationships between landscape characteristics such as residential, commercial and industrial and land surface temperature in Phoenix, Arizona. Furthermore, Stewart and Oke (2012) introduced a new concepts which is known as Local Climate Zones (LCZ). The aim of this concept is to interpret the temperature patterns within the urban context by classify the surface form and cover of the local surroundings area and to present a standardized climate-based classification for thermal studies. A further study by Bechtel and Daneke (2012) also used LCZ to extract thermally homogenous urban structures types in Hamburg, Germany. The results of both studies showed that the method was applicable to capture the temperature pattern in urban areas. In addition, the term of LCZ itself is similar to the urban structure type concept where the zones are mainly divided into different built-up and land cover types.

However, a study about spatially detailed information of urban structure types and their effect on the local characteristics of surface temperature is still missing. Previous studies on surface temperature only worked with moderate resolution images such as Aster and Landsat imagery. For instances, Wardana (2015) analysed the urban surface temperature for green spaces planning using both images. Similarly, Ahmed, Kamruzzaman, Zhu, Rahman, and Choi (2013) employed such moderate resolution imageries in a study about land cover changes and its impact on LST. Thus, VHR images can be used as alternative way to study the impact of urban structure types on surface temperature variations. This research is conducted to address this existing gap by adapting the LCZ approach and analysing its transferability using the combination of Very High Resolution (VHR) images like SPOT 6 and Pleiades and Thermal Infrared (TIR) bands of Landsat. This will allow exploring details of urban structure types and their relationship with thermal effects.

1.2. Research Problem

Previous studies on urban structure types mentioned that spatial patterns can be distinguished into several well defined configurations such as built-up areas, impervious open spaces, urban green areas and other infrastructures types (Heiden, Heldens, Roosner, Segl, Esch, & Mueller, 2012). As different configurations and composition of urban structure types can affect the thermal conditions of cities, further spatial details on its types will deepen the understanding of their impact on UHIs. However, in developing countries, urban structure types are typically very heterogeneous, e.g. areas commonly having a mix of residential, commercial and industrial uses. Hence, study about the effect of configuration and composition patterns in developing countries need to be explored to see the impact of surface temperature patterns.

Furthermore, due to the coarse spatial resolution sensors, results from moderate resolution images have limitations in extracting the urban structure types. Moreover, a research relating surface temperature and urban structure types in the context of developing countries is still unknown. To deal with the heterogeneity of urban areas, it is important to analyze the relationships between land surface temperature patterns and urban structure types employing VHR images to get spatially more detailed information. Thus, classification of LCZ with VHR image can be used to gain spatially more detail information about specific factors which can contribute to high surface temperatures. In short, this study can be used as valuable information for land use planning and urban design policies on mitigating UHIs effect in the context of cities in the developing countries.

1.3. Significance of the Study

The result of this study will contribute to the theoretical and practical knowledge of the LCZ approach in the context of developing countries. The output of this research will clarify the relationships between land surface temperature and urban structure patterns especially in heterogeneous area. In addition, the result is expected to contribute and to obtain practical knowledge regarding the effect of rising surface temperatures in urban areas.

1.4. Research Objectives

The main objective of this research is to analyse the relationships between land surface temperature and urban structure types using the LCZ approach at different spatial and temporal scale in Bandung, Indonesia.

To full fill this objective, the following sub objectives need to be achieved:

1. To analyze the local characteristics of land surface temperature patterns in the study area.
2. To adapt the LCZ method to the local context of a city in the developing countries.
3. To measure the transferability of LCZ method in detecting the main urban structure types using multi-temporal VHR image.
4. To analyze the relationship between land surface temperature and urban structure types.

1.5. Research Questions

In this study, we develop the research questions as follow:

1. Sub – Objective 1 :
   a. What are the trends of land surface temperature?
   b. What are the patterns of land surface temperature?

2. Sub – Objective 2 :
   a. Which LCZ classes can be found in the study area?
   b. What are the spatial patterns of LCZ classes in the study area?
   c. What are the thermal patterns of LCZ classes in the study area?

3. Sub – Objective 3:
   a. How can this LCZ method be translated into an image based classification using VHR images to detect main urban structure types?
   b. How transferable is the LCZ method to be applied to different spatial and temporal images?

4. Sub – Objective 4 :
   a. Does the type of built-up/land use and land cover significantly contribute to surface temperature patterns?
   b. Does the composition of built-up/land use and land cover significantly contribute to surface temperature patterns?
   c. Does the configuration of built-up/land use and land cover significantly contribute to surface temperature patterns?

1.6. Hypotheses

The hypothesis of this study is that type and density of urban structure types significantly contribute to the intensity and pattern of urban surface temperature. Moreover, the anticipated result of the specific objectives can be seen in Table 1.1.

Table 1.1 Anticipated Results

Specific Objectives	Anticipated Results
To map the hotspots of land surface temperature	• Land Surface Temperature Map
To adapt LCZ in local context	• LCZ classes for the city of Bandung
To measure the transferability concept in detecting urban structure types using VHR image	• Transferability results
To analyze the relationship between land surface temperature and urban structure types	• Descriptive statistics • Linear regression

1.7. Conceptual Framework

As mentioned in chapter 1.1, due to unique characteristics of urban structure types and the phenomenon of increasing surface temperature especially in cities of developing countries, we argue further research is required to analyse the relationships between urban surface temperature and urban structure types. At the same time, further research on the UHIs effect with the use of LCZ needs to include also the cities in the developing countries. However, as mentioned in chapter 1.2, the heterogeneous patterns of urban structure types show limitations when extracting them using moderate resolution image. Such images have less problems in differentiate compact areas and open areas or dense trees and scattered trees and etc. However, with the use of VHR images we can extract spatially more detailed information regarding different urban structure types. Finally, we will analyse the relationships between land surface temperature and urban structure types. Figure 1.1 presents the conceptual framework of this research.

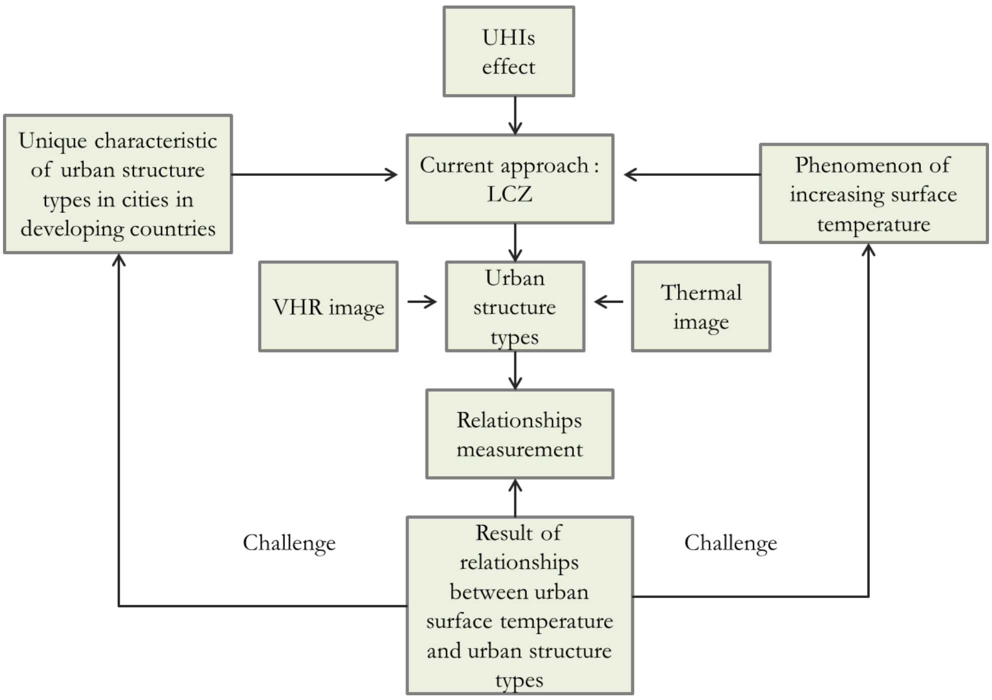

Figure 1.1 Conceptual Framework

1.8. Study Area

Bandung is located in the Western regions of Java islands in Indonesia. It is the capital of West Java province. Based on 2014 survey by Badan Pusat Statistik (BPS), the number of inhabitants living in the city was approximately 2.5 million inhabitants. Topographically, the city lies in the river basin surrounded by several mountains with the altitude nearly around 791 meters above mean sea level. The mean monthly temperature ranges from 18 – 38 °C with annual average temperature of approximately 23.6 °C. Figure 1.2 shows the location of Bandung on the Java Islands.

Figure 1.2 Location of Bandung

Over the past twenty five years the city of Bandung has experienced rapid urban growth where population growth rate increased from 1.35% per year between 1990 and 2000 to 1.49% per year between 2000 and 2010 (Firman, 2012). Moreover, a recent study by Wardana (2015) presented that during 1990 and 2008 there had been a massive land conversion from vacant land (468 ha), rice field (373 ha) and other land use (357 ha) into commercial and services (663 ha), housing (468 ha) and industry (37 ha). A previous study from Ramdani and Setiani (2014) also found out that the surface temperature has increased significantly from 27.5° C in 1999 to 31.7° C in 2009. Based on these socio-economic data, land use and temperature characteristics, selecting Bandung as a case study area will give a better knowledge on UHIs phenomenon especially when studying the relationships between urban surface temperature and urban structure types in cities of the developing countries.

1.9. Thesis Structure

This report is organized into five chapters with the following structure:

1. **Chapter 1 : Introduction**
   This chapter explains background and justification of the study, research problem, significance, research objective and questions, hypotheses, conceptual framework and study area.
2. **Chapter 2 : Literature Review**
   This chapter reviews the concepts that are related to the study. It starts with the Urban Heat Island concept followed by the land surface temperature data processing, followed by a description of local climate zones concept, machine learning algorithm, and object-based image analysis.
3. **Chapter 3 : Research Methodology**
   This chapter describes the methods that are related to this study. It starts with the general approach follow by data requirements, identification of land surface temperature and local climate zones. It also provides the method to apply LCZ approach to VHR images and to analyse the relationship between land surface temperature and urban structure types.
4. **Chapter 4 : Results and Discussion**
   This chapter presents the results and discussion of this thesis. It starts with the local characteristics of land surface temperature, implementation of LCZ, transferability of VHR and the relationships between land surface temperature and urban structure types.
5. **Chapter 5 : Conclusion and Recommendations**
   This chapter presents the conclusion and recommendations for further research

2. LITERATURE REVIEW

This chapter describes the concepts related to this study. It starts with the description of Urban Heat Islands (UHIs). Then, we explain the processes required to the extraction of land surface temperature using thermal remote sensing. After that we explain the LCZ method in relation to urban structure types. Next, we presented the use of Machine Learning Algorithms for image classification. Finally, in the section on extracting urban structure types in VHR imagery, we discuss the concept of object-based image classification that is used in this study.

2.1. Urban Heat Islands (UHIs)

As mentioned early in chapter 1.1, increasing UHIs is one of the recent phenomena faced by urban communities impacted by LULC changes in cities. In the past, measuring UHIs was commonly done by taking in-situ measurements at a particular location. Nowadays, obtaining temperature datasets can be done by using satellite imagery with thermal bands. However, some studies also used a combination of these two methods. For example, Schwarz, Schlink, Franck, and Großmann (2012) extracted surface temperatures from satellite imagery combined with in-situ meteorological measurements to analyze the relationships of air and surface temperature and its implication in Leipzig, Germany.

According to the U.S. Environmental Protection Agency (2014), several factors that contribute to UHIs effect are lack of vegetation cover, surface materials, anthropogenic heat, wind and cloud cover, and topography. In addition, a study from Schwarz and Manceur (2015) mentioned that the composition and configuration of land cover and city size are the most common factors which strongly influence the generation of UHIs. There are two different types of UHIs effects which are Atmospheric Urban Heat Islands (AUHIs) and Surface Urban Heat Islands (SUHIs) (U.S. Environmental Protection Agency, 2014). AUHIs are usually detected by taking direct measurements from thermal thermometers with a fixed meteorological station. SUHIs are generally identified from satellite imagery with the use of thermal band (indirect measurement). An illustration of the relation between surface and air temperature during daytime and night time with different configuration of urban form is presented in figure 2.1. It is shown air temperature in urban downtown is almost similar, while surface temperature is significantly different.

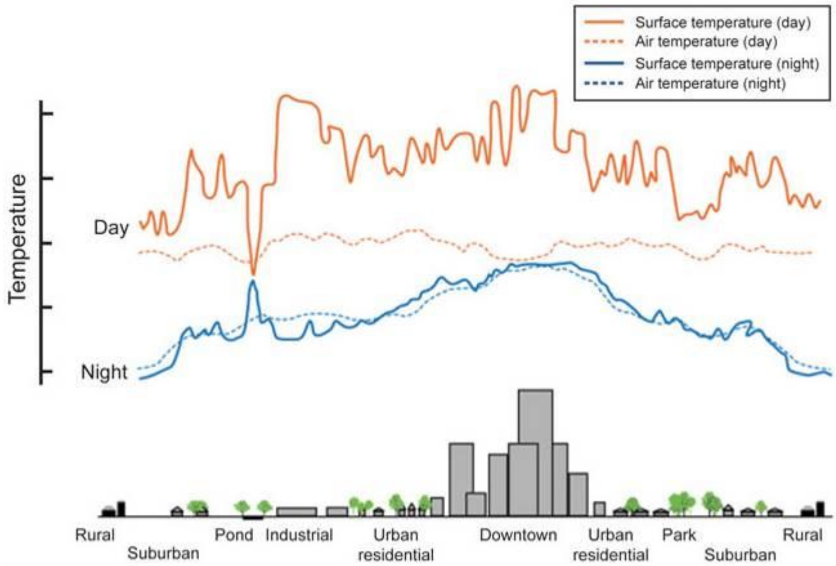

Figure 2.1 Variations between Air and Surface Temperature in Urban Form
(U.S. Environmental Protection Agency, 2014)

2.2. Land Surface Temperature Processing

Thermal Infrared Remote Sensing (TIRS) has been used widely to retrieve LST in urban climate and environmental studies in order to determine surface radiation, energy exchange and human comfort in cities (Weng, 2009). TIRS provides different methods to obtain LST information since most of the energy is directly emitted by the land surface (Yu, Guo, & Wu, 2014). Furthermore, LST can be used not only as an indicator of the energy balance but also as an environmental parameters to determine energy exchange between surface of the earth and the troposphere (Orhan, Ekercin, & Dadaser-Celik, 2014).

In order to retrieve LST from images there are several key parameters that should be taken into account. First, geometric correction needs to be applied in order to get exact locations and appropriate pixel values. Second, atmospheric correction and radiometric calibration is required to determine true surface reflectance values and brightness temperature. After that, NDVI is needed to generate vegetation indices. Here, the NDVI threshold method is calculated using formula which was developed by Sobrino, Jiménez-Muñoz, and Paolini (2004). Last, LST is obtained by calculating brightness temperature and surface emissivity. Figure 2.2 illustrates the steps to extract LST from Landsat-8 OLI TIRS images.

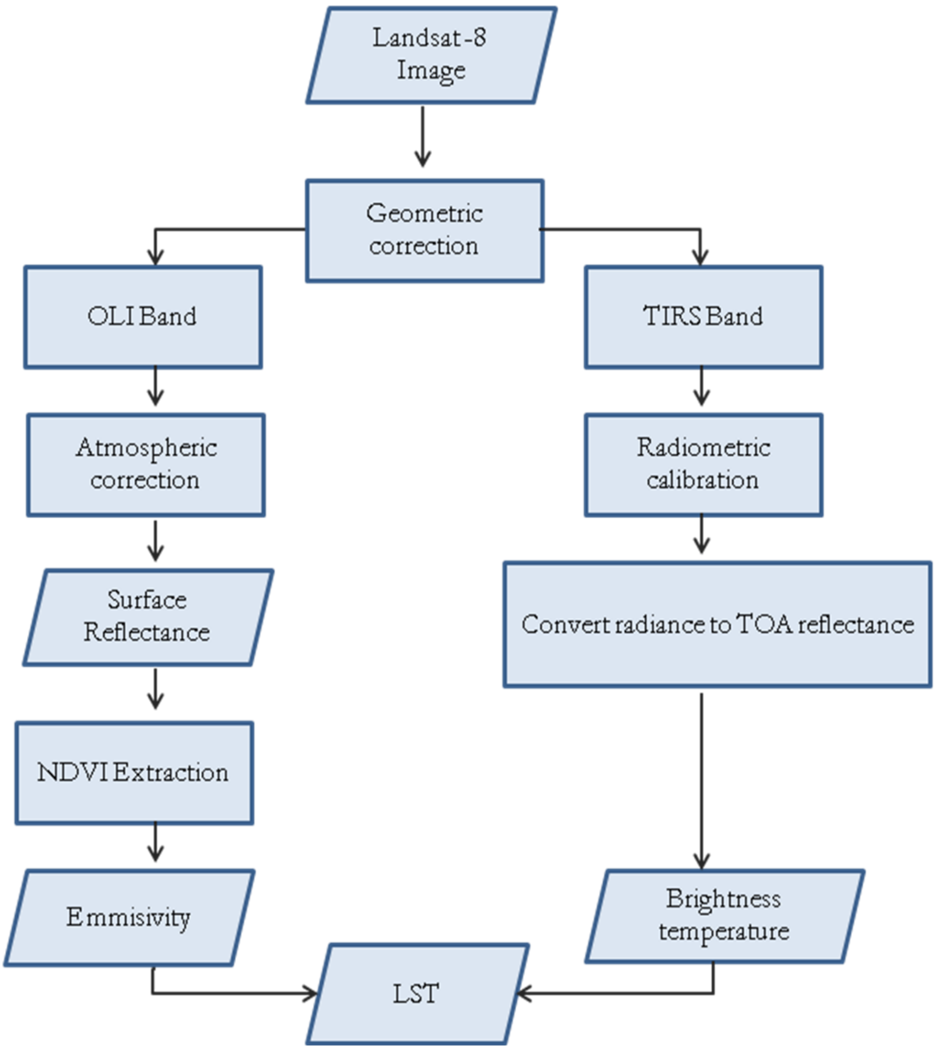

Figure 2.2 Land Surface Temperature (LST) Extraction Processes
(adopted from Jin, Li, Wang, & Shang (2015))

2.3. Local Climate Zones (LCZs) in Relation to Urban Structure Types

LCZs were developed by Stewart & Oke (2009) as a method of dividing cities into different homogenous thermal zones for the purpose of providing urban climate models with a range of possible values for different types of model parameters, e.g. sky view factor, impervious surface fraction, building surface fraction, surface albedo and anthropogenic heat output (Danylo, See, Bechtel, Schepaschenko, & Fritz, 2016). Furthermore, this method provides a standardized classification of urban climate sites where there are 17 local climate zones in 4 landscape series (I. D. Stewart & Oke, 2012). An illustration of LCZs can be seen in Figure 2.3 including a short definition of each class.

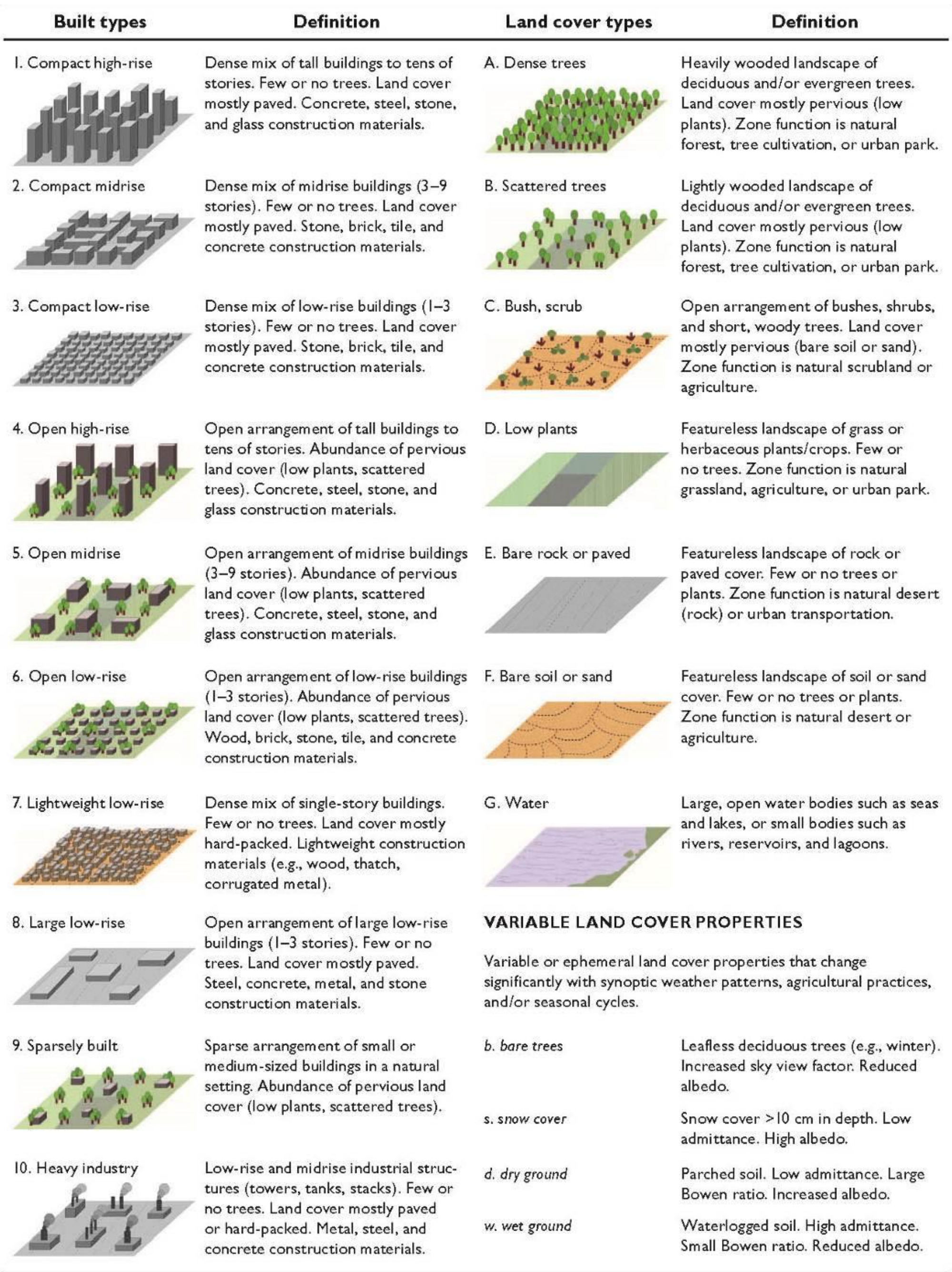

Figure 2.3 Local Climate Zones (I. D. Stewart & Oke, 2012)

In general, LCZs divide the zones into two different main types. The first main type is known as built-up or land use types. This type consists of 10 different zones, e.g., compact high rise, compact low rise, compact mid-rise, heavy industry, lightweight low rise, open high-rise, open low rise, open mid-rise, open low rise, and sparsely built. The second main type is categorized as land cover types. It contains with 7 different zones, e.g., bare soil, bush, dense trees, low plants, paved, scattered trees and water.

In the beginning, the LCZ method was not designed for mapping purpose, but it was rather used to classify urban heat island observation sites (Lelovics, Unger, Gál, & Gál, 2014). However, its relation to spatial and temporal temperature variability with respect to the geographical location has become an important research focus in urban climate studies (Geletič, Lehnert, & Dobrovolný, 2016). In urban planning studies, one of the commonly used terminologies in describing the spatial structure of a city is known as Urban Structure Types (UST). The term itself is used not only to describe the structure of urban pattern but also to map the existing structure of a city. For example, Banzhaf and Hofer (2008) mentioned UST as a spatial indicator to identify the physical and functional factors of the city.

Furthermore, a study from Bechtel et al. (2015) mentioned the aim of the LCZ scheme was to accommodate the configuration of urban structures types based on their climatic properties rather than local relief such as built-up environment or natural vegetation. Thus, LCZ can be used to represent a generic and neutral description of urban structure types for climate studies purpose. Figure 2.4 presents the characteristics of each LCZ classes employing remote sensing. The arrows indicate potential wavelength bands and feature direction. For instances, NIR and SWIR bands are employed to define soil and vegetation land cover. Meanwhile, TIR band is used to find different vegetation and built-up types. In addition, LIDAR/IFSAR datasets can be used to find the height information of each land cover types.

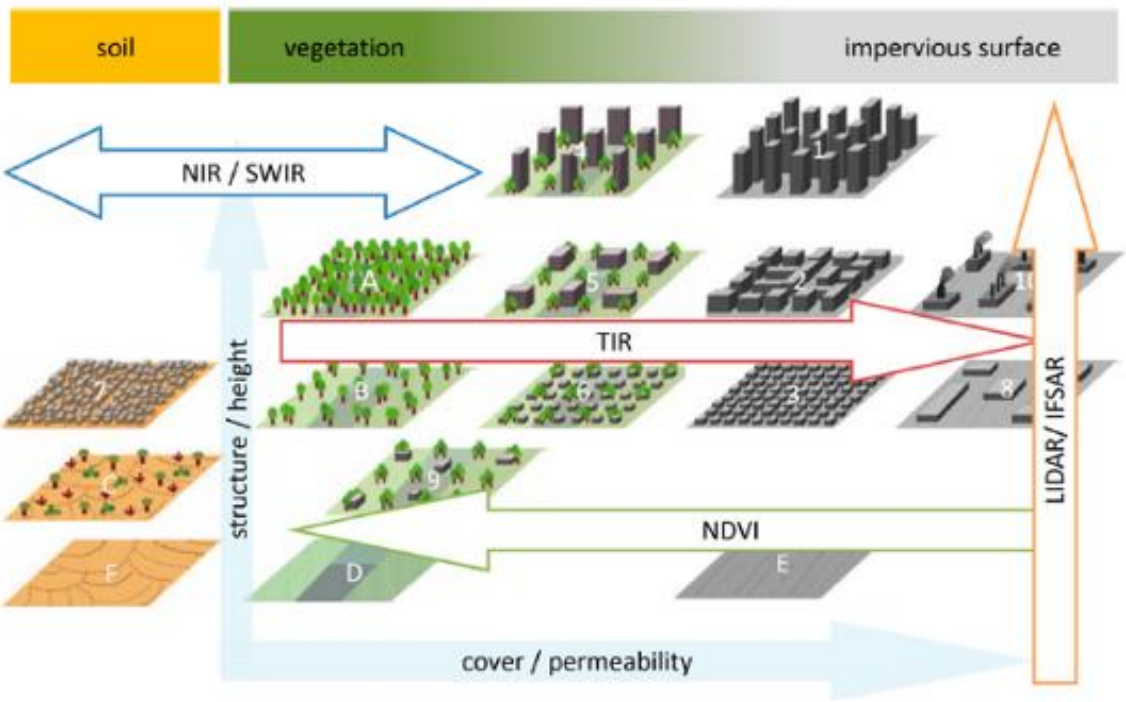

Figure 2.4 Observable Characteristics to Differentiate LCZ from RS (Bechtel et al., 2015)

Since the LCZ method provides an initial approach to standardize the classification of urban structure types in the field of climate studies, many researchers used this term as their primary method in describing the impact of urban structure types on temperature patterns. For example, a study from Middel, Häb, Brazel, Martin, and Guhathakurta (2014) mentioned the impact of urban form and landscaping types on the mid-afternoon microclimate in Phoenix, Arizona using the LCZ approach. A similar study from Geletič et al.,(2016) revealed the use of the LCZ approach to compare the spatial distributions of land surface temperature patterns in the cities of Brno and Prague. Moreover, a study from Leconte, Bouyer, Claverie, & Pétrissans (2015) mentioned the use of the LCZ scheme for Urban Heat Islands assessment in the Great Nancy Area, France to investigate thermal pattern in a homogeneous urban form. All these studies show the importance of the LCZ approach in describing the relation between urban form and temperature patterns.

A major initiative in creating LCZ maps was initiated in Dublin in 2014 where several researchers in the field of remote sensing gathered to develop a world urban database and portal tools (WUDAPT)[1]. WUDAPT was created to bridge the lack of information regarding the aspects of spatial form in cities with the impact on the climate issues. A study from Bechtel et al., (2015) mentioned the objective of WUDAPT is to produce a global spatially database that captures information on urban form and provides this information for climate studies. Several methods as mentioned by Bechtel et al.,(2015) have been applied to map LCZ including manual sampling of individual grids cells using Geo-Wiki, GIS-based approach using building data, digitisation of homogenous LCZ, object based image analysis, and supervised pixel-based approach. The results as mentioned by Bechtel et al., (2015) showed extraction of LCZ with a supervised pixel-based approach using a machine learning algorithm e.g., random forest classifier which has proven as an ideal approach to achieve higher accuracy and computational performance.

2.4. Machine Learning Algorithm

Machine Learning Algorithm (MLA) is known as an effective and ideal approach in image classification for addressing specific problems where our theoretical knowledge is still incomplete, but we do have a significant number of observations or other datasets (Lary, Alavi, Gandomi, & Walker, 2016). Furthermore, study from Lary, Alavi, Gandomi, and Walker (2016) also mentioned the advantages of using Machine Learning, i.e., it does not need a prior knowledge regarding the nature of relationships between data. These algorithms have become a well-known method compared to traditional parametric classifier such as Maximum Likelihood Classifier (MLC). Moreover, MLA is flexible and robust to non-linear and noisy relations among input features and class labels (Im, Beier, & Li, 2013). This type of classifiers can handle complex data and therefore it does not depend on the performance of a predefined model (Belgiu & Drăgu, 2016). Another advantage using MLA is its ability to gain an optimum classification accuracy with a small numbers of training datasets and a high number of input features (Cracknell & Reading, 2014).

There are several different types of MLA that are used nowadays such as Artificial Neural Networks (ANN), Support Vector Machine (SVM), Decision Trees (DT), Neuro-Fuzzy (NF), Genetic Algorithm (GA), and Random Forest (RF) (Lary et al., 2016). However, as mentioned by Bechtel et al. (2015), Random Forest revealed as the best method to extract LCZ since each LCZ have quite different appearances within cities. Furthermore, this algorithm is also used as the standard method in the WUDAPT guidelines.

[1] WUDAPT database can be found in http://www.wudapt.org/

2.4.1. Random Forest

The Random Forest (RF) algorithm is a combination of several tree predictors where each tree depends on the values of vector sampled independently (Breiman, 2001). A study by Wieland and Pittore (2014) mentioned the input feature in RF is classified with every tree in the forest where the trees are trained with the same parameters but in different training sets. Furthermore, these training sets are taken from a bootstrap procedure on the original training data where for each training set the same numbers of vectors are randomly selected with replacement (Wieland & Pittore, 2014).

A study from Cracknell and Reading (2014) found that RF has performed better in terms of classification accuracy compared to other algorithms such as Artificial Neural Network, Support Vector Machines, k-Nearest Neighbors and Naïve Bayes. In addition, as mentioned by Cracknell & Reading (2014), this algorithm is easy to train, computationally efficient, stable and accurate when being applied to sparse training datasets. Therefore, it is an excellent algorithm to be used due to its capability to handle large data and feature sets. Figure 2.5 presents the principle of the RF algorithm which uses a decision tree approach to gain optimal results.

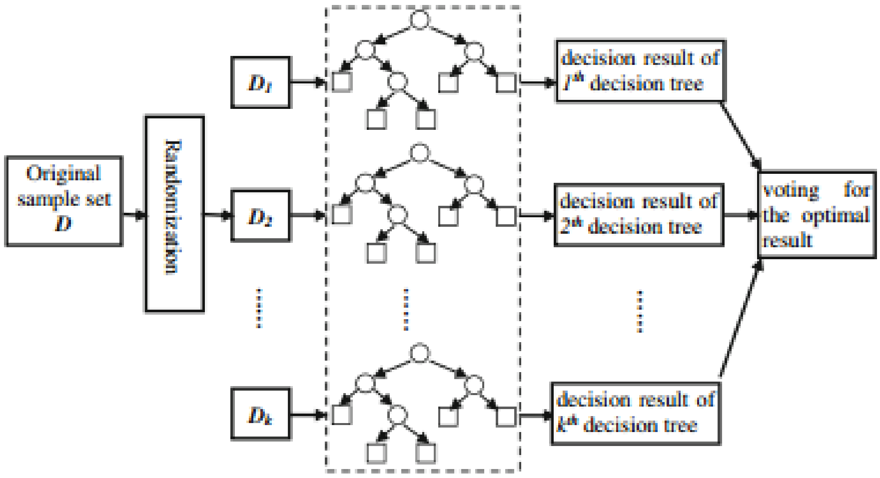

Figure 2.5 Random Forest Flow Diagram (Luo, Huang, Liu, & Feng, 2016)

2.5. Object Based Image Analysis (OBIA)

Extracting spatial information of the urban environment from an image into a single thematic map is considered to be a complex process. Different mapping methods have been introduced in remote sensing studies. For example, Weih & Riggan (2010) mentioned that in the past extracting land use and land cover from remote sensing imagery have been done using a pixel-based method. In addition, as mentioned by Weih & Riggan (2010) this method is mainly based on the multi-spectral techniques which assign a pixel into a specific class considering its similarities in image domain feature. Another method is known as object based image analysis (OBIA). This method is developed to split-up automatically an image into an object based feature class (Castilla & Hay, 2008).

A study by Liu & Xia (2010) found that applying pixel based classification using VHR image leads commonly to low classification accuracy since this method produces a 'salt and pepper effect[2]. In addition,

[2] Salt and pepper effect is a common result of a pixel based classification where close neighbours often have different classes despite being similar due to spectral heterogeneity between each neighbouring pixels.

a study from Myint, Gober, Brazel, Grossman-Clarke, and Weng, (2011) demonstrated that as the spatial resolution becomes smaller, the spectral response from different small-objects in an urban environment exhibit complex patterns in such fine resolution images. Moreover, Myint et al. (2011) mentioned that in a pixel based approach some urban classes share similar spectral responses which can lead to confusion. As consequences, it is important to develop an approach that can deal with non-pixel based classification especially in extracting information from VHR images.

Among various studies by the remote sensing community, OBIA has been introduced as the robust method in classifying VHR image. A study by Blaschke et al. (2014) mentioned the usefulness of OBIA when employing it to VHR images where objects are visually composed of many pixels. Furthermore, OBIA is an effective method for extracting features in VHR since its characteristics are assigned from an image object rather than the pixel (Bhaskaran, Paramananda, & Ramnarayan, 2010). In addition, as mentioned by Bhaskaran et al. (2010), OBIA is based on segmenting an image into homogeneous regions and classifying objects using their spectral, spatial, and textural characteristics. Several studies have been done to demonstrate the usefulness of OBIA image classification in an urban context. For example, the study from Salehi, Zhang, Zhong, and Dey (2012) mentioned the usefulness of this method to classify different land use and land cover in an urban area. Hence, classifying the urban structure using VHR imagery needs to be employed in OBIA.

According to Liu, Guo, and Kelly (2008), in general OBIA requires two major steps which are segmentation and classification. The aim of the segmentation step, as mentioned by Y. Liu et al.(2008), is to extract segments of objects that have same attributes. After the segmentation process, the classification process needs to be done in order to classify the objects based on its attributes and relation between segmented objects (Guo, Kelly, Gong, & Liu, 2007).

2.6. Spatial Metrics for Analysing The Relation between Surface Temperature and Urban Structure Types.

Spatial metrics are quantitative and aggregate measurements obtained from the digital analysis of maps showing the spatial heterogeneity of a landscape at a specific scale and resolution (Herold, Goldstein, & Clarke, 2003). A number of metrics have been developed to measure and describe both composition and configuration of land cover features (McGarigal, Cushman, Neel, & Ene, 2002). A study by Herold et al., (2003) mentioned the advantages of several metrics like Number of Patch (NP), Edge Density (ED) and Contagion (Contag) in analysing the existing urban form pattern over periods of time using raster datasets.

Spatial metrics are also used in several studies on analysing the effects of landscape patterns on land surface temperature patterns. For instances, a study by Liu and Weng (2009) used 11 different metrics to examine the scaling effect on the relationships between landscape patterns and land surface temperature in Indianapolis, United States. Furthermore, a study by Zhou, Huang, and Cadenasso (2011) used 10 different metrics when exploring the effect of land cover patterns on LST in urban landscape. Therefore, the application of spatial metrics can be very useful in understanding the relationship between land surface temperature and urban structure types.

3. RESEARCH METHODOLOGY

This chapter describes the methods to address the related research questions. It begins with the description of the general approach of research methodology, followed by data requirements of this study. Next, we discuss the identification of land surface temperature and local climate zones. Then, we describe the transferability implementation using OBIA approach. In the last part, we present the relationships between land surface temperature and urban structure types.

3.1. General Approach

In general, this study applied an exploratory design approach in order to explore the relationship between land surface temperature and urban structure types. According to Yin (2003), an exploratory design is used to explore situations or conditions in which the intervention being evaluated has not been tested or is not clear. Furthermore, only few studies have been conducted using the LCZ method in cities of the developing countries. For example, LCZ study for sustainable megacities development in Guangzhou, China by Cai, Ren, Xu, Dai, and Wang (2016). Therefore, conducting an exploratory design will give a broader perspective about the relationship between urban structure types and land surface temperature patterns.

As mentioned in chapter 1.6, type and density of urban structure types are major indicators to influence the surface temperature. In order to address this objective, we developed our research methodology (Fig. 3.1), consisting of four phases. In the first phase, we extract the surface temperature from thermal images to verify and map the local characteristics of the land surface temperature. This process allows us to see the pattern of the local land surface temperature in the study area. A local expert was asked to compare and provide feedback regarding the surface temperature result. At the second phase, we adapt the LCZ method in order to define the existing LCZ classes which relates to the surface temperature in the surrounding area. During this phase, we employed moderate resolution images to capture the existing condition in the city based on its LCZ classes. For this phase, a random forest classifier which is the standard LCZ approach was used to extract LCZ classes. In the third phase, we analyse the transferability of the LCZ method to VHR images, which provide more spatial detailed information. As discussed in sub chapter 2.5, OBIA is considered as an effective method to gain a better overall accuracy in VHR image classification. Thus, OBIA was applied for classification of VHR image. Moreover, during this step, we developed a rule set to test the LCZ method with different spatial and temporal VHR image. In the last part, we analyzed the relationships between urban surface temperature and urban structure types using spatial metrics.

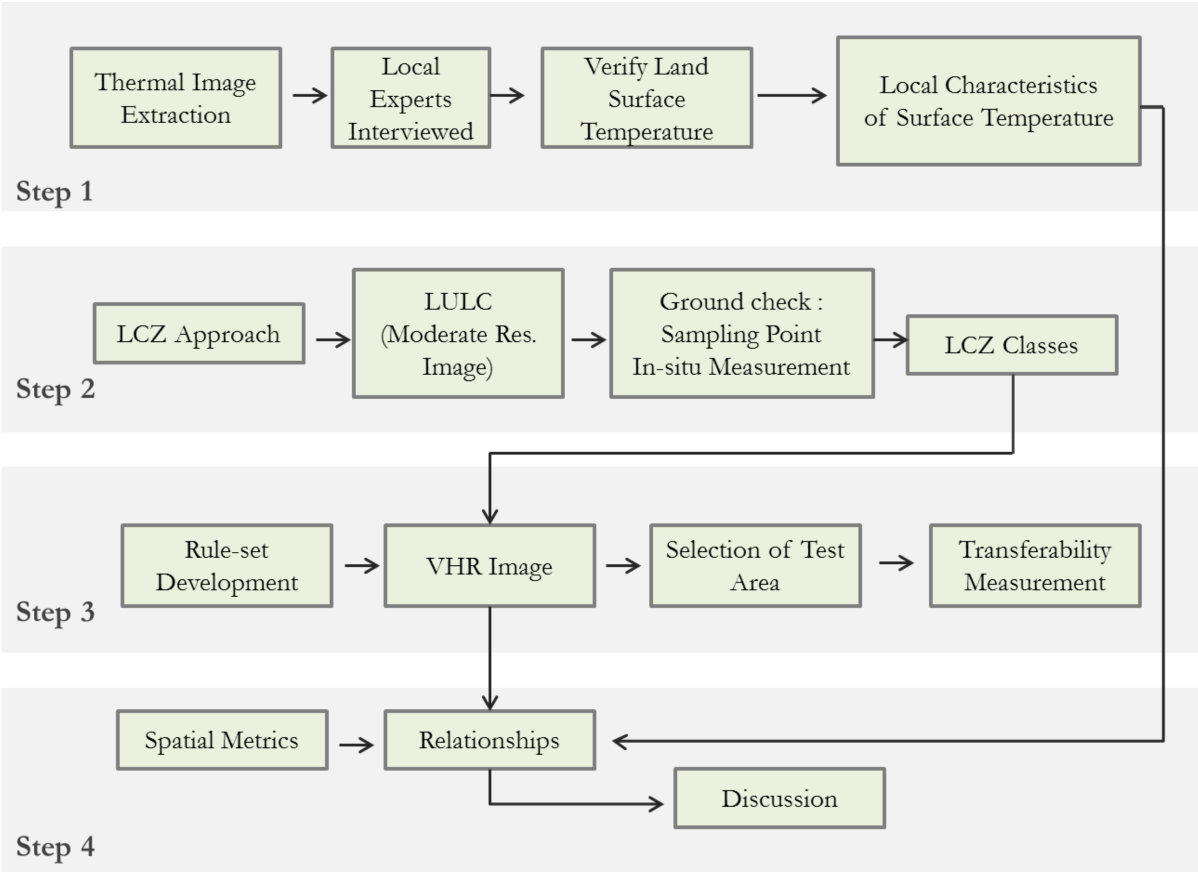

Figure 3.1 Research Methodology

3.2. Data Requirement

In this study, we used two different types of data, namely primary and secondary data. Primary data was collected by sampling of observation points on the ground, collecting site information, interviewing local experts regarding the surface temperature patterns and conducting in-situ thermal measurement at selected locations. Secondary data was taken from several satellite imageries with several additional data such as administration boundaries, land use and air temperature datasets. The details of both datasets are described in the following sub-sections.

3.2.1. Primary Data Collection

According to Hox & Boeije (2005), primary data are collection of original datasets for specific research objectives which used to answer the research problems. In this study, primary data were collected during a one-month fieldwork in October 2016. The following process and type of data are explained below.

First, fieldwork data collection is considered as the important primary data in this study. Several preparations were necessary before conducting this process. In the first step, a base map was created for data collection process. In total, 448 sampling points of built-up and land cover types were collected to define not only the training areas used for training the classification but also test areas which were used as a reference points for the accuracy assessment. The selection of point samples should consider all the variation within each zones/classes. In this study, we applied random stratified sampling in order to define

LCZ classes in the study area. According to McCoy (2005), stratified random sampling assigns a specific number of sample points to each class in proportion to the size or significance of the category. Thus, this method will avoid an uneven distribution of points among the classified category. Figure 3.2 illustrates several types of sampling pattern in the field of remote sensing study.

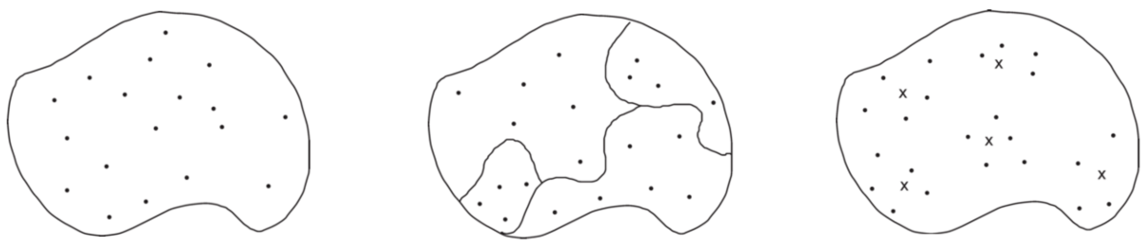

Simple Random Pattern Stratified Random Pattern Clustered Pattern

Figure 3.2 Types of Sampling Pattern (McCoy, 2005)

Four sets of handheld GPS were used to collect these observation points. During this process, six surveyors helped researcher collecting the primary data. We conducted the survey not only by cars and but also motorcycle since in some areas only motorcycle allowed to access the location.

Thermal point measurements were also collected during this time to find out the ground surface temperature value. We conducted in-situ thermal measurements at three different times at the same locations. This consideration was taken because the pattern of surface temperature is based on the sun energy that has been reflected and emitted to the ground. First, we took measurements shortly before the sunrise begins (between 5:30 and 6:30 am). The consideration is because during pre-dawn most of the solar component is less accentuated and thermal emission from natural surfaces like rocks, asphalt and vegetation is at a minimum level (Kuenzer & Dech, 2013). Second, the measurement was performed at daytime during Landsat descending acquisitions time between 10:00 and 10:30 am. We assumed that the surface temperature during this time would be more or less the same as the value extracted from Landsat. Lastly, we took measurements during evening time shortly after the sunset (between 06.00 and 07.00 pm). The reason was because the surface temperature at this time should decrease since most of the energy had been evaporated into the air. Therefore, dawn time, daytime and evening time measurements were used to understand the characteristics of surface temperature.

Furthermore, comparison between in-situ measurement and Landsat acquisition was considered as an important factor to provide authentic information regarding the surface temperature in the study area. Thus, we employed in-situ thermal measurement. Figure 3.3 presents the Testo 830-T2 thermal thermometer that was used to take surface temperature measurement during fieldwork with a precision accuracy of ± 1.5° Celsius and temperature resolution of 0.5° Celsius. In addition, air temperature measurements were also taken during fieldwork not only to get real time air temperature data but also to obtain a comparison with the surface temperature. Although, the accuracy of the digital air thermometer has been considered as limitations in this study, this datasets is considered as one important factor to assess the pattern of surface temperature.

.

Figure 3.3 Digital Air and Thermal Thermometer

Second, an interview with a local expert was conducted to discuss the preliminary results about the trend of surface temperature in Bandung. The aim of the interview was to explore and determine the characteristics of surface temperature in Bandung. This method is considered to be effective since it gives the researcher a comprehensive perspective regarding surface temperature and its characteristics in the study area. We used the topic-focused interview method[3]. One local expert was interviewed during this time. We arranged to meet in Bandung in October 2016. We asked several questions during the interview. For instance, we asked the expert regarding the temperature patterns in Bandung and the factors that influenced the behaviour of temperature especially in the last decade. All of the questions from the interview process can be seen in Appendix 1.

3.2.2. Secondary Data Collection

Concerning secondary data collection, there are two types of images that were used to assess land surface temperature and urban structure types. First, moderate resolution image such as Landsat TM5 and Landsat 8 OLI TIRS were selected where these imageries have a thermal band. In Landsat TM5, the thermal band is located in band 6, while in Landsat 8 OLI/TIRS there are two thermal bands which are band 10 and band 11. Both the images have been resampled to 30 meters resolution. Appendix 2 shows the detailed information regarding these two thermal imageries. Furthermore, according to Roth, Oke, and Emery (1989), there are several parameters to assess UHIs intensities. One parameter is that the UHIs intensity is going to be higher during daytime at the dry season. Therefore, the thermal images will be selected during these times. Wardana (2015) also mentioned that another parameter in image classification is the selection of cloud cover which should be limited to ≤ 10 %. This criterion becomes an important factor to ensure all information from images can be identified precisely. Thus, we only selected images

[3] According to Groenendijk and Dopheide (2003), topic-focused interview technique will ensure that required information is being collected and the topic of discussion can be explored during the interview.

with cloud cover below this criterion. As a result, only eight satellite images with thermal band were selected from 2005 – 2016.

Second, Pleiades and SPOT6 were used to extract detailed information of urban structure types. We acquired a recent Pleiades image from ESA[4] and SPOT6 image from BIG[5]. Both images were obtained with "free of charge" for research purposes. VHR sensors offer panchromatic and multispectral bands, both are very useful to distinguish complex built-up types such as compact low rise and open low rise and vegetation types like dense trees, scattered trees or low plants.

Other types like administrative boundaries and land use were used as supporting data for the image processing. In addition, OSM datasets such as roads and rivers were also used to assist the researcher during the classification process. Table 3.1 provides the dataset that used in this study.

Table 3.1 Ancillary Datasets

No.	Data	Format	Year	Data Sources	Data Collection
1.	Landsat TM 5	Raster	2005, 2007, 2008, 2009	USGS	Download
2.	Landsat 8 OLI - TIRS	Raster	2013, 2014, 2015, 2016	USGS	Download
3.	SPOT 6	Raster	2013	BIG	Order
4.	Pleiades	Raster	2016	ESA	Order
5.	Administration Boundaries	Vector	2011	Bappeda	Institutional Survey
6.	Land use	Vector	2011	Bappeda	Institutional Survey
7.	Road and River	Vector	2015	Open Street Map (OSM)[6]	Download
8.	Photo of ground sampling objects	Documentation	At present	Study area	Field Observation

[4] Pleiades is obtained from European Space Agency (ESA). Images were captured on July, 21 & August, 3 2016. The available image can be found in htpp://www.geo-airbusds.com/en4871-browse-and-order.

[5] SPOT 6 is obtained from Badan Informasi Geospasial (National Geospatial Agency of Indonesia). Image was captured on April 19, 2013.

[6] OSM (Open Street Map) is a project community which aims to make freely available and editable maps. Maps can be downloaded from http://www.openstreetmap.id

3.3. Identification of Land Surface Temperature

The aim of this phase was to determine the local characteristic of the surface temperature in Bandung. This phase was considered as the stepping stone in the research methodology since its results will be used to present the entire picture of the urban surface characteristics in the study area. Furthermore, the results were used not only to identify which areas are detected as either hotspots or cold spots of the surface temperature along the study area but it is also used as a base map to identify the existing of urban structure types.

To have the pattern of the local surface temperature in the study area, we applied the procedure of thermal extraction from thermal satellite imagery. We used multi temporal imagery, e.g., Landsat TM5 and Landsat 8 OLI/TIRS, which were taken from the year of 2005 until 2016 to identify LST. Moreover, it is also important to understand that the images were captured during daylight time between 10.00 and 10.30 a.m.

Several studies suggest that monitoring UHI effects by determining LST from satellite images should be analysed using a daily basis datasets and during night time. For example, a study from Bechtel, Zakšek, and Hoshyaripour (2012) suggested that monitoring diurnal UHI effects should be taken per hour using downscaling LST technique from on board geostationary satellites. However, considering the availability of imageries especially in tropical countries like Indonesia which has a lot of cloud cover, the selection included all available Landsat images that fulfilled the above mentioned criteria. Furthermore, to get the maximum results of the LST, we select the peak of summer time in Bandung. Therefore, we selected the month of September in each year. We assumed that during the same month the temperature characteristics are less different. The information regarding thermal images that were used in this research can be seen in table 3.2.

Table 3.2 Thermal Satellite Images Used in This Study

No.	City	Satellite	Date	Time (UTC)	Cloud Cover
1.	Bandung	Landsat 8	02/09/2016	10: 00 : 40	1 %
2.	Bandung	Landsat 8	15/08/2015	09 : 59 :55	1 %
3.	Bandung	Landsat 8	13/09/2014	10 : 00 : 37	0 %
4.	Bandung	Landsat 8	10/09/2013	10 : 02 : 29	1 %
5.	Bandung	Landsat TM5	15/09/2009	09 : 50 : 15	0 %
6.	Bandung	Landsat TM5	10/07/2008	09 : 45 : 09	1 %
7.	Bandung	Landsat TM5	26/09/2007	09 : 53 : 30	1 %
8.	Bandung	Landsat TM5	04/09/2005	09 : 48 : 36	0 %

3.3.1. Image Pre-Processing

As discussed previously in chapter 2.2 regarding thermal remote sensing, image pre-processing is required before image classification. Therefore, to extract LST from Landsat imagery we applied several pre-processing steps. For instance, radiometric calibration and atmospheric correction should be done in the beginning. However, since the images have been geometrically corrected by USGS, we focused to the following steps.

1. Conversion DN Values to Reflectance and Brightness Temperature

- Top of Atmospheric Spectral Radiance :

$$L\lambda = M_L * Qcal + A_L, \quad (1)$$

Or

$$L\lambda = (L\,Max - LMin) / (Qcalmax - Qcalmin) \times (Qcal - Qcalmin) + LMin$$

Where
ML = band specific multiplicative rescaling gain factor
AL = band specific additive rescaling bias factor
Qcal = quantized calibrated pixel value
LMax = spectral at sensor radiance to Qcalmax (DN=255)
LMin = spectral at sensor radiance to Qcalmin (DN=1)
Qcal max = quantized calibrated pixel value (DN) maximum
Qcal min = quantized calibrated pixel value (DN) minimum

- Conversion of Radiance to Reflectance

$$p = (\pi * L\lambda * d2) / (ESUN\lambda * \cos\theta s) \quad (2)$$

Where
p = Planetary TOA reflectance which is the ratio of reflected versus total power energy
π = Constant (3.14159)
Lλ = Spectral radiance at the sensors aperture (at-satellite radiance)
d = Earth-Sun distance in astronomical units
ESUNλ = Mean solar exo-atmospheric irradiances
θs = Solar zenith angle in degrees, which is equal to θs = 90° - θe ; where θe is the Sun elevation
For Landsat 8 the calculation of ESUNλ can be done as follow:
ESUN= (π*d2) * Radiance Maximum/Reflectance Maximum

- Conversion of Radiance to At-Sensor Temperature:

After the DN values are converted into reflectance, the thermal band needs to be converted from spectral radiance to brightness temperature using the constants from metadata file. Here is the employed equation to convert reflectance into brightness temperature (BT) with the following calibration constants (table 3.3):

$$BT = (K2 / \ln [(K1/L\lambda)+1]) - 273{,}15 \quad (3)$$

Where
K1 = band specific conversion constants 1
K2 = band specific conversion constants 2

Table 3.3 Calibration Constants from Metadata of Satellite Images

Constants	Landsat 8 (Band 10)	Landsat 5 TM (Band 6)
K1	1321.08	1260.56
K2	774.89	607.76

2. Retrieval NDVI and LSE

- Calculating the Normal Difference Vegetation Index (NDVI) :

NDVI is an indicator to analysis and assess whether the target object contains of vegetation or not. The near infrared band and visible red band were used to calculate the Normal Difference Vegetation Index (NDVI). The NDVI calculation can be described as follows :

$$\text{NDVI} = \frac{\text{p (NIR} - \text{Red)}}{\text{p (NIR} + \text{Red)}} \tag{4}$$

Where
ρNIR = Reflectance Near Infrared Band
ρRed = Reflectance Visible Red Band

- Calculating the proportion of vegetation :

The following equation is used to calculate the proportion of vegetation (Pv):

$$\text{Pv} = \left(\frac{\text{NDVI} - \text{NDVIs}}{\text{NDVIv} - \text{NDVIs}} \right)^2 \tag{5}$$

Where
NDVIv = NDVI values for vegetation (0.5)
NDVIs = NDVI values for soil (0.2)

- Calculating Land Surface Emissivity (LSE) :

Land Surface Emissivity is known as a factor to predict emitted radiance. The value will be used to estimate LST. The correction of emissivity will use the NDVI threshold method which was developed by Sobrino et al. (2004). Where pixels with NDVI >0.5 are considered as vegetation and will be given emissivity value of 0.99. In addition, Pixels with an NDVI <0.2 will be considered as built-up area and will be given emissivity value of 0.97. NDVI values between 0.2 and 0.5 are considered as mixtures of soil and vegetation cover and will be retrieved with the following equation:

$$E\lambda = 0.004 \text{ Pv} + 0.986 \tag{6}$$

Where
E = emissivity
Pv = proportion of vegetation

3. Extraction of LST

The last step to extract LST calculation is computed as follows :

$$\text{Ts} = (\text{BT}/(1 + [(\lambda \text{BT}/\text{p}) \ln E\lambda])) \tag{7}$$

Where
Ts = Land Surface Temperature
BT = Brightness Temperature

Since we used multi temporal images to extract surface temperature, therefore we used the model builder in ArcGIS software to reduce processing time. Two procedure steps were taken during this phase. First, we calculated the NDVI and Brightness Surface Temperature. After that, we defined the LST using the maximum and minimum value of NDVI. All the procedures of the LST extraction can be seen in Appendix 3.

3.3.2. Spatial Patterns of Land Surface Temperature

To obtain general pattern of land surface temperature in the study area, we applied the reclassification method due to different temperature value in each year. Quantile classification approach was used to get the same proportion number of data values within each class. We divided the land surface temperature results into four different types e.g., very low (0-25%), low (25-50%), high (50-75%) and very high (75-100%). After that, we assigned each class with value 1 to 4. Then, we combined all years into one LST map by adding the values using the raster calculator tool in ArcGIS. Finally, we synthesized three types of class from the land surface temperature reclassifying result. The first type is the cold areas which represent the cooler areas during the years. The second type is categorized as the areas with moderate surface temperature where its value range is neither cold nor hot. The last type is categorized as the hot areas which represent the areas with high surface temperature. Description of each classification can be seen in Table 3.4.

Table 3.4 Scoring and Classification of LST Patterns from 2005 - 2016

No.	Classification Class	Scoring	Characteristics
1	Cold	8 -15	Low temperature value
2.	Moderate	16 -23	Medium temperature value
3.	Hot	24 -32	High temperature value

3.4. Identification of Local Climate Zones

The main activity in the identification of LCZ is to map the existing built-up/land used and land cover types with the LCZ approach. Mapping LCZs is a crucial step in this research since it will be used to understand the spatial pattern of urban structure types in the study area. To map the entire study area (Bandung city), we used moderate resolution images from Landsat 8 OLI/TIRS from year 2013 and 2016.

3.4.1. Image Analysis

In this phase, a supervised classification method was used to perform the LCZ classification. The training sample sites were based on the sampling points collected during fieldwork. As mentioned in sub chapter 3.2, in total, 448 random points from ground observation were collected (see fig. 3.4). We selected two-thirds (298 points) as the training datasets while the remaining one third (150 points) used as the test datasets for accuracy assessments.

As mentioned in chapter 2.4, the Random Forest (RF) algorithm was used to perform the pixel based approach for the LCZ image classification. The process was conducted in R software which is known as an effective tool for data preparation, calculation and graphic display. We used a comprehensive package for raster pixel based classification such as rgdal, raster, caret, e1071 and randomForest to running the RF classification. In order to prepare ancillary datasets that are used in the classification process such as layer stack, masking image, projection image and visualization, we used ENVI 5.3 and ArcGIS 10.4 software.

During the process in R software, we set up two variables, the number of features used in tree (mtry) and number of variables (ntree) to have an optimal result. In order to get these results, we tested the variables in different scenarios. Hence, trial and error was needed during this process. Finally, the confusion matrix was calculated based on the sampled reference points to obtain the Overall Accuracy (OA) and Kappa coefficient.

We applied the LCZ classification to two different temporal Landsat imageries which are 2013 and 2016. In addition, we selected these years because of several considerations. First, we assumed that the latest years represent best the existing LCZ classes in the study area. Second, since our research aim is to test the transferability of the LCZ method to VHR imagery we selected the years for which were we had available VHR imageries.

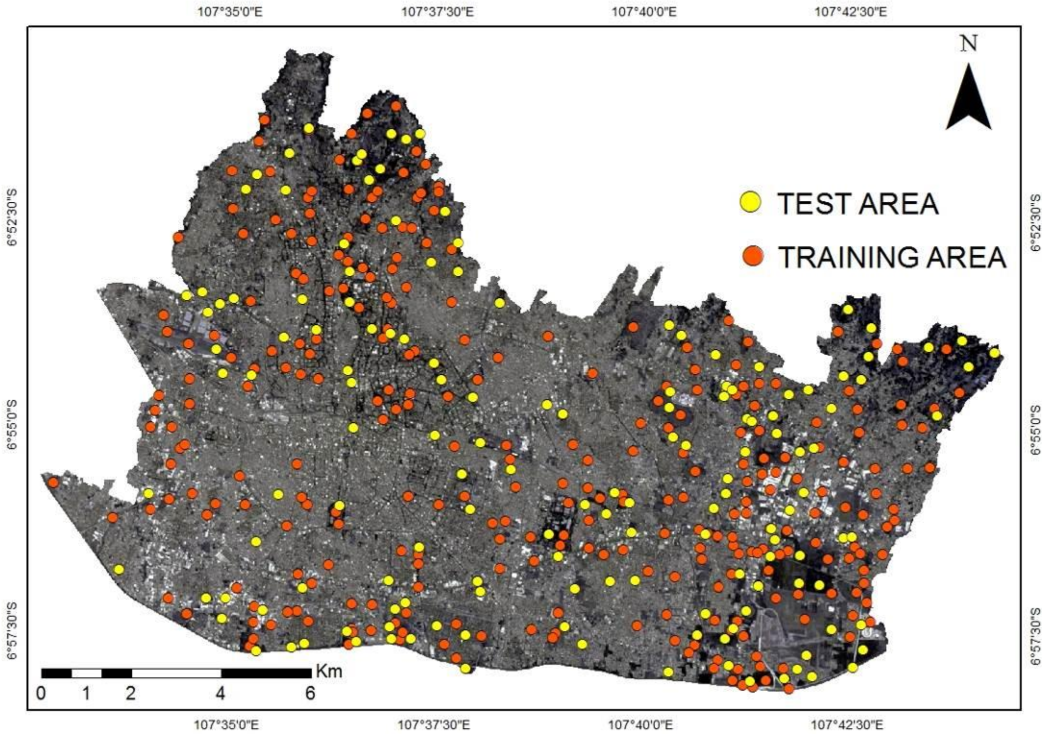

Figure 3.4 Random Points for Training and Test Area

3.5. Transferability Implementation

Transferability refers to the capability of a principles or methods for testing how well the obtaining results can be obtained in another context (Hellström, 2008). The study from Kohli, Warwadekar, Kerle, Sliuzas, and Stein (2013) mentioned the terms of transferability of Object Based Image Analysis (OBIA) concept in the context of slums identification where it refers to the capability of a specific method to obtain a comparable result for different temporal condition with minimal adaptation. Furthermore, as mentioned by Kohli et al., (2013), previous studies have presented that developing rule set acquired by OBIA methods can be used and applied to various context such as subset of same image or different images. Hence, implementing this concept to adapt LCZ method using coarse and fine resolution imagery was considered to be useful.

In this phase, the process started with the selection of the satellite imagery, VHR image pre-processing, selection of test areas and lastly segmentation and classification. Various steps have to be taken since the main activity is to define the details of urban structure types using the LCZ classification. Thus, when aiming at a detailed LCZ classification higher spatial resolution imagery is required. Descriptions of details are given below.

3.5.1. Selection of the Satellite Imagery

As mentioned in chapter 1.2, to extract and distinguish detailed information of urban structure types specifically in the context of heterogeneous urban areas in developing countries, it is necessary to use VHR images to get spatially detailed information of the ground. Additionally, since the object of interest from the LCZ classes mostly consist of different built-up types, VHR images allow to detect these various types of buildings more accurately compared to moderate resolution imagery.

Furthermore, the city contains different vegetation types such as dense tree, scattered tree and low plants. Therefore, highly spatial resolution images are required to differentiate the diversity of this land cover class. In addition, the availability of the Near Infrared (NIR) band is also considered as an important factor when selected VHR imagery. The NIR band can distinguish not only vegetation types but also water class. This is because vegetation tends to reflect higher in NIR spectrum band, while water tends to absorb of NIR light.

Figure 3.5 (a) and (b) and table 3.5 present the coverage area and spatial resolution of the two different VHR images. Pleiades image has a higher resolution for both the panchromatic and multispectral bands compare to SPOT6. In this study, we used a pan-sharpened image. Therefore, the resolution for each image is the same as the panchromatic resolution. Thus after pan-sharping, SPOT 6 has 1.5 metres resolution for each band. Meanwhile, Pleiades resolution is 0.5 metres.

Table 3.5 Resolution Scale of SPOT-6 (2013) and Pleiades (2016)

Image	Panchromatic	Multispectral
SPOT 6	1.5 meters	6.0 meters
Pleiades	0.5 meters	2.0 meters

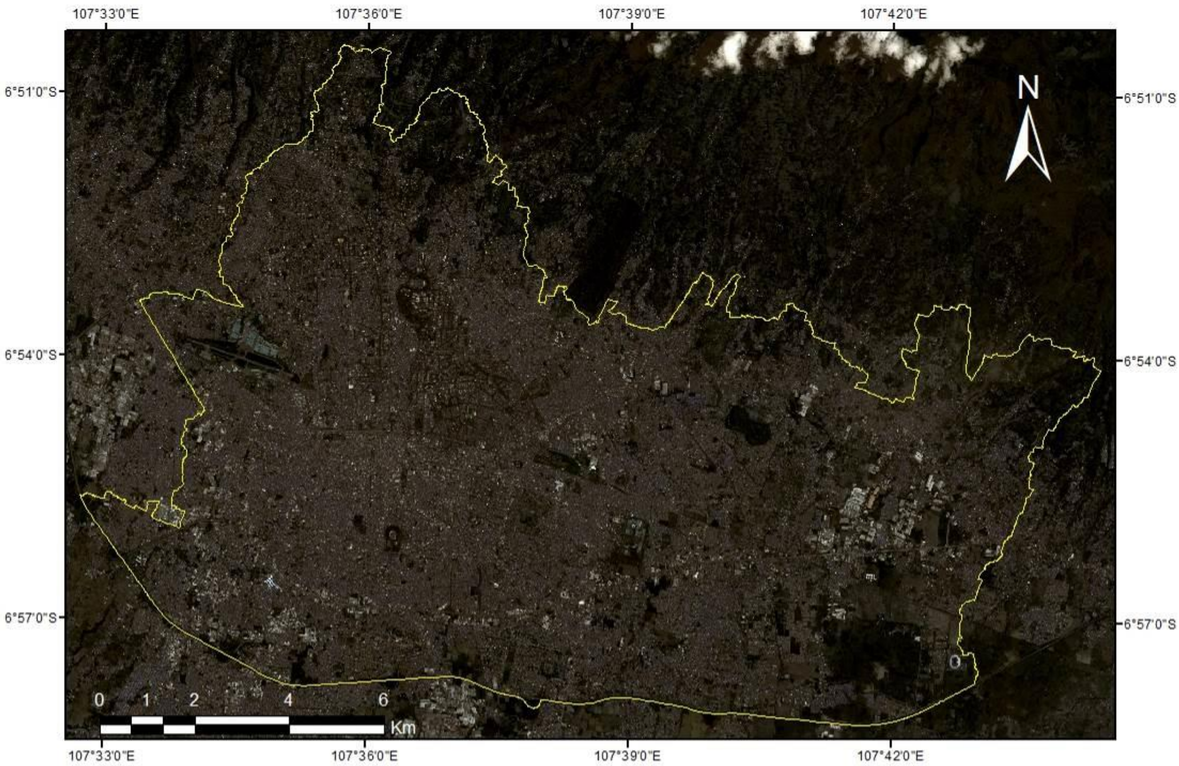

a. SPOT-6 (2013)

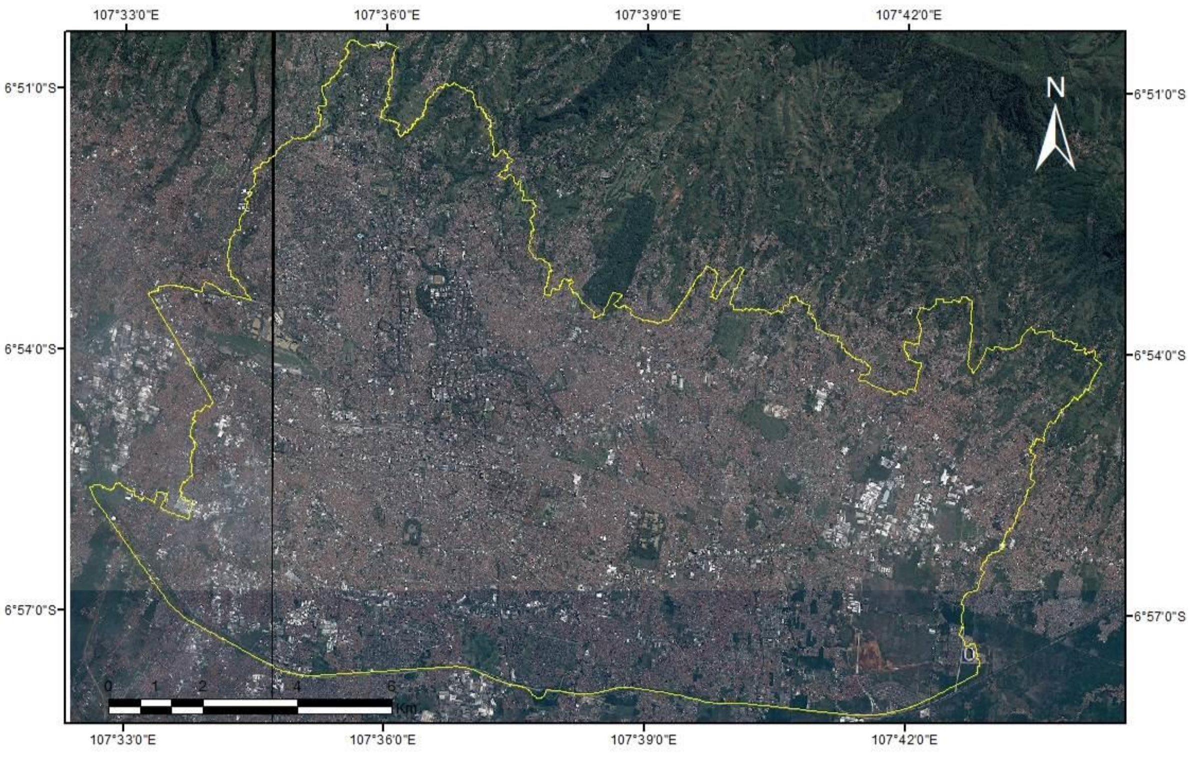

b. Pleiades (2016)

Figure 3.5 VHR Image from SPOT-6 (2013) and Pleiades (2016)

3.5.2. VHR Image Processing

Since we used multi-temporal images, the variations in atmospheric and geometric conditions will be a crucial factor to the outcome. Thus, before performing image processing we need to conduct a pre-processing step to ensure the quality and consistency of input images. According to Astrium (2013), both SPOT6 and Pleiades images have been geometric and radiometric corrected using their internal calibration parameters, ephemeris and altitude measurements.

Based on the metadata that was given from Pleiades and SPOT 6 imagery, the images have different sun angle. The effect of different sun angles will lead into different shaded of relief landscapes where certain features are highlighted. Therefore, correction was needed to ensure the quantitative use from both imageries. In principal, the procedure has been relatively similar to the moderate resolution image. However, there were some differences due to number and characteristics of bands. For example, according to ASTRIUM (2012), converting DN value can be obtained from the gain and bias method with the following formula.

$$Lb\,(p) = \frac{DC(p)}{Gain(b)} + Bias(b) \tag{8}$$

Where
Lb (p) = Radiance in the TOA
DC (p) = DN value
Gain (b) = gain value for specific band
Bias (b) = bias value for specific band

After converting DN values to TOA, we stacked the four band layer into one single image. Then, we performed a sun angle correction by divided the pixel value with the sine of the sun elevation angle using the information of sun elevation on each image. Appendix 4 presents the information regarding sun elevation and its sine value. Similar with the routine process in the moderate resolution image, we applied to build another model builder in ERDAS software to have an efficient process. The model builder was used since we deal with multi temporal images. Each steps of image pre-processing can be seen in figure 3.6.

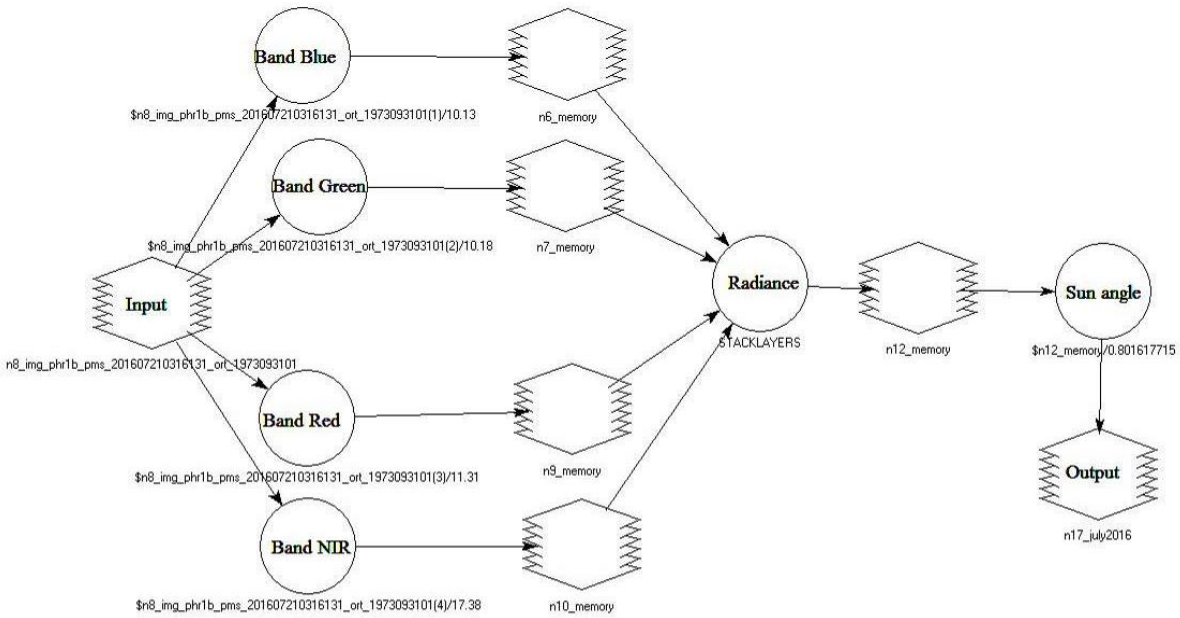

Figure 3.6 Flowchart Process in ERDAS Modeller

3.5.3. Selection of the Test Area

Since our research aim is to assess the transferability of LCZ method using VHR images, test areas should be selected considering various characteristics of urban structure types in the study area. Therefore, it was necessary to consider several aspects before deciding on the location. First, the area should consist several of built-up types such as compact low rise, open low rise and industry. Second, the area should contain different vegetation types like dense trees, scattered trees and low plants. Last, road and water areas were considered also as important features. Water can be found either near to the river or close to paddy fields which are mainly located in the southern part of the city. Thus, based on these considerations, we have selected test areas around Dago and Astanaanyar region.

Both test areas can be seen in figure 3.7a and 3.7b. For the first area, we selected an area in the city centre close to major offices. As can be seen from fig.3.7a, there are various built-up types conwithin this area with several vegetation in the southeast part of the image. Meanwhile, for the second area (figure 3.7b), we choose an area that contains all the LCZ classes. The second test area is located in the South part of the city.

a. Test Area 1 b. Test Area 2

Figure 3.7 Test Area Locations

3.5.4. Segmentation and Classification

Segmentation and classification was applied to produce features from image objects. According to Blaschke (2010), the aim of image segmentation is to divide or partition the image into relatively homogenous groups of pixels. In order to obtain accurate segmentation results, many different algorithms have been developed in the recent years. One of the most widely used algorithms in image segmentation is known as multi resolution segmentation. This segmentation has the ability to produce extremely homogenous objects from different types of data (Baatz & Schäpe, 2000). Various studies in OBIA approach have revealed the advantages of this algorithm in urban areas. For example, study by Salehi, Zhang, Zhong, and Dey (2012) used this algorithm to classify complex urban environment using Quickbird imagery. Furthermore, study by Kuffer, Barros, and Sliuzas (2014) mentioned that this algorithm has the least degree of over and under segmentation compare to different other algorithms (mapping urban slum areas). Thus, we used multi resolution segmentation to extract the built-up and land cover types.

To apply this segmentation in OBIA, we used a new automated parameterisation approach for multi scale image segmentation from Drăguţ, Csillik, Eisank, and Tiede (2014). This approach is known as Estimation Scale Parameter (ESP) 2[7]. ESP2 is used to determine an appropriate Scale Parameter (SP) by an optimisation process. Moreover, the ESP tool mainly contains pre-defined rule set parameters which can be run in eCognition software. The result provides an appropriate of SP value for different level of segmentation. Figure 3.8 presents the current process for extracting scale parameter value from ESP tool.

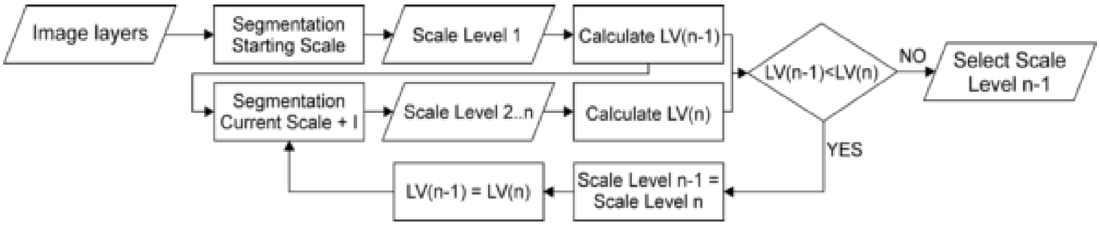

Figure 3.8 Selection of SP Using ESP Approach (Drăguţ et al., 2014)

After creating an appropriate segmentation, we determined a suitable classification approach. We chose to perform assign class algorithm due to its ability to assign an image object to a class using certain threshold values (Trimble Germany GmbH, 2016).

During the segmentation and classification phase, we applied two different development strategies. First, we focused on differentiating the base classes such as water, road, trees, low plants and built-up. Second, we chose again the built-up and trees to implement the remaining classes of LCZ. Therefore, two level of segmentation were applied during this phase. For segmentation level 1, a low value of Scale Parameter (SP) =10, with equal weight (0.5) to shape and compactness were applied. After that, we employed a coarse segmentation from ESP result to segment the zones of trees and built-up area. During this phase, we applied the segmentation level 2 into two categories. For instances, we divided vegetation into two types such as dense trees and scattered trees. Then, we classified built-up area into compact low rise, open low rise, and industry. In this process, we also considered that applying higher SP can result in misclassification. Figure 3.9 shows different result after applying different SP where the building class was detected as vegetation.

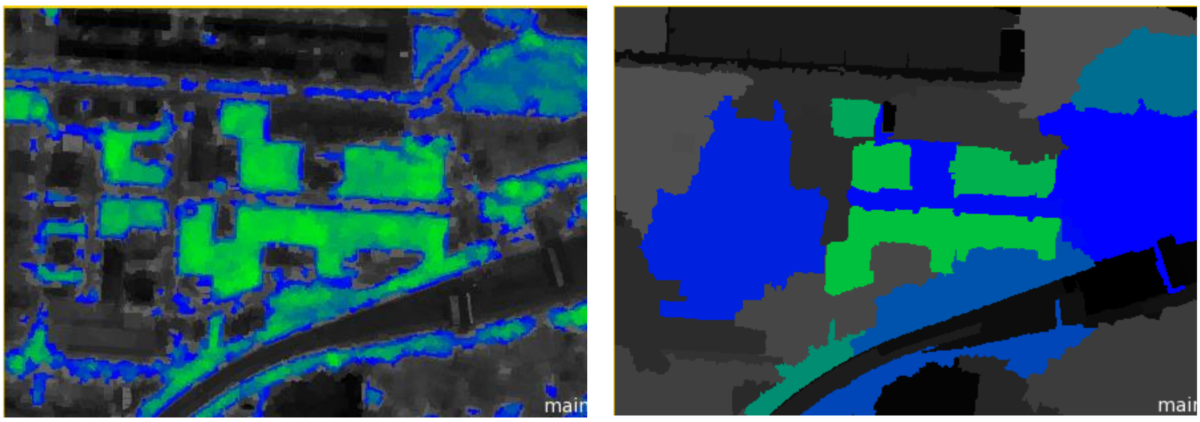

SP = 10 NDVI >0 SP = 300 NDVI >0

High Low Non Veg

Figure 3.9 Different Results in Applying SP in Detecting Vegetation

[7] ESP tool can be found at http://www.ecogntion.com/community.

Regarding the first classification process, we used a threshold from the Normalized Digital Vegetation Index (NDVI) to differentiate vegetation like trees and low plants from built-up areas. Then, we applied a visual brightness threshold to distinguish trees and low plants. We used datasets from Open Street Map (OSM) to define road and water areas especially near the river side. Afterwards, we applied a coarse level segmentation with specific rule set criteria for detected the remaining LCZ class.

During the second level classification, we divided the built-up area into three classes such as open low rise, compact low rise and industry (locally relevant LCZ classes in the study area). We used the GLCM entropy red as an indicator to define the first two built up classes. A study from Kohli et al. (2013) mentioned that the GLCM entropy red was used as a stable parameter to distinct different built-up areas with other classes. Therefore, we assigned different thresholds of GLCM entropy red to define these two classes. After that, we applied visual brightness and extent of the geometry area to define the industrial area. Next, we classified the trees into two different classes such as dense trees and scattered trees.

We developed the classification process using different rule set in eCognition software. In order to test the performance of the rule set, we implemented similar values for the different temporal datasets. During this step, a trial and error process was conducted to find the appropriate threshold values for different land cover classes. The following steps can be seen in Figure 3.10.

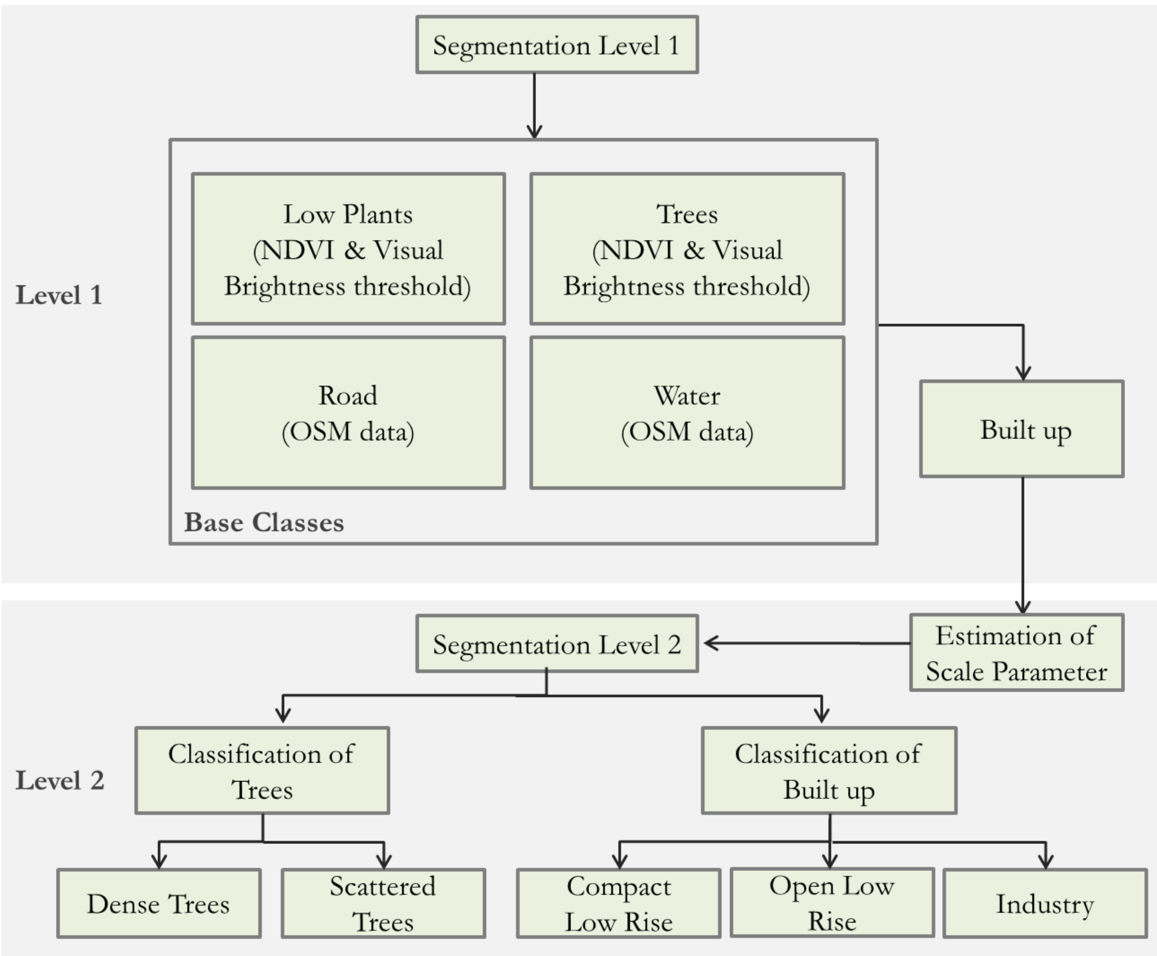

Figure 3.10 Segmentation and Classification Process

3.5.5. Transferability Assesment

In this study, we measure the transferability of the LCZ method across different spatial and temporal locations. Several recent studies focused on the transferability of OBIA methods. For instances, a study by Kohli et al. (2013) discussed the transferability of the OBIA method in detecting slum areas. A study from Belgiu, Drăguţ, and Strobl (2014) also presented the transferability evaluation of using variations of rule set in urban neighbourhood areas. Another study from Tuanmu et al. (2011) mentioned three parameters to measure the transferability of wildlife habitat model. These parameters are spatial transferability, temporal transferability and spatial temporal patterns transferability. The first parameter affirms the result should be of similar accuracy within the same temporal frame. The second parameter emphasize the model should have the same output in different places. Last, the parameter should produce in similar spatial pattern. Moreover, a study by Pratomo, Kuffer, Martinez, and Kohli (2016) mentioned the transferability measurement of rule set development in slum area using both quantitative and qualitative indicators. However, since the emphasis of our research is to analyse the transferability of the LCZ method using VHR imageries in order to see detailed land cover classes in urban areas we only focus on the quantitative measurements comparing the spatial and temporal transferability of LCZ method using VHR images.

For the spatial transferability assessment, we analysed the accuracy results between the first and second test area by looking into its producer accuracy, user accuracy, overall accuracy and kappa statistics for all LCZ classes. For the reference, 130 random points were created and assigned its LCZ class (see figure 3.11). Meanwhile, for the temporal transferability assessment, we measure the accuracy changes between the two images (2013 and 2016). After that, comparison between the results from latest VHR imagery and moderate resolution was done to get insights regarding the implementation of different resolution imagery.

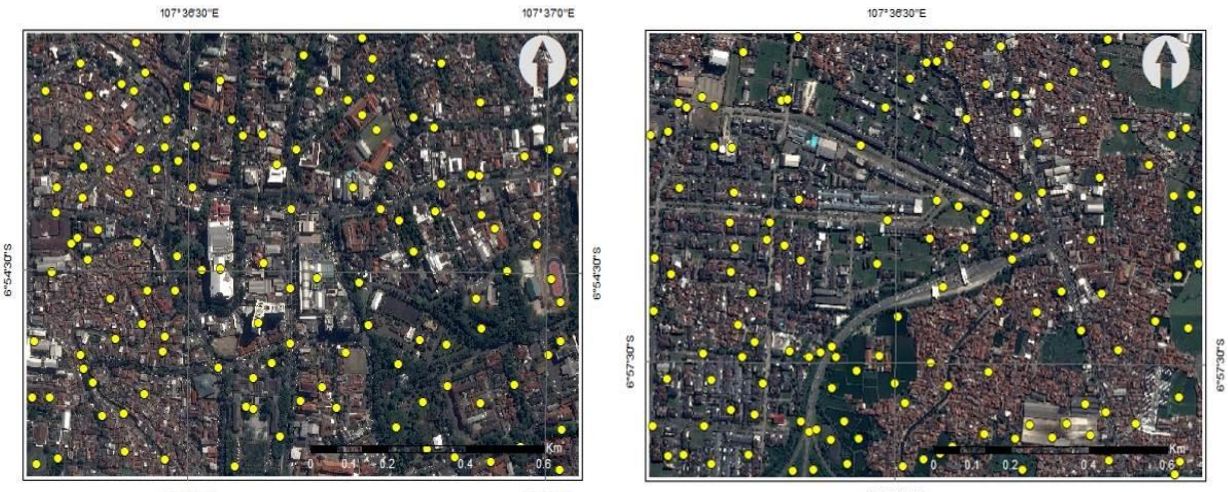

Figure 3.11 Random Points for Confusion Matrix Accuracy Assessment in VHR Image

3.6. Relationships between Land Surface Temperature and Urban Structure Types

As discussed in the conceptual frameworks, we analysed the relationships between land surface temperature and urban structure types to see whether correlation or significance among them exists. We argue there are correlations between the values of land surface temperature and urban structure types. Therefore, we performed two main analyses to define these issues. Details are described in the following sub-sections.

3.6.1. Variations of Land Surface Temperature and Urban Structure Types

Spatial distributions pattern and descriptive statistics analysis from LST and LCZ were conducted in order to find the relationships between their patterns. We performed the analysis overlaying the surface temperature with the VHR images to analyse the spatial patterns of surface temperature at micro scale. We argue that analysing the relationship at micro scale will a give more detailed perspective and knowledge regarding the patterns of surface temperature. We used the sampled points from fieldwork as our reference. Then, LST values were overlaid with each LCZ type for these points. In addition, we applied box plots summarizing for each LCZ the LST values to see their variations Furthermore, the mean LCZ temperatures were evaluated by the analysis of variance (ANOVA). This technique is most commonly-used for comparing means in order to find out whether the means of two or more groups are different. ANOVA also uses F-Test to statistically test the results. Difference between these factors indicates that there is a certain degree of relationships between LCZ and LST.

3.6.2. Composition and Configuration Patterns

For identifying how urban structure types affects the land surface temperature, composition and configuration pattern were explored using the landscape metrics method. The selection of metrics to analyse the relationship between land surface temperature and urban structure pattern were based on previous studies. For example, a study from Connors, Galletti, and Chow (2013) mentioned the use of several metrics like Percentage of Landscape (PLAND), Aggregation Index (AI), and Number of Patches (NP) in assessing the relationships between urban landscape and land surface temperature. Furthermore, another study from Feng and Myint (2016) also used these metrics to explore the effects of neighbouring land cover pattern on LST of central building objects. PLAND were used to represent the composition of urban structure types. PLAND value equals to zero percentage means there is no patch represent a certain type of class, while value equals to one hundred means that on class covers 100% of the areas. Meanwhile, AI and NP were used as parameter to represent the configuration pattern of urban structure types. AI equals to 0% means the landscape is maximally disaggregated, while AI equals to 100% means the landscape is maximally aggregated. High NP means area consists of a many fragmented land cover types, while low NP means area contains of few patches. In this analysis, Urban Structure Types were grouped into three different types which are built-up (compact, open low rise and industry), vegetation (dense, scattered tree and low plants) and water. Each type was converted into a binary raster map. Furthermore, since the value of PLAND, AI and NP varies in different radius, sensitivity analysis was applied to identify the optimal radius of correlation coefficient results. A circular of 30 m radius was chosen to perform this sensitivity analysis in accordance with spatial resolution of Landsat image. These operations were conducted in FRAGSTAT software using moving window tools.

The correlation analysis was performed between land surface temperature and urban structure type based on the percentage cover from PLAND value and configuration value from AI and NP using bivariate correlation in SPSS. Pearson correlation coefficients were analyzed to define significant relationships between composition and configuration pattern and land surface temperature value. Finally, a simple linear regression method was generated to explore the relationship between land surface temperature and the composition and configuration pattern of urban structure type.

4. RESULTS AND DISCUSSION

This chapter describes and discusses the results of this study. It starts with the extraction of the land surface temperature and its spatial pattern. Secondly, the implementation of the LCZ method is discussed assessing its accuracy and its thermal pattern characteristics. Next, transferability result using OBIA approach in VHR images is described. In the last part, the relationships between land surface temperature and urban structure pattern are explained using descriptive statistics and spatial metrics.

4.1. Local Charateristics of Land Surface Temperature

4.1.1. Land Surface Temperature Trend

In this section, the land surface temperature patterns in Bandung from 2005-2016 are analysed (see table 4.1). Overall, the minimum temperature was found in the range of 13 – 22°C while, the maximum temperature was recorded in the range of 35-42°C. In addition, the mean temperature was seen at around 26-31°C. The lowest value for minimum, maximum and mean can be found in the year of 2005 where the minimum, maximum and mean was recorded at 13°, 35° and 28° Celsius respectively. Meanwhile, the highest value for the minimum temperature occurred in 2009 and 2015 (21°C), and the highest value of maximum and mean temperature occurred in 2013 (42° and 31°C).

Table 4.1 Land Surface Temperature 2005-2016

Year	Land Surface Temperature (in °C)			
	Min	**Max**	**Mean**	**Range**
2005	13.31	35.25	28.26	21,94
2007	14.25	37.22	29.27	22,97
2008	17.47	34.46	26.39	16,99
2009	21.06	38.38	30.82	17,32
2013	14.97	42.28	31.32	27,31
2014	20.11	37.51	30.51	17,40
2015	21.34	36.02	29.28	14,68
2016	17.41	36.84	28.41	19,43

In addition to the overall trend, the range difference between minimum and maximum temperature was calculated to be around 15 – 23 °C. The lowest intensity occurred in 2015 with 15°C, whereas the highest intensity was found in 2007 with 23°C. Moreover, the average difference between minimum and maximum temperature during this last decade was ± 20°C.

The highest range value between maximum and minimum happened during the year 2013 (27°C). Meanwhile, the lowest value occurred in the year of 2008 (17°C). This striking difference can be influenced by variations in the intensity of solar radiation during that time or other factors such as cloud cover or water vapour.

It can be concluded that the land surface temperature trend in Bandung city tends to slightly increased between the years 2005 and 2009. However, this trend slightly changed showing lower values between 2013 until now. Despite the slight decrease in 2008, the overall trend of surface temperature shows an increasing trend.

As shown in figure 4.1, the mean surface temperature values had a fluctuate trend between 2005 and 2016. There were ups and downs in the mean temperature values from 2005 until 2009, with slight an increase from 28°C until 30°C despite of the slight decrease in 2008. Meanwhile, after year of 2013 the trend seems to be slightly decreased from 31°C to 28°C in 2016.

Figure 4.1 Mean Land Surface Temperatures

The spatial patterns of land surface temperature in Bandung from 2005 – 2016 are shown in Figure 4.2. Equal interval method was used to classify the temperature datasets. This is applied to emphasize the relative amount of attribute values compare to the other values. Therefore, it divides the range of attributes value into equal-sized range. For example, areas with the same colour on the maps showed the same range of temperature.

As presented in Figure 4.2, it can be seen that the spatial patterns of land surface temperature in the recent decades seems to have a similar patterns. The hotspots areas are mainly located in the central and western part of the city, while the cold spots tend to be found in the eastern part of the city. Furthermore, it shows different variations for each year in terms of highest and lowest temperatures among those areas. For example, the locations of areas with the highest temperature tend to be unstable while the areas with lowest temperature are relatively more stable.

A quite different spatial pattern of temperature can be seen in the year of 2013. In this year, the maximum range of temperature between 40-45°C (dark red colour) occurred in the south western part and some areas in the north part of the city. Meanwhile, the minimum range of temperature as shown in light red colour (10-15°C) was found in the north eastern and south eastern part of the city. Hence, both the maximum and minimum range of the temperature was seen only in this year.

The difference between each year LST maps can be affected by various factors such as the weather condition from different days, speed and direction of the wind when satellite captures the image. Other sources from human activities e.g., energy consumption from buildings and transportation can be also influenced to the LST result. However, the most important factors to be considered are the existing of UST where each location consists of different types of building, vegetation and other types.

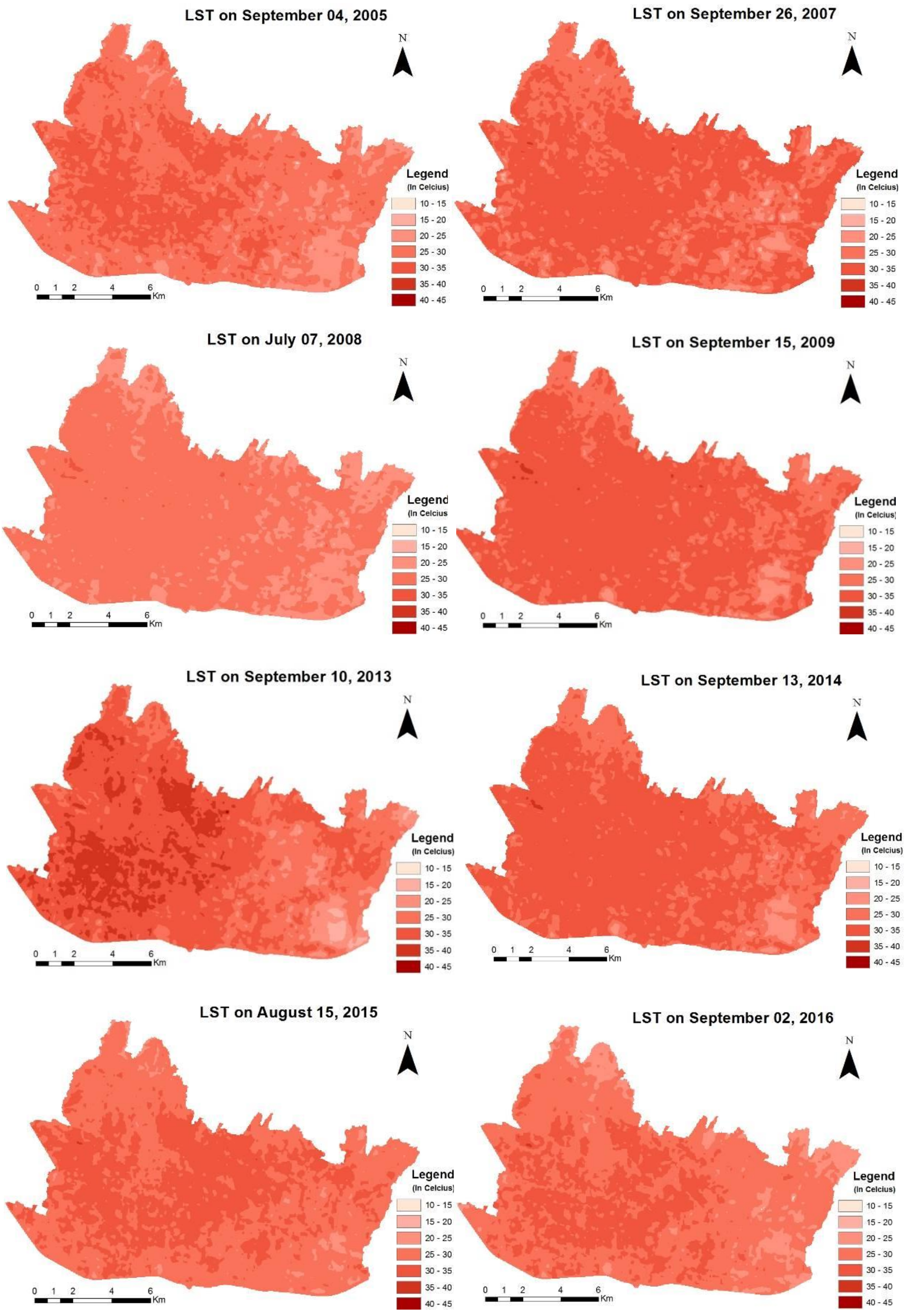

Figure 4.2 Land Surface Temperatures from 2005 to 2016

4.1.2. Land Surface Temperature Patterns

In this sub chapter, the land surface temperature pattern in Bandung from 2005-2016 are analysed. In general, from figure 4.3, it can be observed the hot areas are mainly located in the central, west and southwest part of the city. Meanwhile, the cold areas (areas with consistent lower temperature values) are mostly located in the northwest, northeast and southeast part of the city. The moderate areas mostly occurred in an intermediate zone between hot and cold areas. In addition, this type is mostly concentrated in the northwest of the city.

.

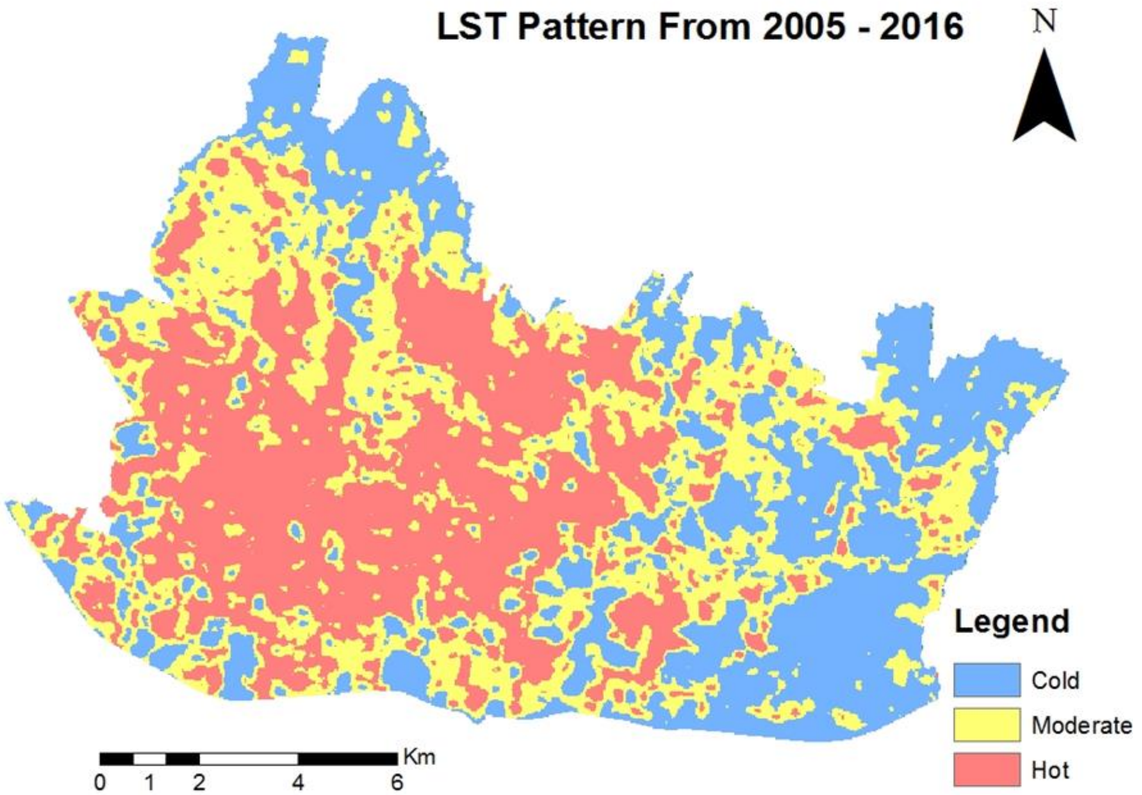

Figure 4.3 LST Patterns in Bandung 2005 - 2016

From the proportion of total area as shown in table 4.2, 37% (62 km²) of total area is covered by the hot temperature area. The hot area performs as the largest area among the three classes. Meanwhile, 33% (56 km²) of area is covered by moderate temperature areas. The cold class area appears to be the smallest area among the three classes with only 30% (51 km²) of the total area. To sum up, there is no significant difference in the total amount of area between each temperature class in Bandung city. This means the temperature patterns in city of Bandung tends to be uniformly distributed across the region.

Although anomaly or quite different land surface temperature pattern appears from 2005 until 2016, the result can be used as an overview for investigating the local characteristics of surface temperature in the study area. All in all, this evidence clearly indicates that the pattern of land surface temperature in Bandung can be well recognized by its geographic locations where hot temperature areas are located mostly in city centre while low temperature areas occurred close to urban fringe in the southeast part of the city.

Table 4.2 LST Pattern Characteristics from 2005 -2016

Temperature Class	**Total Area (in km²)**	**Proportion of Total Area (%)**
Cold	50.75	30
Moderate	55.69	33
Hot	61.98	37
Total	168.42	100

4.2. Implementation of LCZ

To implement the LZC method, we applied a transformation procedure from its concept into the image domain perspective. Thus, visual interpretation from real world characteristics is needed to get the characteristics of each LCZ classes before doing image classification. We started this subchapter by describing the existing of LCZ classes in the study area. After that, we present the LCZ classification results. Later on, we discuss the findings from thermal measurement which reflect on each LCZ Classes.

4.2.1. Spatial Pattern of Local Climate Zone

Based on the ground observation results of LCZ classes during fieldwork and visual interpretation from both images, we found only 9 different LCZ classes in Bandung. These classes are Compact High Rise (LCZ 1), Compact Low Rise (LCZ 3), Open Low Rise (LCZ 6), Heavy Industry (LCZ 10), Dense Trees (LCZ A), Scattered Trees (LCZ B), Low Plants (LCZ D), Road/Paved (LCZ E) and Water (LCZ G). However, due to lack of height information to differentiate Compact High Rise (LCZ1) from Compact Low Rise (LCZ3) in Landsat imagery, we used only 8 LCZ Classes for image classification process. The result of these observations can be seen in figure 4.4 and 4.5. For built-up types, the locally relevant of LCZs in the study area can be identified into three different classes e.g., Compact Low Rise, Open Low Rise and Industry. Meanwhile, for the land cover types, the locally relevant of LCZs can be found into several classes e.g., Dense Trees, Scattered Trees, Road, Low Plants and Water. Furthermore, results of LCZ classification for the entire city are presented in figure 4.6 and 4.7.

In general, it can be seen that the spatial pattern of LCZ classes in Bandung are mostly dominated by built-up types. Meanwhile, land cover types like vegetation occurred only in several part of the city. Similar results are also found for others types such as roads and water bodies which appeared only in a small part of the city.

Within the class of built-up types, we found that compact low rise mostly appears compare to other types. For example, compact low rise largely dominates the built-up area (shown in red colour in Fig. 4.6 and 4.7). Meanwhile, open low rise occurs scattered in the south, east and north-west part of the city. Moreover, industrial area as shown in grey colour can be found only in the south west and north east. For the land cover types, it is shown that vegetation areas with dense trees, scattered trees and low plants are more common compare to non-vegetation areas like road and water. Low plants can be found in the south east of the city. Meanwhile, dense and scattered trees occur in the north east and north west of the city. Both tree types are located closely to each other. Furthermore, paved/road areas exist along the area. It has a circular pattern connecting one area to another area. However, a different pattern is shown for the water class. A small number of water areas can be only found in the southern part of the city (shown in blue colour).

a. Compact Low Rise (LCZ 3)

b. Open Low Rise (LCZ 6)

c. Heavy Industry (LCZ 10)

Source: Landsat image (left); Fieldwork observation (centre); Pleiades image (right)

Figure 4.4 LCZ Built-up Types Ground Condition

a. Dense Trees (LCZ A)

b. Low Plants (LCZ D)

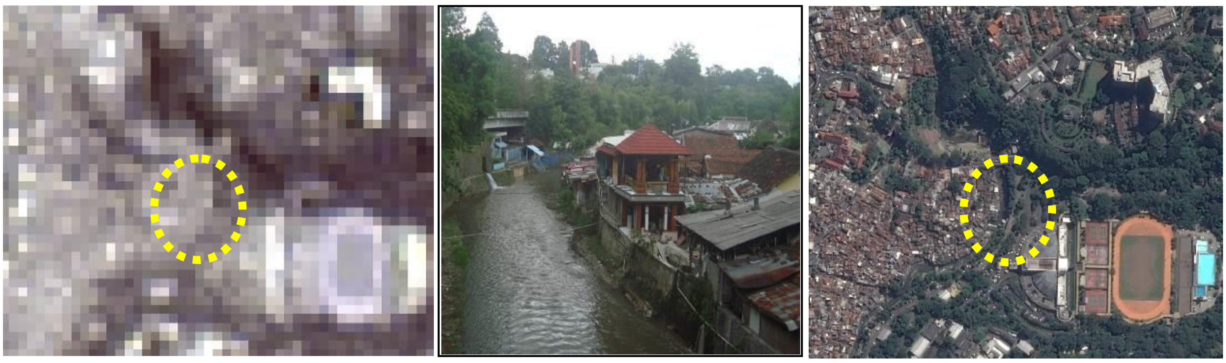

c. Water / River (LCZ G)

Source: Landsat image (left); Fieldwork observation (centre); Pleiades image (right)

Figure 4.5 Land Cover Types Ground Condition

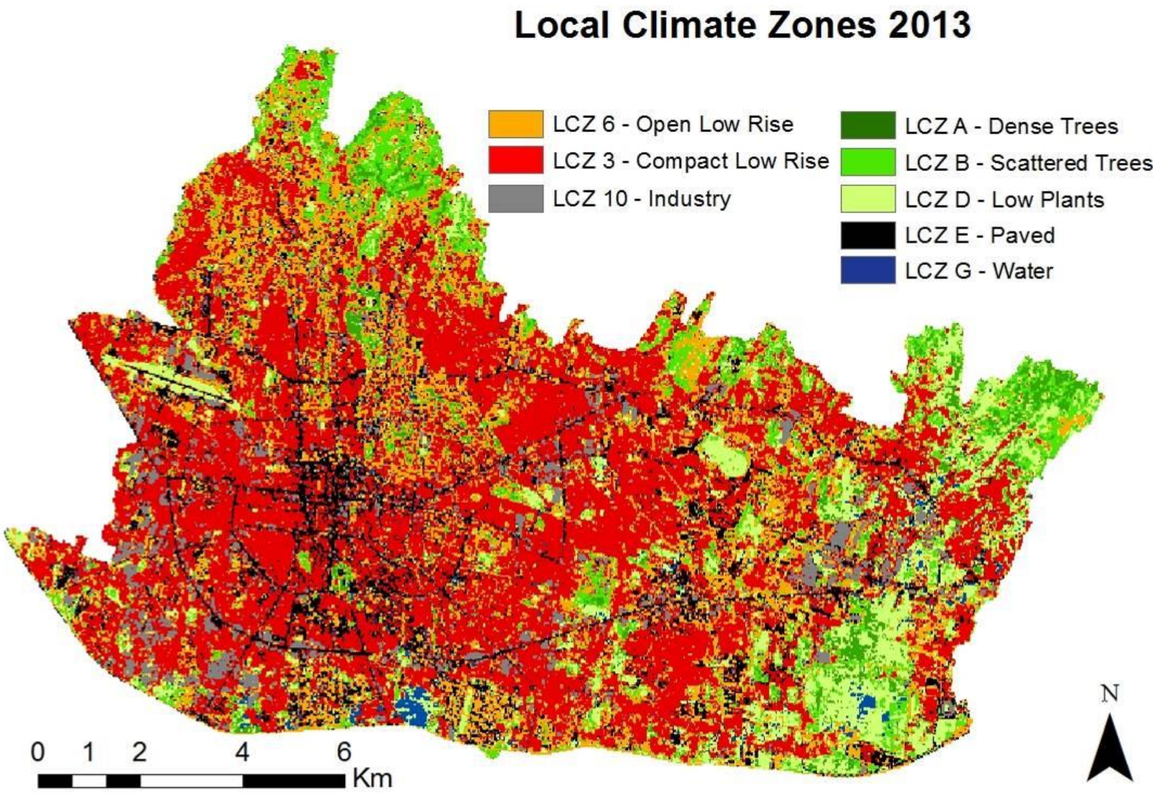

Figure 4.6 LCZ Maps 2013

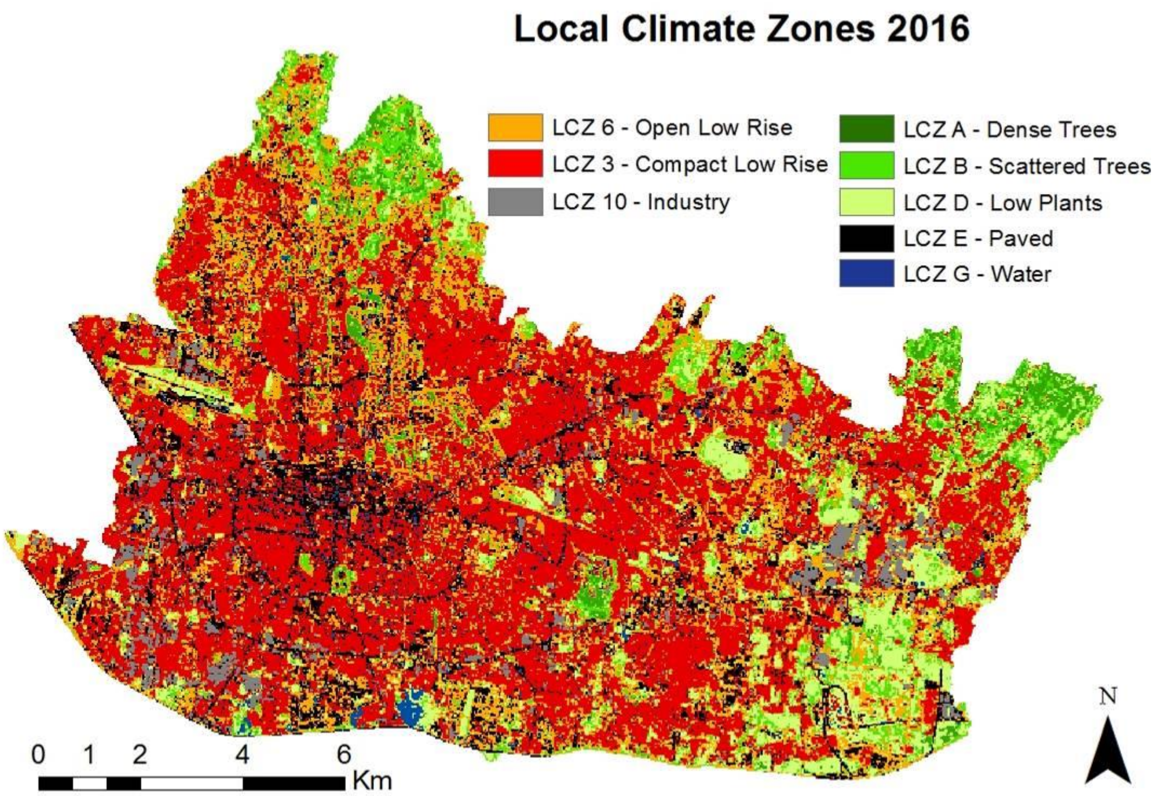

Figure 4.7 LCZ Maps 2016

As mentioned in sub chapter 3.4.4, to extract the spatial pattern of LCZ in the study area, we tested the LCZ approach into two different temporal Landsat images. As a result, the LCZ spatial pattern in Bandung city shows a different number in its total area coverage (km²) or the proportion of total area (%) between these periods of time (see table 4.3). For the built up types, the open low rise area shows a relatively stable trend among the others built up types. The overall proportion of total area ranged from 20-21%, or approximately around 35 km². However, a different trend is shown by compact low rise areas, it increased from the total of 72 km² (42%) in 2013 to almost 75 km² (44%) in 2016(an increase by 2 %). I Industrial areas decreased suddenly from 9.7 km² (9%) in 2013 into 7.2 km² (7%) in 2016. For the land cover types, in the vegetation area, dense trees shows a stable trend between the two years with around 5 km² (3%). Meanwhile, scattered trees decreased slightly from 13 km² (8%) in 2013 to 12 km² (7%) in 2016. However, a significant change occurred in low plants area which decreased from 17 km² in 2013 to 14 km² in 2016, or decreased by almost 3%. In addition, the two remaining classes present a difference results. For instance, paved/road class increased significantly between these two year periods from 15 km² in 2013 to 19 km² in 2016, or increased by almost 2%. On the other hand, water area shows a decreasing trend from almost 4 km² (2%) in 2013 to 2 km² (1%) in 2016. Thus, water area has lowest share among all LCZs classes with just only one percentage in its total area. To sum up, the spatial patterns of LCZs in Bandung are mostly dominated by the compact low rise type in its built up types while the land cover types are dominated by three main types: low plants, dense and scattered trees.

.

Table 4.3 Land Cover Trend of LCZ Classes in Bandung

LCZ Class	**Area (in km²)**		**Proportion of Total Area(%)**	
	2013	**2016**	**2013**	**2016**
LCZ 3 - Compact Low Rise	71,98	74,48	42,74	44,22
LCZ 6 - Open Low Rise	33,34	34,78	19,79	20,65
LCZ 10 - Industry	9,24	7,24	5,49	4,30
LCZ A - Dense Trees	5,35	5,38	3,18	3,19
LCZ B - Scattered Trees	13,13	12,36	7,80	7,15
LCZ D - Low Plants	16,95	13,92	10,06	8,45
LCZ E - Paved	15,06	18,24	8,94	10,83
LCZ G - Water	3,38	2,02	2,01	1,20
Total	168,43	168,42	100,00	100,00

The accuracy assessment report of the LCZ approach for Bandung can be seen in fig. 4.8. In general, the overall accuracy of LCZ classification between 2013 and 2016 resulted in the range of 66% - 69%, while Kappa statistics had a range of 0.61-0.66 (see Appendix 5). In 2013, the lowest accuracy was found in the open low rise class. Both user and producer accuracy resulted with 41% and 42%. Water tends to have the highest difference between user and producer accuracy (40%). On the other hand, the highest accuracy can be seen in heavy industry with 80% both in user and producer accuracy. A similar result was also obtained in 2016, the lowest accuracy was found in open low rise. It is shown that both user and producer accuracy resulted with 42% and 43%. Meanwhile, heavy industry still had the highest accuracy for both user and producer accuracy with 91% (and increased by 10%). Other types are relatively stable. Moreover, with the coarse spatial resolution of Landsat TM, it was difficult to distinguish the quite large areas with heterogeneous mix of LCZ types. The reflectance of various types such as open low rise, paved/road and scattered tree has been very close. Thus, the number of correctly classified between these classes became lower compare to other classes. Furthermore, this result also happened due to the spectral variability within each class in the selected training samples.

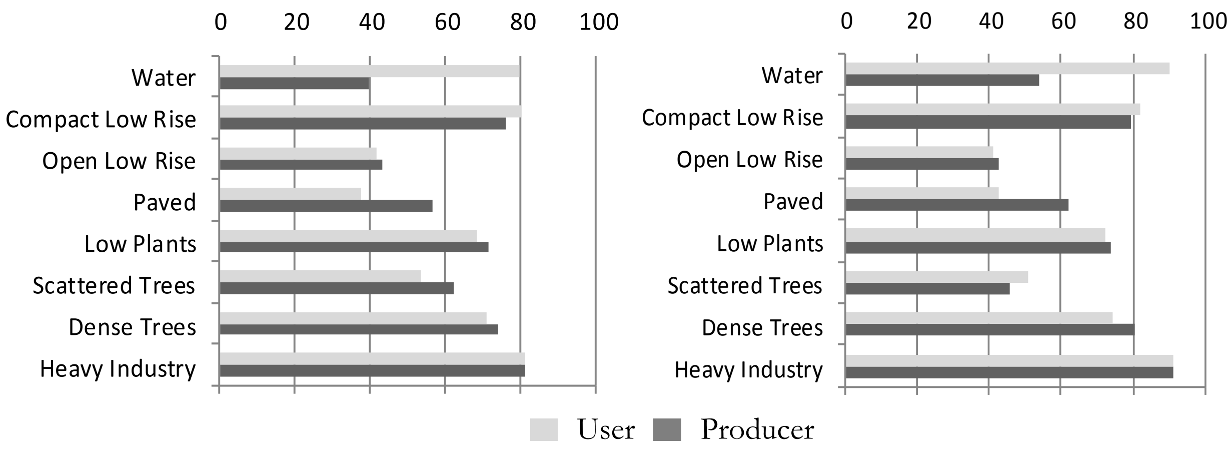

a. 2013 b. 2016

Figure 4.8 Accuracy Assessment Using Moderate Resolution Image

4.2.2. Thermal Patterns of Local Climate Zone

From the previous change detection analysis, we selected several areas of interest to verify the surface temperature in the case study area. The selected areas were chosen as representatives of change detection consisting of three different categories namely hot area, cold area and unstable area. Figure 4.9 presents these areas.

Based on surface temperature detection, several thermal points were chosen randomly with discrete uniform distribution method where a finite number of classes are likely to be observed. This consideration was taken since the LCZ classes within the study area were not equally distributed. For example, in one area of interest, the area consists of industry and vegetation therefore the distribution of thermal points was only chosen within these existing classes. Thus, the thermal points of the each class are not equally similar.

During fieldwork in October, 2016 the weather conditions in Bandung were mostly rainy. Heavy rain and storm happened in most of the region. Solar radiation is known as one of the important factors in analyzing the behaviour of surface temperature. During rainy days, temperature tends to become closer to minimum value. Thus, taking measurements at this time can create noisy results. Therefore, we only collected the thermal measurement when the day was sunny to get stable temperature data.

Figure 4.10 shows the distribution of thermal points in this research. During the thermal measurements, we have obtained 45 thermal points from different LCZ classes. From this result, it can be seen that the LCZ classes of compact high rise, compact low rise and heavy industry have higher temperatures compare to the other types such as dense trees, scattered trees and low plants. For example, we found that during October the minimum surface and air temperature was recorded with around 19° Celsius in an area of low plants type in the morning. In addition, the maximum temperature was found in an area of compact high rise with 24° Celsius.

However, during daylight the behaviour of temperature pattern has shown a significant change. In paved areas, the temperature increased in the range of 12-15°C compare to the morning measurement. This situation might be occurred due to characteristics of paved area. For example, paved areas are mostly located in an open area. In an open area, energy from the sun is directly received and stored into the ground. In addition, paved areas are commonly made from asphalt and concrete surface which are easy to absorb sun's energy. Therefore, temperature in paved became high. Meanwhile, in areas of compact high rise and compact low rise, the energy from the sun tends to be reflected back into space by their rooftop material. Hence, the temperature in this class is slightly lower with an increase around 8-12°C.

We also found during night time that the temperature in areas of vegetation and low plants tend to significantly decrease, because most of the energy has been freely released into the air during this time. The decrease particular happened in areas which are not surrounded by buildings. On the contrary, areas with compact buildings had a low decrease on their surface temperature. This might be happened because most of the energy in this area was still being trapped in the air. The results from the thermal point measurements are presented in Appendix 6.

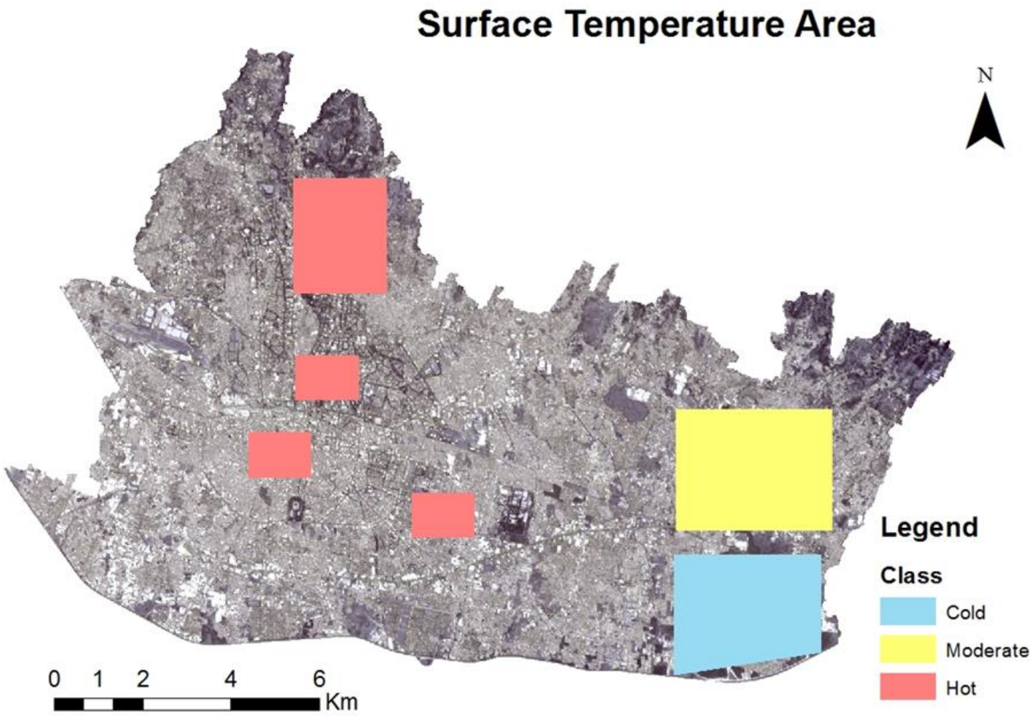

Figure 4.9 Surface Temperature Detection Areas

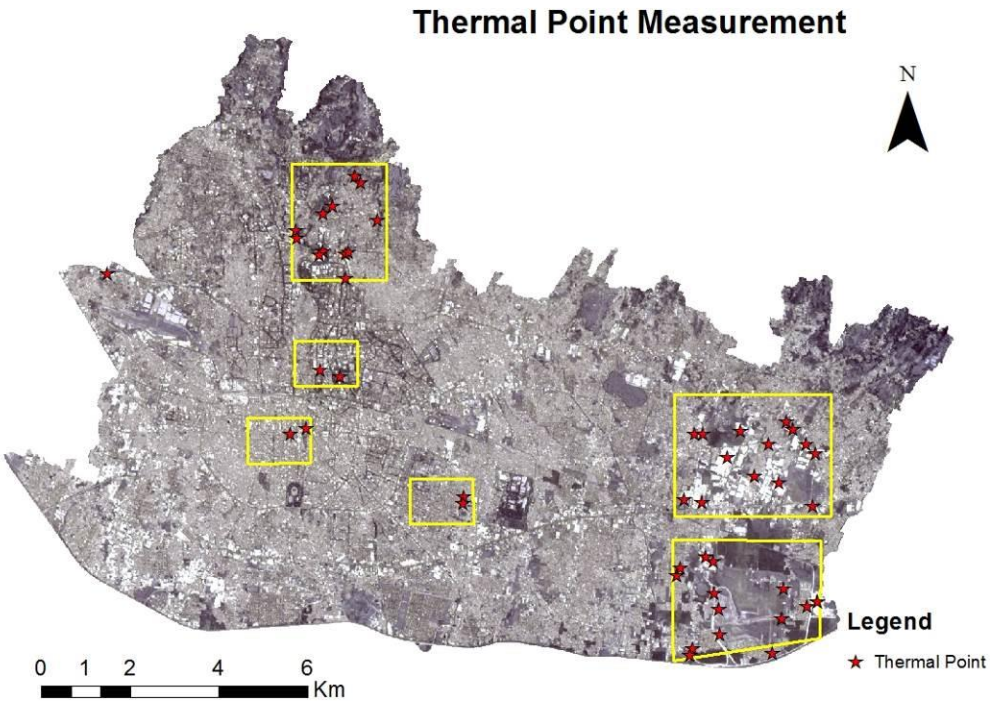

Figure 4.10 Thermal Point Measurements Taken During Field Work

The results of thermal measurements can be seen in the figure 4.11, 4.12 and 4.13. For the first area, we selected the area around Gedebage region. This area has been classified as a cold area. In this area, mixing types of LCZs has been found like heavy industry, open low rise, compact low rise and paved area. According to the visual image from figure 4.11, overall the selected area consists of more than half of low plants cover. This area is located in the north, centre and south part of the selected area (TA7). Meanwhile, built up types such as compact low rise tends to concentrate only in the east and west part (TA 14). The open low rise can be found in the south east of the area (TA9). Only small areas of other built-up types like industry can be found (TA3) in this area.

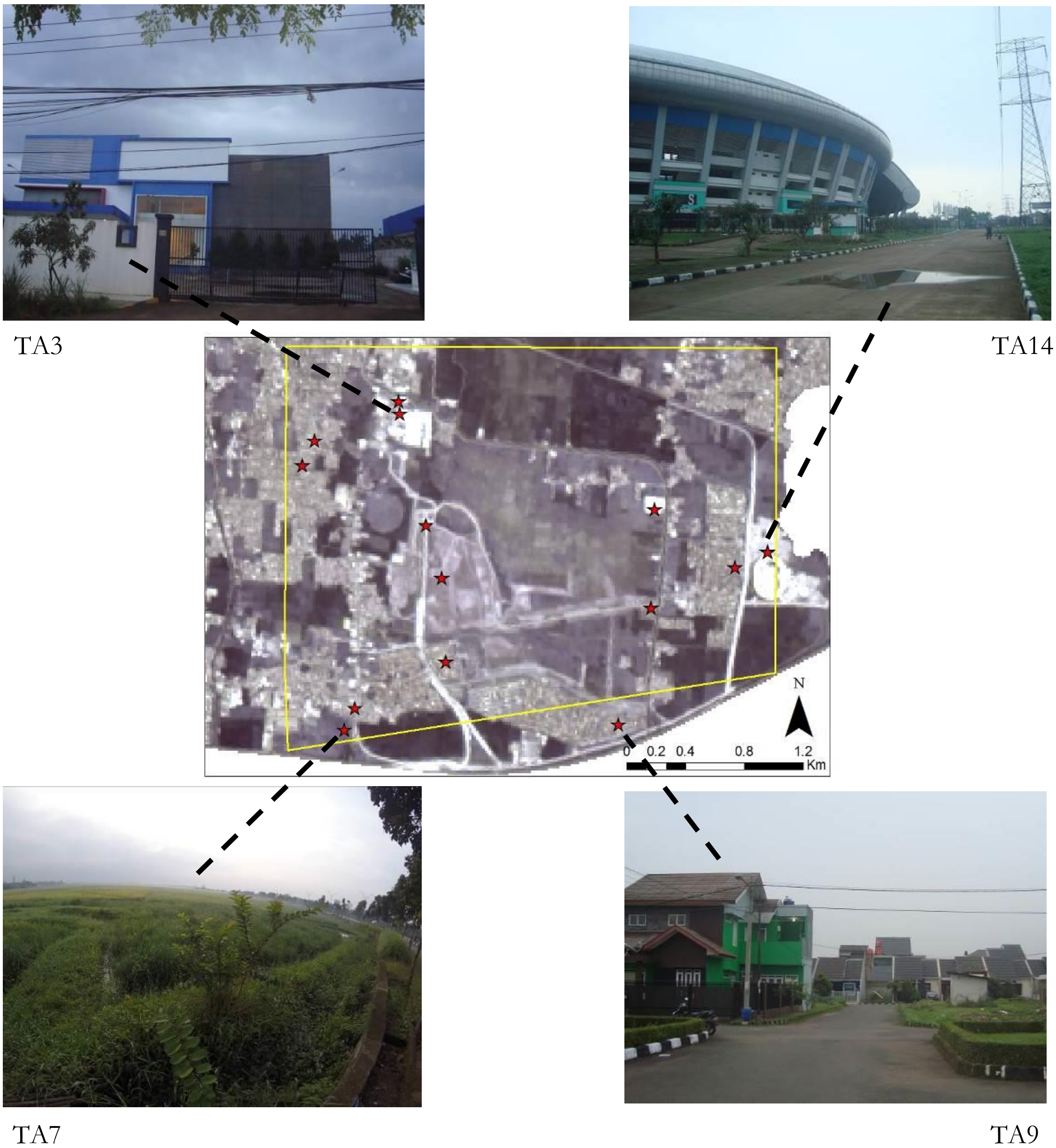

Figure 4.11 Thermal Measurements in Gedebage Area

For the second area of interest, we selected an area around North Gedebage and Panyilukan region as moderate area. In this region the LCZ classes consisted mainly of heavy industry. It can be seen from figure 4.12, where almost half of the area contains industrial buildings from small industry (TB6) into heavy industry (TB5). Another type recorded was compact low rise in the east and west part of the selected area. Low plants (TB9) also appeared in a northwest and southeast of the area, located near the industrial area (TB6).

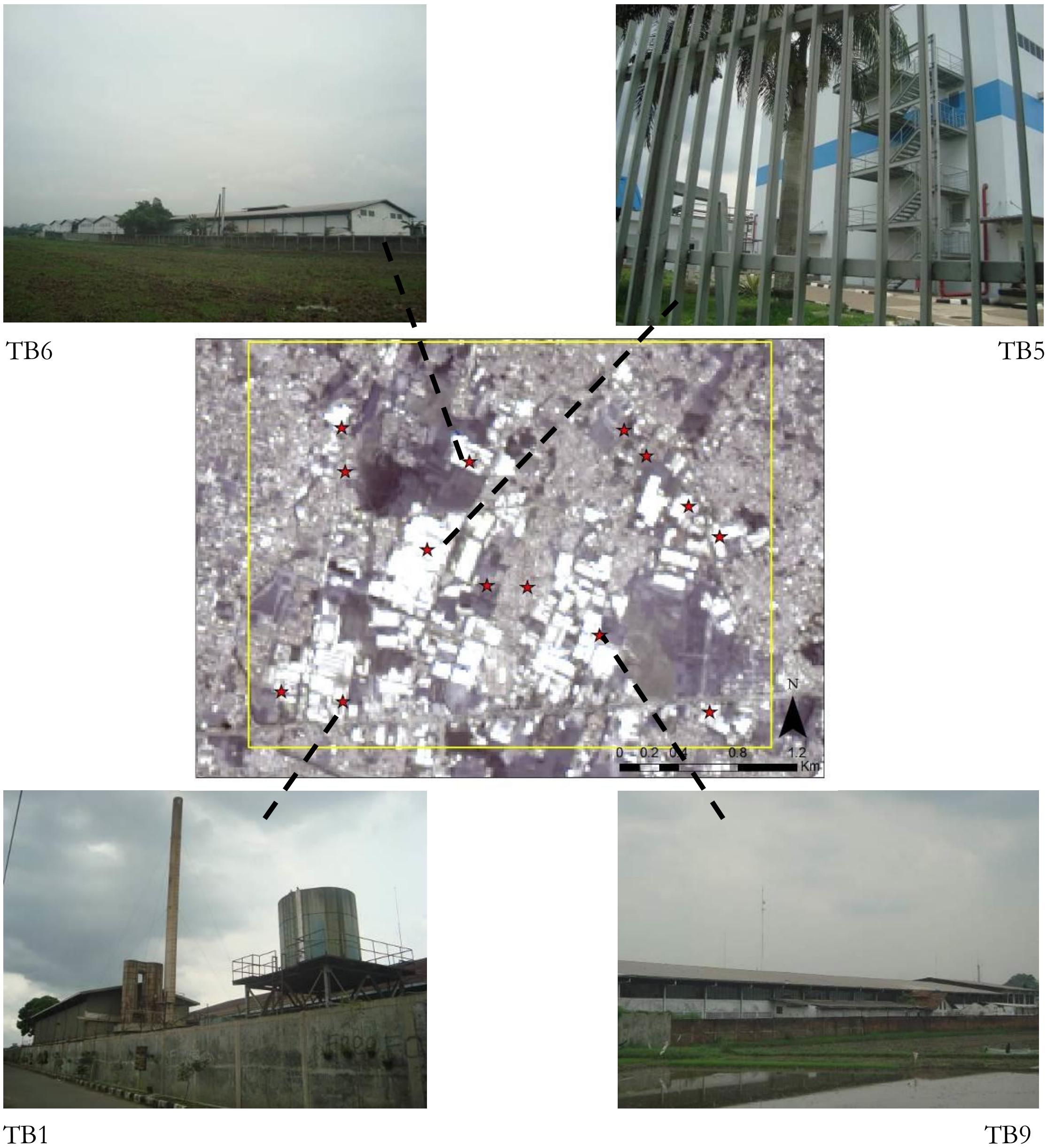

Figure 4.12 Thermal Measurements in North Gedebage and Panyilukan Region

For the last selected area, we choose an area around Dago region as a hot area where the temperature increased during the years. This area is known as one of the crowded areas during weekdays due to existence of public spaces like offices, public shopping, hospitals, universities and other public amenities. In addition, the characteristics of LCZ types within this area consisted of mixed use building types, dense trees, and scattered trees. From figure 4.13, it is shown that there are a lot of compact high rise buildings (TC1) and compact low rise (TC11). Although, this area contains a mixed use of building types also vegetation is present such as scattered trees (TC7). Based on visual image interpretation, the built-up tends dominate this area while vegetation only appears in the north part of the area. In the city centre, the areas mostly are covered by built-up types with less vegetation cover.

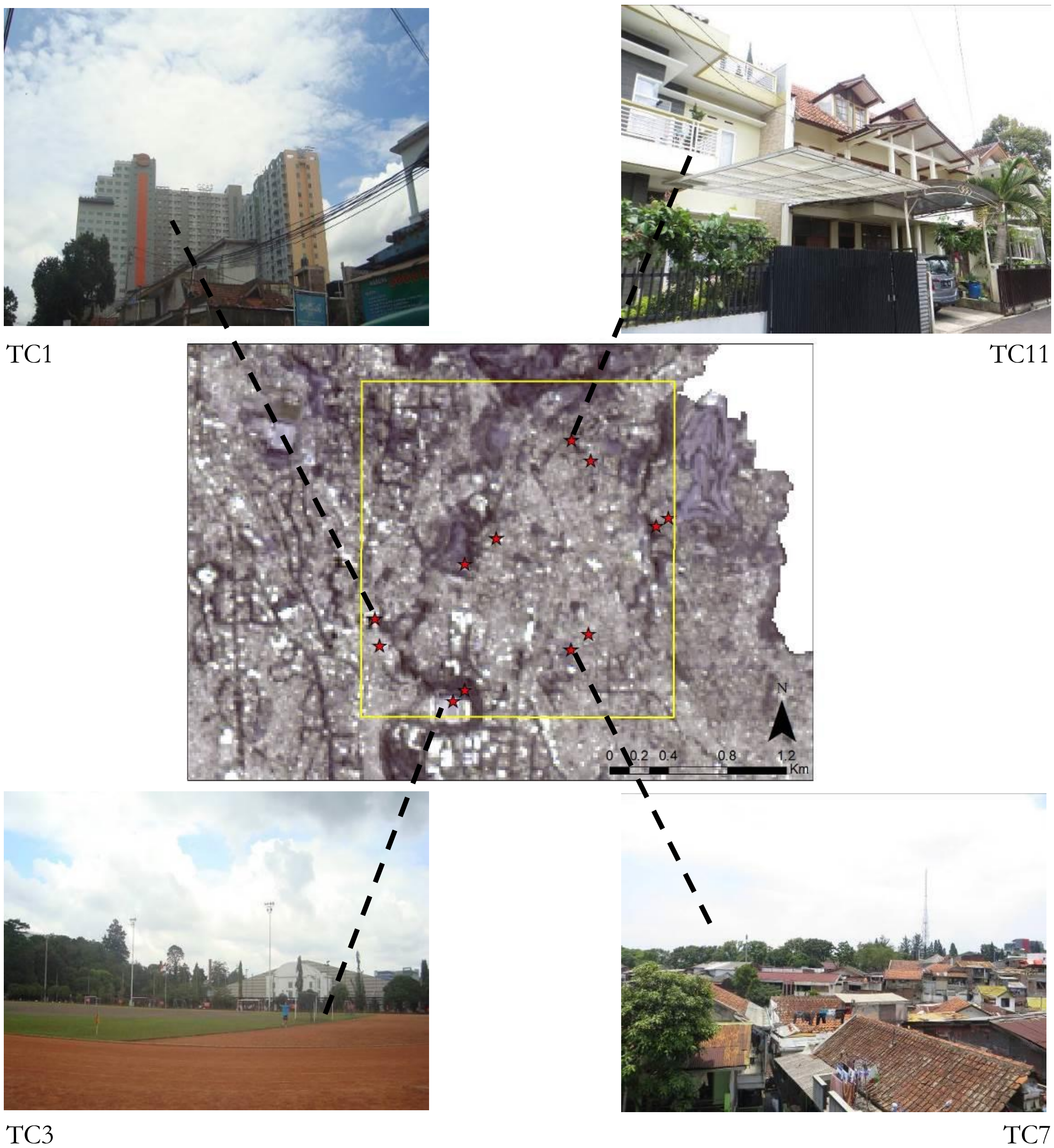

Figure 4.13 Thermal Measurements in Dago Region

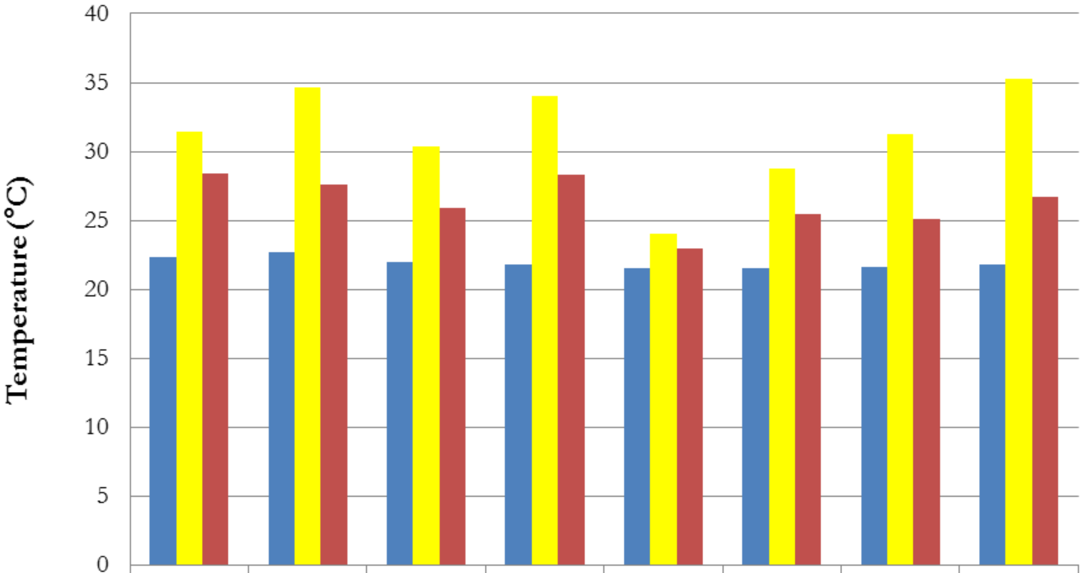

	Compact High Rise	Compact Low Rise	Open Low Rise	Industry	Dense Trees	Scattered Trees	Low Plants	Paved
Morning	22.3	22.7	22	21.8	21.5	21.5	21.6	21.8
Daylight	31.4	34.6	30.4	34	24	28.8	31.3	35.3
Night	28.4	27.6	25.9	28.3	23	25.5	25.1	26.7

Figure 4.14 Result from Average Thermal Temperature Taken During Field Work

Figure 4.14 shows the average of the thermal point measurements at three different times (taken during field work) for all LCZ classes. In general, it can be observed that the average mean temperature shows a similar pattern between the LCZ classes, where the average temperature increased between morning and daylight time. Meanwhile, the average temperature decrease after daylight time. The lowest average thermal value occurred in the morning time, while the highest average is captured during daylight time.

In the morning time, the highest average temperature occurred in the built up classes. For instance, compact low rise had a temperature value of 22.7°C, while the other two classes (open low and compact high rise) had value between 22 - 22.3°C. On the other hand, the lowest temperature can be found in the vegetation classes such as dense trees and scattered trees where both had temperature value of 21.5°C.

During the daylight time, the highest average temperature is found in the paved area with temperature value of 35.3°C. In addition, the second largest temperature occurred in the compact low rise with a temperature value of 34.6°C. On the contrary, the lowest average temperature is captured in areas of dense trees area with a temperature value of 24°C.

In the night time, the highest average temperature found in two different classes which are compact high rise and industry with almost 28.4°C. Meanwhile, the lowest average temperature occurred in areas of dense tree class with 23°C. The other classes such low plants, scattered trees and open low rise had temperature range value between 25 -26°C.

Based on the results of the average temperature from the thermal measurements, it can be seen that there has been a significant change between morning and daylight time. For example, in paved and compact low rise, an increase of almost 13-14°C occurred. However, only the dense trees class shows stability throughout the day with a range of less than 3°C. This means that dense vegetation coverage especially trees tend to reduce the heat effect, while other land cover types with non-vegetation coverage tends to absorb heat radiation.

To identify whether the values of surface temperature from thermal measurement can also reflect the values of air temperature measurement, we compared both datasets. In addition, the correlation between surface temperature and air temperature were assessed to understand certain correlation between surface and air temperature. The findings can be used as an indication about the relationships between surface and air temperature.

Table 4.4 Correlation of Surface Temperature and Air Temperature

		Surface Morning	Air Morning
Surface Morning	Pearson Correlation	1	,241
	Sig. (2-tailed)		,107
	N	46	46
Air Morning	Pearson Correlation	,241	1
	Sig. (2-tailed)	,107	
	N	46	46

		Surface Daylight	Air Daylight
Surface Daylight	Pearson Correlation	1	,464**
	Sig. (2-tailed)		,001
	N	46	46
Air Daylight	Pearson Correlation	,464**	1
	Sig. (2-tailed)	,001	
	N	46	46

**. Correlation is significant at the 0.01 level (2-tailed).

		Surface Evening	Air Evening
Surface Evening	Pearson Correlation	1	,486**
	Sig. (2-tailed)		,001
	N	46	46
Air Evening	Pearson Correlation	,486**	1
	Sig. (2-tailed)	,001	
	N	46	46

**. Correlation is significant at the 0.01 level (2-tailed).

From table 4.4, it can be seen that the temperature measurements for both surface and air temperature during daylight and evening time are positively correlated. However, the air temperature and surface temperature in the morning has a very low correlation. Furthermore, based on the results shown in Appendix 6, it can be observed that during daylight and night time the land surface temperature are consistently higher compared to the air temperature. In fact, during fieldwork, we found out that the air and surface temperature patterns from each LCZ classes tend to be similar. For instance, when air temperature slightly increased during daylight time, the same conditions also happened for the land surface temperature. On the other hand, when the air temperature suddenly decreased during night time, the surface temperature also showed similar results. Thus, as indicated by the statistics in table 4.3, there is a positive correlation between air and surface temperature.

Interpretation of the results discussed above only present pragmatically findings since measurements were not taken continuously. Further investigations especially with hourly real time ground air temperature measurement data would be precisely accurate for answering the relation between air and surface temperature patterns. All in all, these results showed that the surface temperature pattern reach its highest value during daylight time when the sun is located vertically above the ground.

4.3. Transferability Implementation Results

4.3.1. Rule-set Development

In order to map Urban Structure Types (UST) represented by LCZ classes in VHR imageries, we built up a rule set in eCognition software to transform the real world features into image domain features. As mentioned in sub chapter 2.3, to transform the LCZ approach from real world features into image domain features, we had to define the specific characteristics specifically when it applied in VHR imagery like texture, shape and geometry. Subsequently, we found that some characteristics are difficult to obtain from the image. Therefore, we employed additional datasets from Open Street Map (OSM) which was very helpful to acquire the road and water class.

Additionally, we also found that most built-up areas in Bandung consists of two types of buildings e.g., compact and open low rise. These types of buildings can be recognized by its roof materials, footprint, size and shape. Thus, image texture helped to separate both classes. For the vegetation land cover class, the NDVI value was used to distinguish several classes of vegetation. Hence, our rule set was able to produce several land cover classes based on the LCZ approach. In table 4.5, the conceptualisation process from real word features into image domain feature for VHR image are shown

.

Table 4.5 Real World Features Into Image Domain Feature in VHR Image

LCZ Class	Real World Features	Image Domain Features
Compact Low Rise	Dense buildings, no trees, mostly paved	Texture : GLCM Entropy Red High
Open Low Rise	Open arrangement buildings, abundance of pervious land cover	Texture : GLCM Entropy Red Low
Industry	Industrial building structures	Texture : GLCM Entropy High, Shape : Regular, Visual Brightness High
Dense Trees	Heavily wooded landscape	NDVI High, Geometry : Area larger
Scattered Trees	Lightly wooded landscape	NDVI High, Geometry : Area smaller
Low Plants	Grass, plants/crops, no trees	NDVI Low, Texture : GLCM Entropy Red Low, Visual Brightness Low
Road	Paved cover	Shape : Regular
Water	Lakes, rivers, or reservoirs	NIR Low, Texture : GLCM entropy blue low

During the transferability implementation process from the VHR image, we used a personal computer with 4 GB of RAM and 2.3 GHz System Processor. We are aware that this computer specification is not performed for a high computation process especially under time constraints. Therefore, we selected a small area of image for testing the approach. We selected a subset of two square kilometres which contains all LCZ classes. Then, we tested the rule set for two different locations and two different years (2013 and 2016).

4.3.2. Segmentation and Classification

As discussed in the previous chapter, we apply two levels of segmentation. The first level is to select the base class, where the second level was used to separate trees and building types. The results for both segmentation and classification are discussed below.

A. Level 1 Phase

In this phase, we extracted the four main land cover classes: Trees, Road, Water, and Low Plants. Next, we assigned the unclassified class as a built up class. We apply this first level of segmentation and classification to different temporal images. However, during this phase we found that the threshold value needs to be adjusted due to different temporal image characteristics. As discussed in sub chapter 3.1, we used two different images, namely SPOT for years 2013 and Pleiades for years 2016. Therefore, several threshold modifications were needed to have an optimal image classification. The results can be seen in figure 4.15 (a) and (b). In the 2013 image, we can see that a lot of trees are detected which mostly blocked road classes. This means that we need to increase the minimum threshold of the Normalized Different Vegetation Index (NDVI). Meanwhile, the minimum threshold for NDVI value of 2016 image was not changed since classification of trees have been similar to image 2013 after adaptation. In general, the threshold values were obtained in a trial and error process due to different characteristics of both images.

Figure 4.15 Levels I Phase Before and After Adaptation

We also used threshold modification of visual brightness parameter using this formula:

$$(\text{Mean Blue Band} + \text{Mean Green Band} + \text{Mean Red Band}) \,/\, 3 \qquad (9)$$

This visual brightness parameter can be used to detect variations between vegetation areas and non-vegetation areas. As a result, we found trees have low brightness value with darker colour. On the other hand, the class of low plants has higher brightness value with lighter colour. Appendix 7 presents all the modification value done in the adaptation process.

B. Level 2 Phase

In level 2 segmentation, we used the image subset from the first area (year of 2016). Before performing the segmentation, we tested the ESP tool to determine the Scale Parameter (SP) for a particular image. The result shows that in for second level segmentation the ESP tool recommended using the SP of 207. However, the recommended SP value seems not to be equally fit enough to segment the built up types. Since the aim of the second level segmentation is to define built up and trees types, a coarse level of segmentation is urgently needed during this process. Therefore, we tested again the SP value from 200, 250, 300, 400 and 500. The result based in visual inspection showed that SP of 300 was equally enough to distinguish trees types, however for built up types a SP of 500 was considered as the best fit value to define built up types. Thus, we used different level of SP for these two different land cover types.

As it can be seen from figure 4.16 and 4.17, applying different scale parameters could affect the results especially when extracting building types and trees. For example, trees with a SP 10 are detected separately while SP 300 is able to appropriately distinguish scattered and dense trees (Figure. 4.16 (b)). In addition, results from lower SP for built-up areas have divided small objects and large buildings into several parts (Figure 4.17(a)). On the other hand, a higher SP for built-up areas has unified small objects into one large area (Figure 4.17(b).

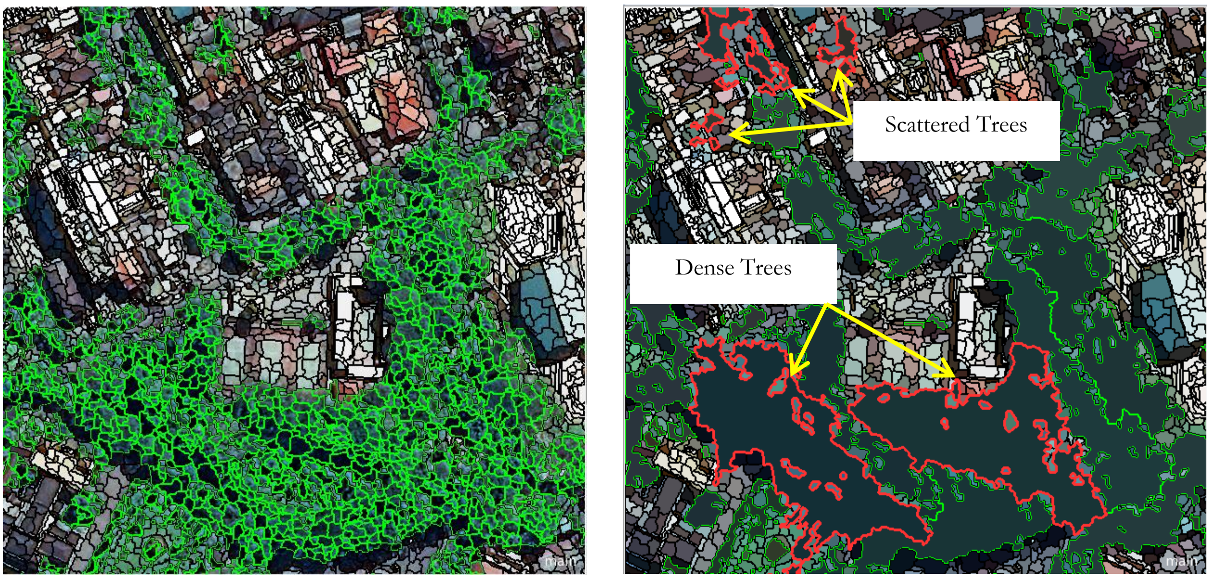

a. Trees with SP = 10 b. Trees with SP = 300

Figure 4.16 Effect of Different of Scale Parameter for Tree Classes

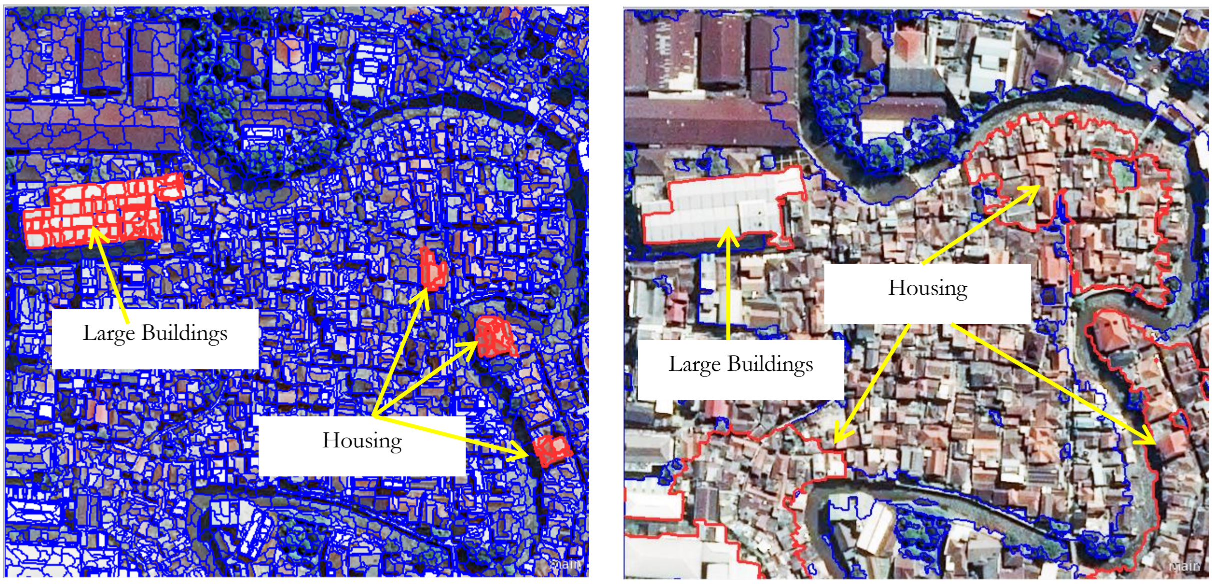

a. Built-up with SP = 10 b. Built-up with SP = 300

Figure 4.17 Effect of Different of Scale Parameter for Built-up Types

Next, we performed classification for extracting detailed of tree and built up types. For tree types, we applied the characteristics of geometry area, where the larger number of geometry area (heavy) is classified as dense trees. On the contrary, the smaller number of geometry area (light) is classified as scattered trees. We assumed that dense trees have a larger canopy area compare to dense trees. Therefore, we used the threshold value of higher than 0.2 hectare to define the dense trees and below than 0.2 hectare to classify the scattered trees.

In the next stage, we applied a classification of built up types. As discussed in sub chapter 3.5., the study from Kohli et al.,(2013) mentioned the usage of image texture as a stable parameter for the classification of built up areas. We found that the GLCM entropy red and blue are able to capture the difference between non-built-up, open arrangement built-up and dense built-up. For example, figure 4.18 (a) shows that low class (blue colour) is identified as a non-built-up area (water area). Meanwhile, the high and very high classes which are represented in green and white colour are detected as built-up area. In this study, we choose to use GLCM entropy red to distinguish built-up, showing good results. In addition, as shown in figure 4.18 (b), after using threshold values it can be seen that open low rise areas were found in the medium class (grey colour) while compact low rise fall into the high and very high class (blue and white colour). The rule set development process can be seen in Appendix 8.

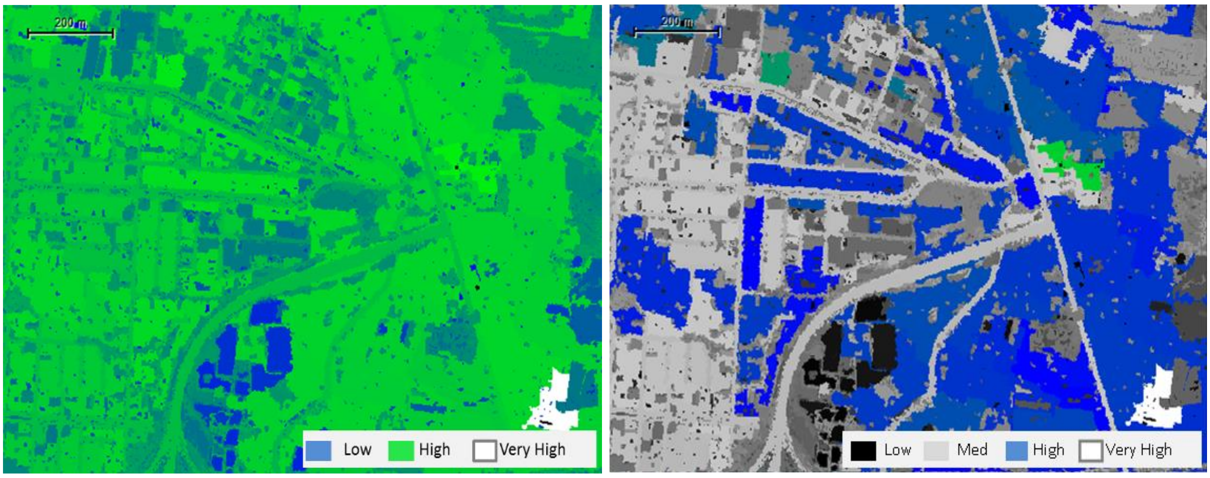

a. GLCM Entropy Blue b. GLCM Entropy Red

Figure 4.18 GLCM Entropy Values

As a results, 8 (eight) LCZ classes have been classified simultaneously. For the land cover types such as road, water, low plants, dense and scattered tree, we found that most of them have been correctly located (as the same as the visual interpretation from image). Meanwhile, for the built up types, we discovered that in some areas of compact low rise and open low rise are incorrect. This shows that between these two classes misclassification occurred. A possible reason for this problem is a mix up location between these two classes. For example, we found that within the open low rise areas also compact low rise exists and vice versa. Hence, we argue that the heterogeneity of built up types could be one of the problems behind the results.

Further experiments could explore the built-up classification using additional datasets like LIDAR and stereo images which has height information for improving the classification results. However, since producing different built up and land cover types using rule set development needs a lot of resources (e.g. time due to trial and error approach), we argue that the result still allow to analysis the general patterns of LCZs and their impact on surface temperature.

4.3.3. Transferability Assessment

As mentioned in chapter 3.5, the transferability assessment aims to measure the transferability of LCZ approach in different spatial and temporal characteristics. A quantitative method was used to determine the observable results of LCZ classification. Therefore, we employed two measurements, e.g., spatial transferability and temporal transferability measurements.

For the spatial transferability, we analysed the results of LCZs extraction from two selected areas of 2016 image. First, we discussed the spatial transferability in the first test area. As we can see from figure 4.19, the area mostly consists of two main types of urban structure pattern which are built up/land use types and land cover types. For the built up types (fig. 4.19(a)), the compact low rise types were detected in the western, centre, and northern part of the image while the open low rise were located mostly in the south east of the image. We notice a randomly pattern of built up areas in the study area. We argue that this is caused by the heterogeneity of mixed urban structure in Bandung where one area or zones might consist of several types of land use.

For the land cover types (fig 4.19(b)), we found that dense trees mostly occurred in the south east of the image (near to open low rise area). Meanwhile, scattered trees existed in small parts of the image. A similar result is also found for areas of low plants. However, we discovered a small number of water located besides a large building. This result might be happened since water is very similar to the shadow in the image domain characteristics. But in overall, water was classified correctly in the river area as shown in the blue colour. Moreover, we also found roads were appropriately extracted from image.

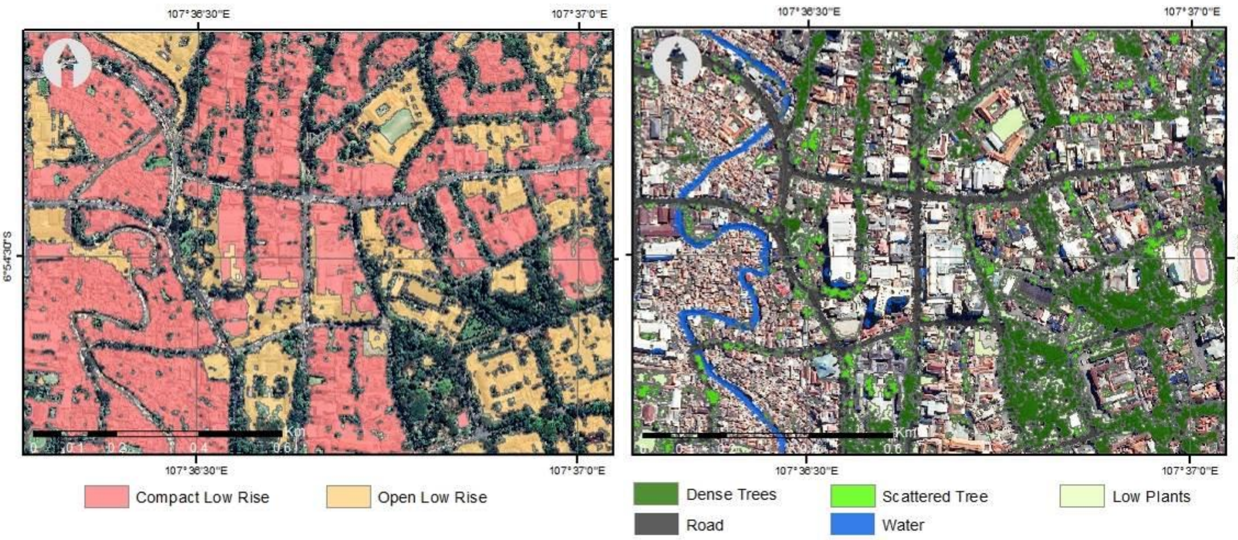

a. Built-up / Land Use b. Land Cover

Figure 4.19 Results of Extracted LCZs in Test Area 1

In the second area, we see a different result compare to the first test area. Although small parts of mixed built up types are present, the built up patterns were found to be more organized (see fig. 4.20(a)). For example, compact low rise areas were mostly located in the eastern part of the image. Meanwhile, open low rise areas occurred in the western part of the image. Moreover, in this area, we found an industrial building in the south eastern part of the image. For the land cover types (see fig. 4.20(b)), we found low plants mostly located in the northern part while dense and scattered trees were randomly located across this area. The water class can be found not only in the river area but also in the south and west part of the image. All in all, from the two selected areas, it can be seen the detailed of urban structure types based on the LCZ approach where mostly mixed types of built-up and land cover were existed.

a. Built-up / Land Use b. Land Cover

Figure 4.20 Results of Extracted LCZs in Test Area 2

The accuracy of confusion matrix assessment of the LCZs classification for the first and second test are can be seen in fig. 4.21.

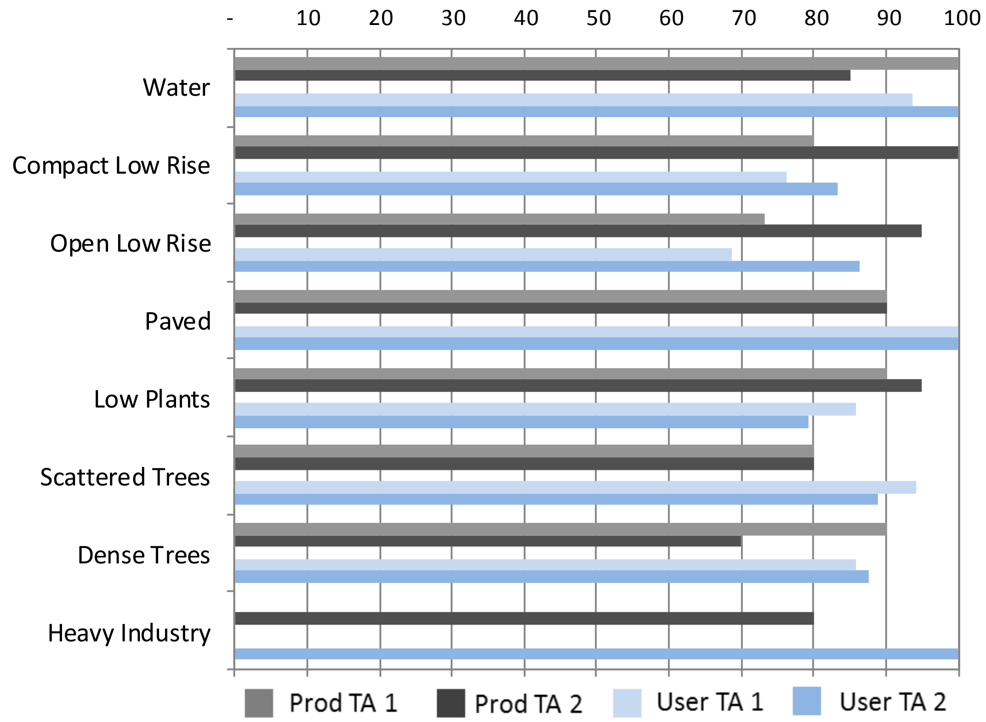

Figure 4.21 Accuracy Assessments between First and Second Test Area

For the built-up or land use types, both producer and user accuracy from compact and open low rise in the second test area resulted in a higher accuracy compared to the first area. However, we could not compare industrial class due to the absence of industry in the first area. For the land cover types, we found a different trend between producer and user accuracy results. For instance, dense trees have a producer accuracy of 90% in the first area, which is higher than the second area (70%) while the user accuracy in the first area (86%) is slightly lower than the second area (88%). Meanwhile, for scattered tree and low plants, both the producer accuracy and user accuracy are slightly higher in the first area in compared to the second area. However, for the road and water class, producer and user accuracy performed much better in the second test area.

The overall accuracy of the second area (89%) is slightly higher than the first area (86%) (see Appendix 8). We argue that the results of the first and second test area are quite similar due to a low difference value. Therefore, we can conclude that the spatial transferability of the LCZ approach using a rule set is generally considered good. Although, several adaptation were applied but the rule set can be used as an alternative approach specifically to have detailed of built-up/land use and land cover types in urban areas.

For temporal transferability, we applied the rule set to different images of two years. Comparison between SPOT 6 (2013) and Pleiades (2016) are presented in Figure 4.22 and 4.23.

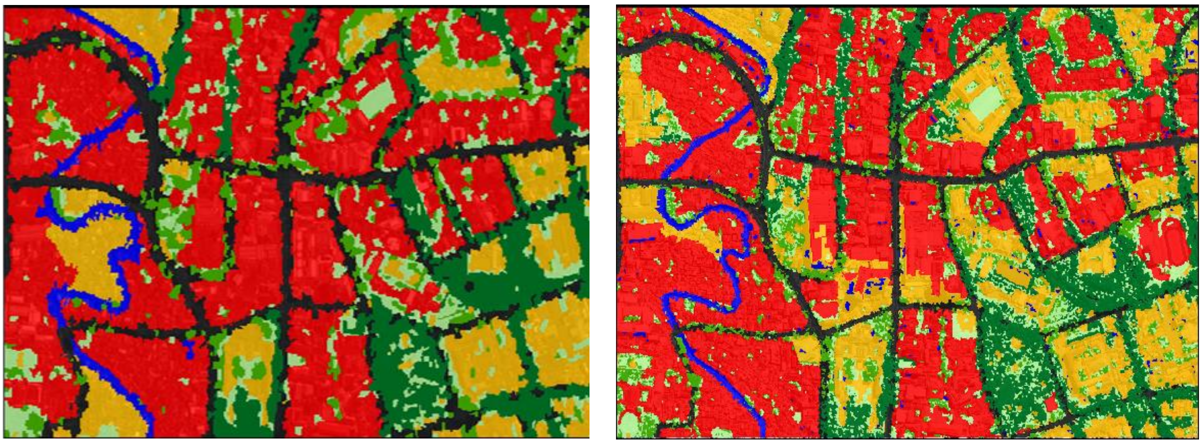

a. SPOT 6 (2013) b. Pleiades (2016)

Open Low Rise, Compact Low Rise, Industry, Water
Scattered Tree, Dense Trees, Low Plants, Road

Figure 4.22 Spatiotemporal Patterns of LCZ in Test Area 1

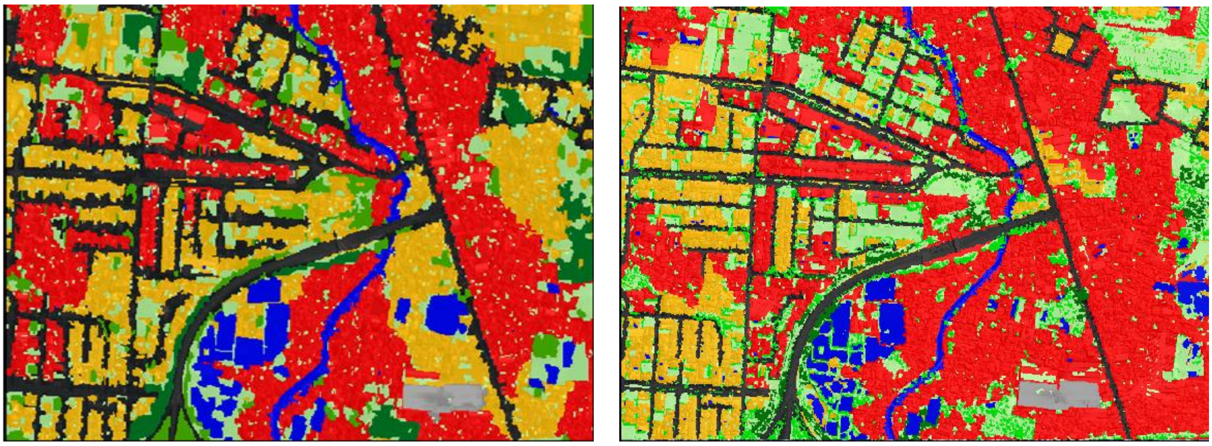

a. SPOT 6 (2013 b. Pleiades (2016)

Open Low Rise, Compact Low Rise, Industry, Water
Scattered Tree, Dense Trees, Low Plants, Road

Figure 4.23 Spatiotemporal Patterns of LCZ in Test Area 2

According to Figure 4.22, we notice some differences in the LCZ classification between SPOT 6 (2013) and Pleiades (2016) in the first area. For example, the open low rise areas that are located near the river in the west direction and several areas in the north-west were changed into compact low rise. Meanwhile, for the land cover types no significant changes occurred during 2013 and 2016.

In the second area (fig. 4.23), we found several differences between open low rise and compact low rise in the western part of the image. For example, based on the visual interpretation of the area around, this part should be classified as a compact low rise instead of an open low rise. This might have happened due to misclassification, also the overall accuracy in 2013 is lower than 2016. Furthermore, we noticed in the eastern part both built-up and land cover types are relatively similar during these years.

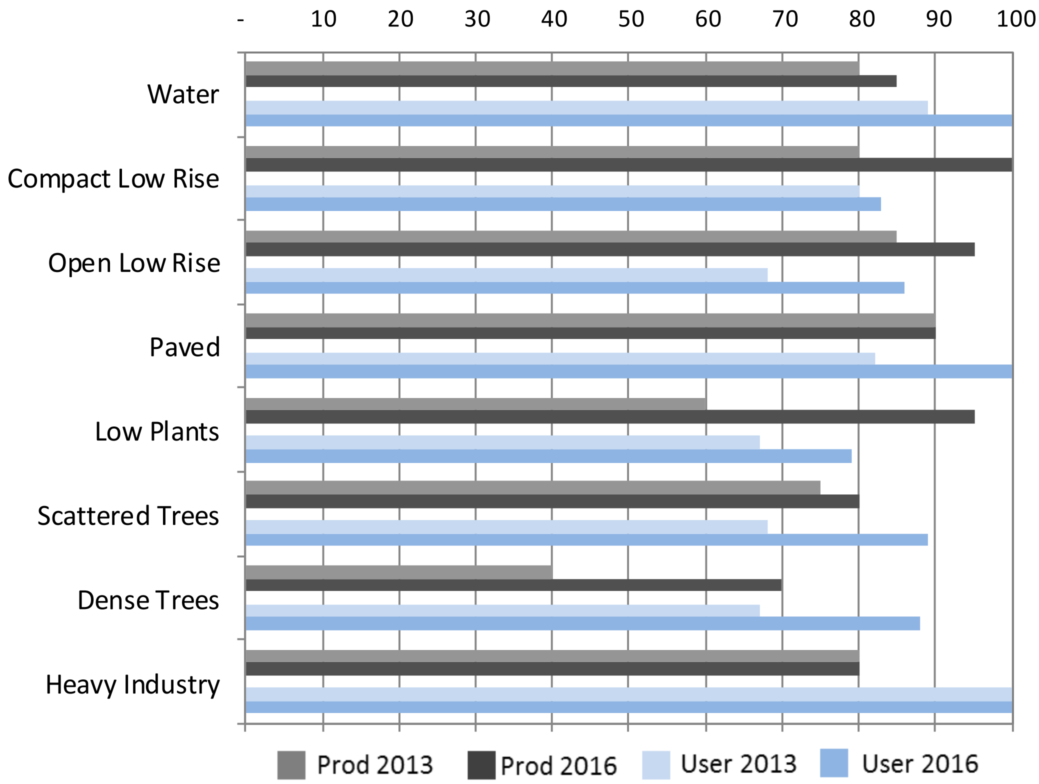

Figure 4.24 Accuracy Assessments between 2013 and 2016 Image in the Second Test Area

We compared the accuracies of both images to analyse the temporal transferability results. We used the second test area since all of the LCZs were present. In general, the average value of producer and user accuracy obtained in 2016 is much higher compared with 2013 (see figure 4.24). For example, built up classes such as compact and open low rise gained above 95% in producer accuracy for the 2016 image while for the 2013 image, producer accuracy results were below 85%. Similar results also found for the land cover types. Both producer and user accuracy from the dense trees, scattered tree and low plants for the 2016 image are slightly higher than 2013 image. However, from fig. 4.25, we notice the differences in the first area are relatively lower with only 3% compare to the second test area (14%). Therefore, the temporal transferability of LCZ is better for the first test area compared to the second test area. Furthermore, the overall accuracy of Pleiades for both subset areas is consistently higher than for the SPOT imagery. For example, Pleiades overall accuracies are range from 86 to 89%, while SPOT6 range from 76 to 82%. Thus, it can be concluded the higher resolution results not only in a higher overall accuracy but also in more detailed information. However, since the average overall accuracy results from both images are not significantly difference, we argue the transferability of the LCZ approach across both images (Pleiades and SPOT6) using an OBIA rule set is still acceptable and can be used to get spatially detailed information of built-up/land use and land cover pattern in urban areas.

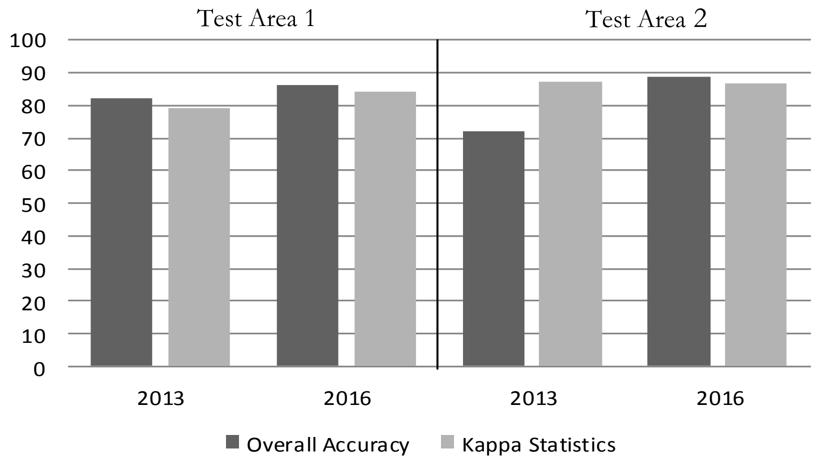

Figure 4.25 Comparison of Temporal Transferability Assessments

In the next step, comparison between coarse and fine resolution imagery was performed. In general, we found there are similar patterns for the built-up types both in first and second subset (see figure 4.26 and 4.27). For example, both compact and open low rise are mainly located in the same location. Meanwhile, industry areas in the coarse imagery are presented more often compared to the VHR imageries. For the land cover types, slightly different pattern are shown between the images. Vegetation types such as dense tree, scattered trees and low plants in the coarse imageries are found less compared to the VHR imageries. However, a significant difference is shown for road areas where in coarse imageries the results show irregular patterns, while in the VHR imageries the patterns are regular. This can be caused by two different factors which are spatial resolution and method of image classification.

Pixel based classification mainly assume that individual classes are defined by similar spectral properties. Meanwhile, object based image analysis uses a different approach. OBIA uses not only spectral and texture but also shape features in the classification process. Furthermore, the segmentation approach becomes an important factor in OBIA since the output defines different objects simultaneously and could lead to better classification result. Thus, these findings demonstrate that OBIA employed to VHR imageries has the advantages not only improving accuracy but also presenting spatially more detailed information about urban structure types. Furthermore, the OBIA approach could lead to better classification results.

Overall, implementation of LCZ method using VHR image in Bandung city has shown a good result. Different built-up and land cover types can be found and extracted more precisely from images. Although only eight classes can be generated from image classification process due to lack of height information, however the diversity of urban structure types in developing countries can be clearly seen. For example, informal settlements (slums) can be detected between areas of compact low rise, close to the river and less vegetation. Furthermore, additional datasets such as LIDAR data might be considered to give better results. Height information from LIDAR can be applied to extract other LCZ classes such as Compact High Rise and Compact Mid Rise. To conclude, LCZ method can be used as an approach in urban climate study to see detailed information of urban structure types.

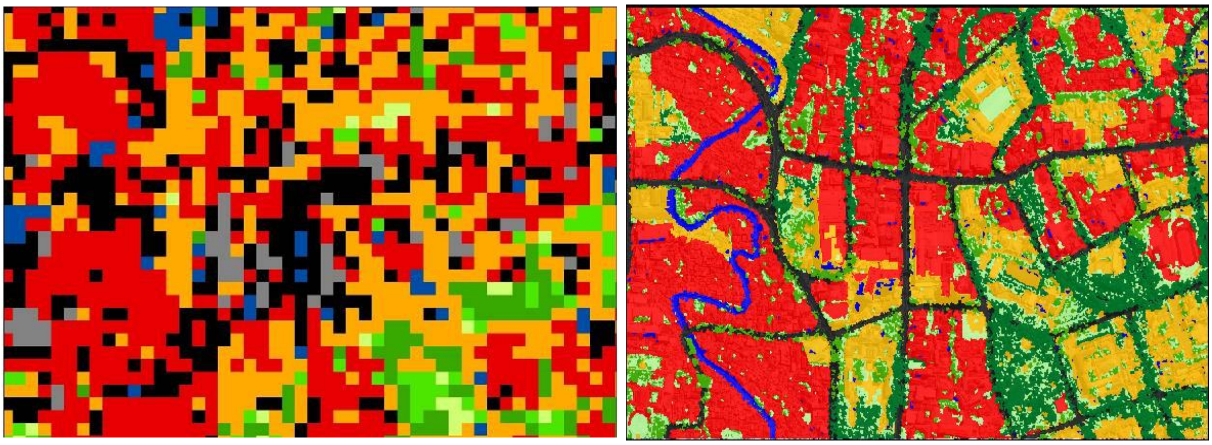

a. Landsat Image   b. Pleiades Image

Figure 4.26 Comparison Result between Coarse and Fine Resolution Imagery in Test Area 1

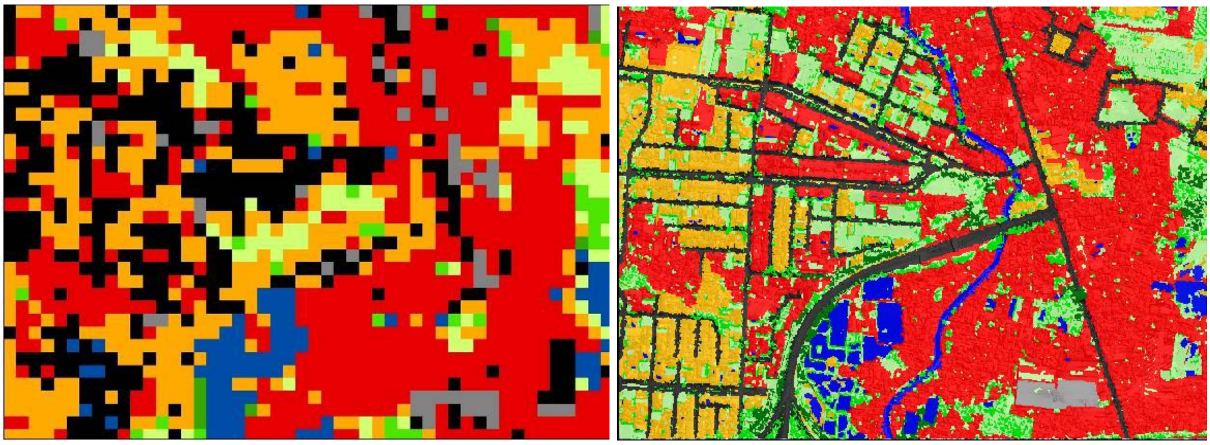

a. Landsat Image   b. Pleiades Image

Figure 4.27 Comparison Result between Coarse and Fine Resolution Imagery in Test Area 2

4.4. Relationship between Land Surface Temperature and Urban Structure Types

4.4.1. Effects of Urban Structure Types on LST

Spatial distributions between surface temperature and LCZ were analysed to investigate their degree of correspondence. First, the mean LST of each LCZ classes were sorted and summarized using box plots analysis. The results in figure 4.28 show differences in the surface temperature between each LCZ. Built-up types like industry, open low rise and compact low rise tend to have higher surface temperatures ranging from 33.8 – 34°C in 2013 and 29.5 – 30°C in 2016, while for vegetation such as dense trees, scattered trees and low plants the values are lower ranging from 32.2 – 32.7°C in 2013 and 27.7 – 28.4°C in 2013. A similar pattern appears for water where the values are lower with 32.8°C in 2013 and 28.9°C in 2016. Meanwhile, roads show as the highest value among the land cover types with 33.7°C in 2013 and 29.4°C in 2016. From this result, we can also see that industries are very homogenous while other classes (e.g. dense trees) have very heterogeneous temperatures (this might depend on the size of the area or whether the pixel is a boundary pixel).

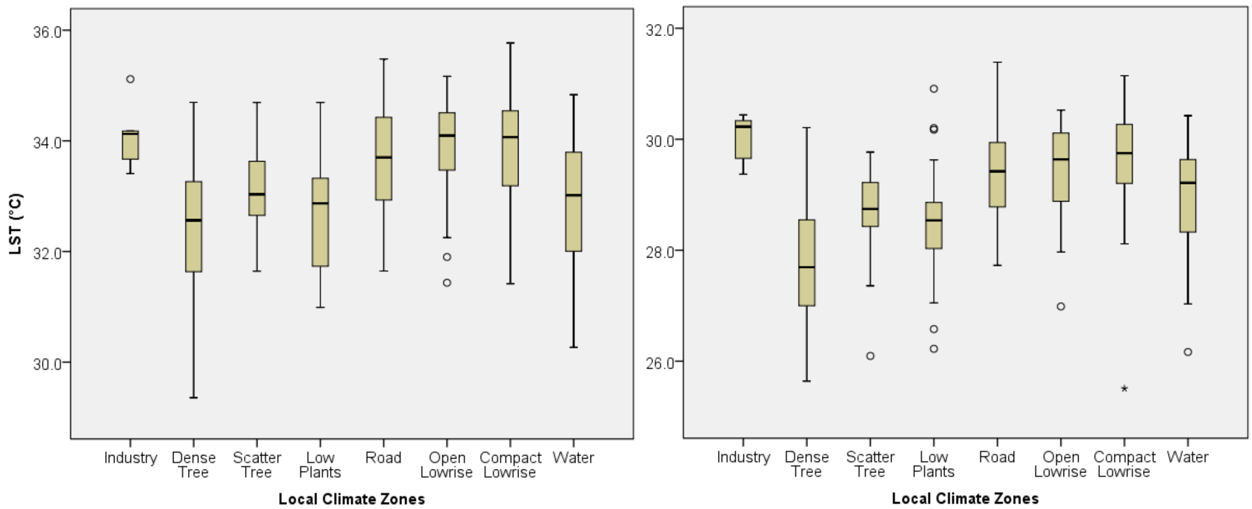

(a). 2013 (b). 2016

Figure 4.28 Boxplots LST and LCZ between 2013 and 2016

Based on these findings, it can be said that the types of urban structure contribute differently to the temperature pattern in its surrounding area. For example, built-up types and roads tend to increase the average of surface temperature due to their surface material. Meanwhile, vegetation types such as trees and low plants plays a major role in reducing the surface temperature because of evapotranspiration processes which keep the surrounding area cool. Therefore, the spatial distribution of this urban structure types will directly affect the temperature pattern.

Second, analyses of variances was conducted to see how significant the influence of each class to the surface temperature patterns. The hypothesis for this analysis is that the values of surface temperatures between each LCZ are significantly different. Hence, we can distinguish high and low values of surface temperature from each LCZ. To test the hypothesis that type of urban structure has a significant effect to the surface temperature value, a one way ANNOVA was performed. Prior to conducting the ANNOVA approach, the assumption of homogeneity of variances was conducted using Levene Statistics Test. Based on the results from table 4.6. it can be seen that both p-value are more than .05, the p-value in 2013 was 0.06, while p-value in 2016 was 0.23. This means that temperature variances between each LCZ in both years were equally distributed. Thus, it indicates that ANNOVA test can be used for testing significance between each LCZ temperature values.

The result from ANNOVA test showed the values of temperature in each class were significant, with F (7, 257) = 10.98, p-value = 0.000 in 2013 and F (7, 257) = 16.79, p-value = 0.000 in 2016. Since the results from the ANNOVA test yielded a significant result, the null hypothesis of no differences between the means was rejected. Therefore, a Post Hoc using Tukey HSD Test was conducted to find the significant difference of surface temperature values between each LCZ classes.

Table 4.6 Results of the Homogeneity of Variances and ANNOVA Test

Year	Test of Homogeneity of Variances		ANNOVA	
	Levene Statistic	Sig.	F	Sig.
2016	1.353	0.226	16.791	0.000
2013	1.951	0.062	10.986	0.000

The multiple comparisons from Post Hoc Test associated with land surface temperature across the eight groups of LCZ are reported in Table 4.7. It shows that several comparisons were statistically significant ($p < .05$). For the built-up types, a similar pattern resulted between compact and open low rise where both types were significantly different with all vegetation class. In addition, the compact low rise was significantly different from the water class with p-value range between 0.000 – 0.026. Meanwhile, industry was significantly different only from dense trees class. However, a different result was found in the comparison between industry and low plants where in 2013 (p=0.071) while in 2016 (p=0.009). We argue that significant difference exists if for both years that result is similar. Therefore, it can be said that these two classes is not significantly different. For the land cover types (vegetation), scattered trees, dense trees and low plants were significantly different from the built-up types like open and compact low rise. However, we also found there is significant difference in the land cover types. For example, roads are significantly different from dense trees and low plants.

All in all, types and variances of built-up and land cover have shown a significant difference about surface temperature patterns. Built-up types like compact low rise which consists of dense residential area is found to have the highest surface temperature values, e.g. caused by absence of vegetation cover in the surrounding areas. A similar result is also found in open low rise areas where less vegetation exists. Furthermore, materials like asphalt or concrete roads play a significant role to the contribution of surface temperature where road class consistently has high temperature for the two years. However, abundance of trees and plants tend to reduce the heat effect from solar radiation.

Table 4.7 Multiple Comparison Results between Each LCZ Classes

LCZ Class		**.Sig**		**LCZ Class**		**.Sig**	
		2013	**2016**			**2013**	**2016**
Industry	Dense Tree	0.013	0.000	Road	Industry	0.983	0.825
	Scattered Tree	0.475	0.055		Dense Tree	0.000	0.000
	Low Plants	0.071	0.009		Scattered Tree	0.301	0.024
	Road	0.983	0.825		Low Plants	0.001	0.000
	Open Low Rise	1.000	0.919		Open Low Rise	0.989	1.000
	Compact Low Rise	0.999	0.983		Compact Low Rise	0.992	0.946
	Water	0.134	0.198		Water	0.068	0.372
Dense Tree	Industry	0.013	0.000	Open Low Rise	Industry	1.000	0.919
	Scattered Tree	0.081	0.051		Dense Tree	0.000	0.000
	Low Plants	0.917	0.061		Scattered Tree	0.047	0.008
	Road	0.000	0.000		Low Plants	0.000	0.000
	Open Low Rise	0.000	0.000		Road	0.989	1.000
	Compact Low Rise	0.000	0.000		Compact Low Rise	1.000	0.998
	Water	0.716	0.216		Water	0.001	0.189
Scattered Tree	Industry	0.475	0.055	Compact Low Rise	Industry	0.999	0.983
	Dense Tree	0.081	0.051		Dense Tree	0.000	0.000
	Low Plants	0.520	0.926		Scattered Tree	0.043	0.000
	Road	0.301	0.024		Low Plants	0.000	0.000
	Open Low Rise	0.047	0.008		Road	0.992	0.946
	Compact Low Rise	0.043	0.000		Open Low Rise	1.000	0.998
	Water	0.855	0.971		Water	0.000	0.026
Low Plants	Industry	0.071	0.009	Water	Industry	0.134	0.198
	Dense Tree	0.917	0.061		Dense Tree	0.716	0.216
	Scattered Tree	0.520	0.926		Scattered Tree	0.855	0.971
	Road	0.001	0.000		Low Plants	1.000	0.356
	Open Low Rise	0.000	0.000		Road	0.068	0.372
	Compact Low Rise	0.000	0.000		Open Low Rise	0.001	0.189
	Water	1.000	0.356		Compact Low Rise	0.000	0.026

Note: Sig: Significant value (p-value); Number of samples (N) : 265

4.4.2. Effects of the Composition Pattern of Urban Structure Types on LST

As discussed in sub chapter 3.6.2, for identifying the relationship between land surface temperature and composition of urban structure types, PLAND metrics were used to calculate the percentage of landscape occupied by each patch type in the two selected areas. The moving window analysis tool was used with a circular kernel option to capture the composition pattern value in this area. However, a sensitivity analyses were performed to find the highest correlation coefficient for different radii. We selected radii from 30-150 meters to obtain optimum correlation coefficient results from for different urban structure types.

As shown in table 4.6, the correlation coefficient between LST and the PLAND of urban structure types show different results. In built up types, the highest correlation coefficient are found for the radius of 90 m with range of 0.60 to 0.61. This means land surface temperature and built up density have positive and strong correlation. A similar result is obtained for vegetation density with the highest correlation for the radius of 90 m. However, the correlation coefficient tends to be the opposite of the built up correlation. The correlation between land surface temperature and vegetation density has a negative and strong correlation ranging from -0.50 to -0.59. On the other hand, the highest correlation for water density is found in the radius of 30 m with a range of -0.29 to -0.41. This means land surface temperature and water density have negative and weak correlation. Moreover, the p-value from all urban structure types are also found lower than 0.01, which means the correlation results between LST and PLAND value are statistically significant between these two years.

Table 4.6 Correlation of LST and Density of Urban Structure Types in Different Radius of PLAND

No.	Radius (m)	Built-up		Vegetation		Water	
		2016	2013	2016	2013	2016	2013
1	30	0.451	0.439	-0.489	-0.414	-0.291	-0.413
2	60	0.579	0.561	-0.554	-0.482	-0.254	-0.408
3	90	0.609	0.604	-0.593	-0.496	-0.234	-0.39
4	120	0.592	0.603	-0.573	-0.475	-0.223	-0.371
5	150	0.573	0.567	-0.525	-0.427	-0.201	-0.344

Based on the correlation coefficient results, the radius of 90 m was selected since it gave the highest correlation coefficient between land surface temperature and urban structure type density especially for the dominant types which are built-up and vegetation. After that, the mean value of land surface temperature was assigned to each value of PLAND in 90 m radius. Sample of observations were selected only for the intersection pixels between each urban structure types with the observed urban structure density from PLAND. Next, correlation and regression analysis were conducted between mean temperature and PLAND values.

The correlation results between mean of land surface temperature and urban structure type density is shown in table 4.3. In general, the correlation coefficients between mean temperature and urban structure type density show moderate and strong results. However, we found that there was slightly different direction between each urban structure types. For example, the correlation coefficients between mean temperature and built-up density has a positive direction with a range from 0.71 (2013) and 0.82 (2016). Meanwhile, the correlation coefficients for vegetation and water density have a negative direction. For vegetation density, the value are 0.69 (2013) and 0.82 (2016). For water density, the values are ranging from 0.79 to 0.80.

Table 4.6 Correlation of LST and Density of Urban Structure Types in Different Radius of PLAND

Year	Built-up - Mean LST			Vegetation - Mean LST			Water - Mean LST		
	Pearson Correlation	Sig.	N	Pearson Correlation	Sig.	N	Pearson Correlation	Sig.	N
2016	0.821	0.00	1000	-0.816	0.00	700	-0.805	0.00	547
2013	0.707	0.00	1000	-0.692	0.00	700	-0.789	0.00	547

Note: Sig = Significant value (p-value); N = Number of Observations

Table 4.7 presents the statistics result of a simple linier regression analysis from the relationship between mean surface temperature and urban structure density between 2013 and 2016. In general, the regression equation results show that the LST can be estimated when urban structure types change by 1%. Furthermore, R^2 value indicates the percentage of variation[8] from the observation value which can be described by the regression line. Thus, it measures how close data are to the fitted regression line. Each relationship between Mean LST and urban structure types will be discussed below.

Overall, the R^2 value between mean LST and each urban structure range from 0.50 to 0.68. For example, the relationship between built-up density and mean LST has a R^2 value of 0.50 – 0. 68. The coefficient value on the regression equation has an average of 0.05. This means the temperature will increase by 0.5°C when built-up density expands by 10%. For the relationship between vegetation density and Mean LST, R^2 value obtained are 0.48 – 0.67. The regression coefficient was found in the average of -0.04. This means the vegetation temperature will decrease by 0.4°C when the vegetation density expands by 10%. Furthermore, a similar result occurred for the relationships between water density and mean LST. R^2 value has a range of 0.62 – 0.65 with an average of -0.11 in the regression coefficient. This means the water temperature will decrease by 1.1°C when water density expands by 10%. Scatterplots of each density types and mean LST between year 2013 and 2016 can be seen in figure 4.29. In general, the scatterplots show that built-up and vegetation density has a large range from 0-100%, while water tends to have a low density of range with range only from 0-50%. This means areas with water are smaller than an area with radius of 90m.

Table 4.7 Regression Statistics of Urban Structure Types Density and Mean LST

Year	Built-up -Mean LST		Vegetation -Mean LST		Water -Mean LST	
	Equation	R^2	Equation	R^2	Equation	R^2
2013	Y = 30.613 + 0.05 X	0.50	Y = 34.617 - 0.04 X	0.48	Y = 34.615 - 0.12 X	0.62
2016	Y = 26.698 + 0.04 X	0.68	Y = 30.214 - 0.04 X	0.67	Y = 30.308 - 0.09 X	0.65

To sum up, this finding suggests that composition of urban structure types has become important parameters to understand the pattern of surface temperature. High densities of built-up area and road pavement have shown as a factor to increase the surface temperature value. Meanwhile, high densities of vegetation and water have proven as the factor to reduce the surface temperature value.

[8] If the R^2 value close to 0, it indicates the total variation of observation values to the fitted regression line are big. Meanwhile if the R^2 value close to 1, it indicates the total variation of observation values to the fitted regression line are small

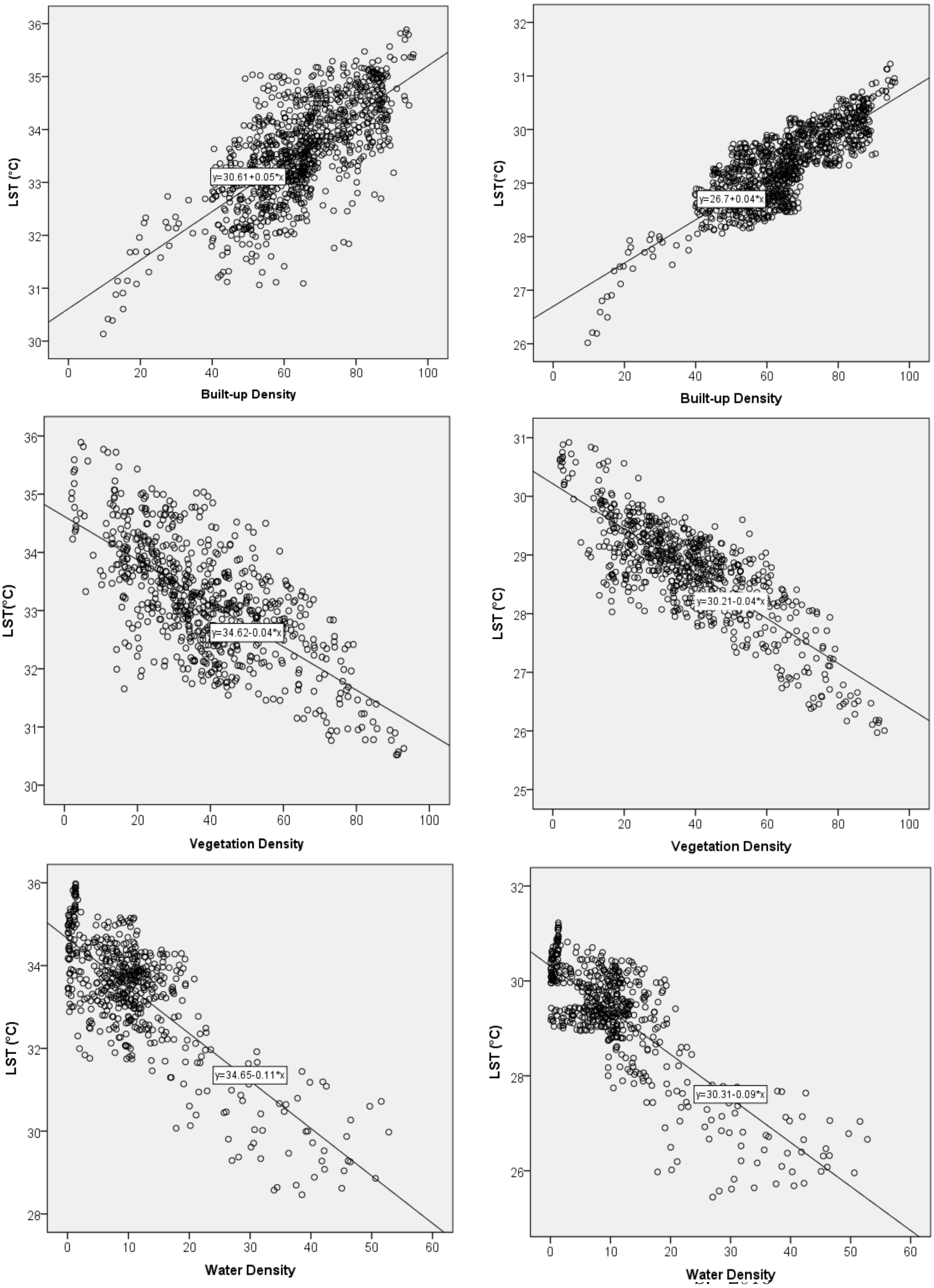

Figure 4.29 Boxplots LST and Density of Urban Structure Types between 2013 and 2016

4.4.3. Effects of the Configuration Pattern of Urban Structure Types on LST

As described in Section 3.6.2, for identifying the relationship between land surface temperature and configuration of urban structure types, Aggregation Index (AI) and Number of Patches (NP) were used to measure the spectrum of the landscape pattern. Both metrics were also calculated using moving window method with a radius of 90 m. This selected radius was chosen to be consistent with previous analysis. Samples were chosen by limiting observations only to intersection pixels between each urban structure types with the observed result of aggregation index and number of patches.

For the aggregation index, the correlation results between the mean of land surface temperature and aggregation index 2013 and 2016 is shown in table 4.8. In general, the correlation coefficient between mean temperature and aggregation index varies from 0.38 – 0.75. There are two different types regarding the direction and strength of the correlation results. First, the correlation coefficient between mean temperature and built-up aggregation index shows a positive and moderate result with 0.65 in 2013 and 0.75 in 2016. Meanwhile, the coefficients for vegetation and water aggregation index have a negative direction. The coefficient for vegetation has obtained values ranging from -0.68 to 0.73 (moderate), while the coefficient for water is slightly lower with a range of 0.37 – 0.45 (low).

Table 4.8 Correlation of Mean LST and Aggregation Index

Year	Built-up - Mean LST			Vegetation - Mean LST			Water - Mean LST		
	Pearson Correlation	Sig.	N	Pearson Correlation	Sig.	N	Pearson Correlation	Sig.	N
2016	0.748	0.00	803	-0.731	0.00	534	-0.456	0.00	207
2013	0.645	0.00	803	-0.683	0.00	534	-0.374	0.00	207

Note: Sig = Significant value (p-value); N = Number of Observations

Table 4.9 presents the statistics result of simple linier regression analysis from the relationship of surface temperature and aggregation index between 2013 and 2016. In general, the R^2 value varies from 0.14 to 0.56. For the relationships between temperature and built-up, the R^2 value has a range from 0.42 to 0.56. This means around 42-58% of variance from the regression line result can be well explained. The coefficient shows in a positive value with an average of 0.17, which means the temperature will slightly increase by 2°C when the built up aggregation index increase by 10%. Meanwhile, in the vegetation, R^2 value is slightly higher compare to other types with a range of 0.47-0.53. The coefficient shows a negative value which means the temperature tend to decrease when vegetation aggregation index increase. However, a low value of R^2 was found in water with a range of 0.14 - 0.21. This result explains the variation around the regression line is quite high. Scatterplot of each aggregation index types and mean LST between year 2013 and 2016 can be seen in Appendix 9.

Table 4.9 Regression Statistics of Mean LST and Aggregation Index

Year	Built-up - Mean LST		Vegetation - Mean LST		Water - Mean LST	
	Equation	R^2	Equation	R^2	Equation	R^2
2013	Y = 14.682 + 0.16 X	0.56	Y = 34.039 - 0.07 X	0.53	Y = 34.779 - 0.08 X	0.21
2016	Y = 16.837 + 0.18 X	0.42	Y = 38.658 - 0.07 X	0.47	Y = 38.980 - 0.08 X	0.14

For the Number of Patches (NP), the correlation results between mean of land surface temperature and number of patches is shown in table 4.10. In general, the correlation coefficient between mean temperature and number of patches varies from 0.51 to 0.68. For the built-up area, the correlation result presents a moderate and negative direction ranging from -0.51 to -0.71. This means a low number of patches tends to increase the temperature, while high number of patches tend to decrease the temperature. Furthermore, these results indicated that the more aggregated built-up areas are the more the surface temperature increases. A similar result also appears for water with range from -0.68 to -0.78. This indicates the more aggregated water tends to be the more the surface temperature will increase. However, a different result occurs for vegetation cover. The coefficients show in a positive value with range of 0.56 – 0.68. This means the more fragmented vegetation tends to be the more the surface temperature values will increase.

Table 4.10 Correlation of Mean LST and Number of Patches

Year	Built-up - Mean LST			Vegetation - Mean LST			Water - Mean LST		
	Pearson Correlation	Sig.	N	Pearson Correlation	Sig.	N	Pearson Correlation	Sig.	N
2016	-0.710	0.00	803	0.684	0.00	534	-0.679	0.00	207
2013	-0.512	0.00	803	0.561	0.00	534	-0.776	0.00	207

Note: Sig = Significant value (p-value); N = Number of Observations

Table 4.11 presents the statistics result of simple linier regression analysis from the relationship between surface temperature and number of patches. In general, the R^2 value varies from 0.27 to 0.59. For the relationships between temperature and built-up, the R^2 value has a range from 0.27 to 0.51. This means around 27-54% of variance from the regression line result can be well explained. The coefficient shows a negative direction with average of 0.2 which means the temperature will decrease by 2°C when the number of patches increases by 10%. A similar result found in the water with R^2 value range from 0.46 to 0.59. Meanwhile, in the vegetation, R^2 value has range of 0.32-0.47. The coefficient shows in a positive value which means the temperature tends to decrease when vegetation number of patch increase. Scatterplots of each number of patches types and mean LST between year 2013 and 2016 can be seen in Appendix 10.

Table 4.11 Regression Statistics of Mean LST and Number of Patches

Year	Built-up - Mean LST		Vegetation - Mean LST		Water - Mean LST	
	Equation	R^2	Equation	R^2	Equation	R^2
2013	Y = 30.070 - 0.22 X	0.51	Y = 27.519 + 0.10 X	0.47	Y = 29.780 - 0.32 X	0.46
2016	Y = 34.323 - 0.21 X	0.27	Y = 32.179 + 0.09 X	0.32	Y = 34.358 - 0.45 X	0.59

These findings indicate that the configuration patterns of urban structure types play a significant role in impacting the surface temperature pattern. More aggregated built-up areas with highly fragmented vegetation tend to increase the intensity of surface temperature, while less aggregated built-up areas with low fragmented vegetation areas tend to decrease the intensity pattern. Understanding the relationship between the spatial pattern of urban structure types and surface temperatures is considered as an important factor on mitigating the effect of land surface temperature. Density or size of green spaces supports cooling effects for the neighbourhood areas. The benefits of having large green spaces especially in urban area appears to be significant in reducing thermal effect from solar radiation. Furthermore, the thermal effects from solar radiation can be also reduced with a better configuration pattern on designing the neighbourhood area. Therefore, for future planning policy and guideline development, planners and policy makers should consider both the composition and configuration pattern of urban structure types for mitigating LST effect.

5. CONCLUSION AND RECOMMENDATIONS

This chapter presents the summary of results and recommendations of this research. It begins with the conclusion of this study, followed by explanations regarding the limitations encountered. At the end, we provide several recommendations for further studies.

5.1. Conclusion

The overall aim of this study was to analyse the relationships between land surface temperature and urban structure types in Bandung, Indonesia. To achieve this objective, four sub objectives and nine research questions had to be answered. Summary of results and conclusion for each sub-objective are presented below.

The first objective investigated the local characteristics of land surface temperature in Bandung between the years 2005 and 2016. The results (Figure 4.1) show that the surface temperature is showing fluctuating values over the years. Between 2005 and 2013, LST increased while from 2013 until 2016 a slightly decrease happened. There are several possible reasons why this occurred. First, it might have happened due to the use of thermal images that only represented surface temperature pattern on a specific day. An image might be taken in one of an unusual hot or cold weather. Thus, different images could lead to represent different surface temperature patterns. Second, the anthropogenic heat effect from human activities such energy consumption from building and transportation can also alter the behaviour of temperature patterns. Last but not least, the existing of UST can be also influenced the temperature patterns. For instance, complex built-up like densely built-up neighbourhoods without vegetation might be have higher LST values compared to low density neighbourhoods surrounding with dense vegetation types. Furthermore, this result demonstrates the uncertainties of surface temperature detection since it depends on the availability of thermal images and temperature patterns.

Regarding the spatial pattern of surface temperature as shown in Figure 4.3, areas with high surface temperature (hot) are mostly concentrated in the central and west part of the city. Meanwhile, areas with low surface temperature (cold) are located in the northwest, northeast and southeast of the city. Furthermore, according to table 4.3, the proportions of these areas are relatively similar. This clearly indicates that the pattern of land surface temperature in Bandung is influenced by its geographic locations.

The second objective was set to adapt the LCZ method to a city of developing countries. Two questions need to be answered to fulfil this objective, which is the spatial pattern and thermal pattern of LCZ. In general, the spatial patterns of LCZ in Bandung are mostly dominated by built-up types, as shown in table 4.3, more than two thirds (70%) of total area consist of this type, while less than one third (30%) contains land cover types. For the built-up types, compact low rise is found as the dominant type compare to other types e.g., open low rise and industry. Meanwhile, dense trees, scattered trees and low plants are the dominant features of land cover. Dense and scattered trees are found in the northwest and northeast part of the city, while low plants e.g., agricultural fields are concentrated in the southeast part of the city. In addition, a small number of water areas with less than 2% of the total area can be found in the south part of the city. Thus, these findings indicate the city is very compactly built-up in the central and west part while in east part is more mixed use zone (less compact). Furthermore, the overall accuracy of classifying the LCZ with a random forest classifier using moderate resolution images was found to range from 66-69%.

For the thermal patterns, fieldwork results found mostly built-up types like compact high-rise, compact low rise and heavy industry to have high temperature values compare to the land cover types. The temperature patterns during daylight have shown a significant increase with an average increase by 8-12°C for the built-up types and 12-15°C for the paved areas. Meanwhile, in the evening, temperature patterns showed a slightly different trend for each LCZ class where areas of vegetation tend to have lower temperatures compare to built-up and other land cover types.

The third objective focused at the transferability of implementing LCZ for VHR image. In order to implement the LCZ method in VHR images, an OBIA rule set was developed using a segmentation and classification approach. Within a rule set, LCZ method can be defined by several characteristics from image domain features. For example, built-up types e.g., compact low rise, open low rise and industry can be recognized from its roof materials, footprint, size and shape using GLCM entropy red threshold value. Meanwhile, vegetation types e.g., dense trees, scattered trees and low plants can be distinguished by the size and shape using the NDVI, visual brightness and total area (Appendix 7).

About the spatial transferability assessment, we notice the second test area is more transferable than the first test area due to a higher overall accuracy results. For the temporal transferability assessment, we found that the overall accuracy results from Pleiades imagery (2016) are slightly higher than SPOT 6 (2013). Pleiades overall accuracies are range from 86 to 89%, while SPOT6 are ranging from 76 to 82%. However, since the differences of overall accuracies between these images are small, we argue the LCZ approach is transferable to different VHR imageries. Furthermore, we noticed that the results using OBIA provides a higher accuracy compare to pixel based classification. Thus, these findings reveal that higher spatial resolution images with OBIA has an advantages not only improving accuracies but also presenting spatially more detailed information about urban structure types compared to moderate resolution imagery.

Finally, the fourth objective was to explore the relationships between land surface temperature and urban structure types. Three questions need to be answered. In general, the results showed that not only does the type of urban structure significantly affect the values of land surface temperature, but so does the composition and configuration patterns. First, there were statistically significant differences between the values of surface temperature and urban structure types. For instance, built-up types like compact low rise and open low rise which consisting of dense residential area are found to have the highest surface temperature values. In contrary, vegetation types like dense trees and low plants are discovered with low surface temperature values.

Regarding the composition pattern, we noticed that the total percentage of density cover plays as an important role. High percentage cover of vegetation and water types significantly reduces the magnitude of LST while high percentage cover of built-up tends to significantly increase the magnitude of LST. The configuration of urban structure types also matters. We found that the increase or decrease of LST pattern can be significantly be influenced by the configuration or spatial arrangement of urban structure types. For instances, an increase in aggregation index of vegetation and water tends to decrease the value of LST. In contrast, an increase of the aggregation index of built-up types leads to an increase of the LST value. Furthermore, a low number of patches in vegetation areas (indicating less fragmentation) can significantly decrease LST. Meanwhile, a low number of patches in built-up are can significantly increase LST. Hence, these findings confirm the contribution of configuration pattern of urban structure types on the surface temperature.

All in all, implementation of LCZ method using VHR image in Bandung city can be used as a potential application not only for climate study but also other urban studies like informal settlements and landscape planning especially in cities of developing countries. Despite heterogeneity of urban structure types in cities of developing countries, the LCZ approach has been able to capture the configuration of built-up and land cover types. Thus, this method will be very useful to see spatially detailed information about urban structure types.

5.2. Limitations in the Research

Some limitations in this research are listed as follow:

1. The availability of thermal satellite products
   The selected thermal images were considered as a key limitation during this research. The availability of thermal images especially in tropical countries depends on the existence of cloud cover. Furthermore, the selected days of the thermal images does not offer a comprehensive LST patterns in the study area. Thus, it will be hard to identify precisely the land surface temperature trend since the temperatures values of a specific day might be not representative for the general trend during the study period.
2. Extraction of Local Climate Zone Method
   In total, 8 out of 17 LCZs were identified in the study area. However, several classes with height characteristics like compact high-rise, compact mid-rise and open mid-rise could not be applied in classification process due to limited information in image domain feature. Therefore, these classes were not included in the image classification results.
3. Hardware Specifications
   When mapping LCZ in a large areas using very high resolution imagery, we encountered limitations with the hardware system used. Using VHR imagery within an OBIA approach has a high computational demand. Hence, producing a classification of large areas using VHR is still considered as an obstacle. Thus the computation process employing our rule set could not be implemented for the entire city (results are only obtained for subsets.
4. Selecting the most appropriate method for image classification
   Although the OBIA has given higher overall accuracy compared to the pixel based classification, we still found limitation when using this approach. Firstly, the result of appropriate segmentation parameter is still based on a trial and error process. In addition, the results of the scale parameter (SP), smoothness and compactness parameter depend on the value that we chose (Drăguţ et al., 2014). Second, selecting appropriate threshold values using image domain feature information was very time consuming.

5.3. Recommendations

For future research, this study recommends as follow:

1. Selecting night TIR imagery and hourly air temperature
   Further investigations of the surface temperature variability during night time can be used to utilize further study the surface temperature characteristics. Therefore, further studies could apply multiple daytime and night time thermal images of different seasons to clarify diurnal and seasonal variations regarding the relation between land surface temperature and urban structure types. In addition, hourly air temperature dataset can be applied to have precisely comparison of surface temperature patterns.
2. Incorporation of different datasets
   Although this study used VHR images e.g., Pleiades (0.5 meter) and SPOT 6 (1.5 meter) after pan-sharpening, detailed information like built-up types with different height are still hard to extract. Thus,

combining VHR and Light Detection and Ranging (LIDAR) data can very useful for future research, especially to classify different heights of built-up types.

3. Selection of the most appropriate spatial metrics
   For future research, selecting different variables of spatial metrics are considered to be useful in finding the effect of configuration pattern between land surface temperature and urban structure types such as connectivity and proximity metrics.

LIST OF REFERENCES

Ahmed, B., Kamruzzaman, M., Zhu, X., Rahman, M., & Choi, K. (2013). Simulating Land Cover Changes and Their Impacts on Land Surface Temperature in Dhaka, Bangladesh. *Remote Sensing*, *5*(11), 5969–5998. https://doi.org/10.3390/rs5115969

Argueso, D., Evans, J. P., Pitman, A. J., & Luca, A. Di. (2015). Effects of city expansion on heat stress under climate change conditions. *PLoS ONE*, *10*(2), 1–19. https://doi.org/10.1371/journal.pone.0117066

ASTRIUM. (2012). Pléiades Imagery User Guide, *2*(October), 118. Retrieved from http://blackbridge.com/geomatics/upload/airbus/Pleiades User Guide.pdf

Astrium, S. (2013). SPOT 6 & SPOT 7 Imagery - User Guide, (July), 117. Retrieved from http://www.intelligence-airbusds.com/spot6userguide/

Baatz, M., & Schäpe, a. (2000). Multiresolution Segmentation: an optimization approach for high quality multi-scale image segmentation. *Angewandte Geographische Informationsverarbeitung XII. Beiträge Zum AGIT-Symposium Salzburg 2000, Karlsruhe, Herbert Wichmann Verlag*, 12–23. https://doi.org/Export Date 6 May 2013

Banzhaf, E., & Hofer, R. (2008). Monitoring Urban Structure Types as Spatial Indicators With CIR Aerial Photographs for a More Effective Urban Environmental Management. *IEEE Journal of Selected Topics in Applied Earth Observations and Remote Sensing*, *1*(2), 129–138. https://doi.org/10.1109/JSTARS.2008.2003310

Bechtel, B., Alexander, P., Böhner, J., Ching, J., Conrad, O., Feddema, J., Mills, G., See, L., Stewart, I. (2015). Mapping Local Climate Zones for a Worldwide Database of the Form and Function of Cities. *ISPRS International Journal of Geo-Information*, *4*(1), 199–219. https://doi.org/10.3390/ijgi4010199

Bechtel, B., & Daneke, C. (2012). Classification of local climate zones based on multiple earth observation data. *IEEE Journal of Selected Topics in Applied Earth Observations and Remote Sensing*, *5*(4), 1191–1202. https://doi.org/10.1109/JSTARS.2012.2189873

Bechtel, B., Zakšek, K., & Hoshyaripour, G. (2012). Downscaling Land Surface Temperature in an Urban Area: A Case Study for Hamburg, Germany. *Remote Sensing*, *4*(10), 3184–3200. https://doi.org/10.3390/rs4103184

Belgiu, M., & Drăgu, L. (2016). Random forest in remote sensing: A review of applications and future directions. *ISPRS Journal of Photogrammetry and Remote Sensing*, *114*, 24–31. https://doi.org/10.1016/j.isprsjprs.2016.01.011

Belgiu, M., Drăguţ, L., & Strobl, J. (2014). Quantitative evaluation of variations in rule-based classifications of land cover in urban neighbourhoods using WorldView-2 imagery. *ISPRS Journal of Photogrammetry and Remote Sensing*, *87*, 205–215. https://doi.org/10.1016/j.isprsjprs.2013.11.007

Bhaskaran, S., Paramananda, S., & Ramnarayan, M. (2010). Per-pixel and object-oriented classification methods for mapping urban features using Ikonos satellite data. *Applied Geography*, *30*(4), 650–665. https://doi.org/10.1016/j.apgeog.2010.01.009

Blaschke, T. (2010). Object based image analysis for remote sensing. *ISPRS Journal of Photogrammetry and Remote Sensing*, *65*(1), 2–16. https://doi.org/10.1016/j.isprsjprs.2009.06.004

Blaschke, T., Hay, G. J., Kelly, M., Lang, S., Hofmann, P., Addink, E., Queiroz Feitosa, R., van der Meer, F., van der Werff, H., van Coillie, F., Tiede, D. (2014). Geographic Object-Based Image Analysis - Towards a new paradigm. *ISPRS Journal of Photogrammetry and Remote Sensing*, *87*, 180–191. https://doi.org/10.1016/j.isprsjprs.2013.09.014

Breiman, L. (2001). Random forests. *Machine Learning*, *45*(1), 5–32. https://doi.org/10.1023/A:1010933404324

Cai, M., Ren, C., Xu, Y., Dai, W., & Wang, X. M. (2016). Local Climate Zone Study for Sustainable Megacities Development by Using Improved WUDAPT Methodology – A Case Study in Guangzhou. *Procedia Environmental Sciences*, *36*, 82–89. https://doi.org/10.1016/j.proenv.2016.09.017

Castilla, G., & Hay, G. J. (2008). Image objects and geographic objects. *Object Based Image Analysis*, (Khun 1962), 817. https://doi.org/10.1007/978-3-540-77058-9_5

Connors, J. P., Galletti, C. S., & Chow, W. T. L. (2013). Landscape configuration and urban heat island effects: Assessing the relationship between landscape characteristics and land surface temperature in

Phoenix, Arizona. *Landscape Ecology*, *28*(2), 271–283. https://doi.org/10.1007/s10980-012-9833-1
Cracknell, M. J., & Reading, A. M. (2014). Geological mapping using remote sensing data: A comparison of five machine learning algorithms, their response to variations in the spatial distribution of training data and the use of explicit spatial information. *Computers and Geosciences*, *63*, 22–33. https://doi.org/10.1016/j.cageo.2013.10.008
Danylo, O., See, L., Bechtel, B., Schepaschenko, D., & Fritz, S. (2016). Contributing to WUDAPT: A Local Climate Zone Classification of Two Cities in Ukraine. *IEEE Journal of Selected Topics in Applied Earth Observations and Remote Sensing*, *9*(5), 1841–1853. https://doi.org/10.1109/JSTARS.2016.2539977
De Gregorio Hurtado, S., Olazabal, M., Salvia, M., Pietrapertosa, F., Olazabal, E., Geneletti, D., D'Alonzo, V., Si Leo, S., Reckien, D. (2015). Understanding How and Why Cities Engage with Climate Policy : An Analysis of Local Climate Action in Spain and Italy. *TeMA - Journal of Land Use, Mobility and Environment*, *8*(NOVEMBER), 23–46. https://doi.org/10.6092/1970-9870/3649
Drăguţ, L., Csillik, O., Eisank, C., & Tiede, D. (2014). Automated parameterisation for multi-scale image segmentation on multiple layers. *ISPRS Journal of Photogrammetry and Remote Sensing*, *88*, 119–127. https://doi.org/10.1016/j.isprsjprs.2013.11.018
Feng, X., & Myint, S. W. (2016). Exploring the effect of neighboring land cover pattern on land surface temperature of central building objects. *Building and Environment*, *95*, 346–354. https://doi.org/10.1016/j.buildenv.2015.09.019
Firman, T. (2012). Urbanization and urban development patterns. *The Jakarta Post*. Retrieved from http://www.thejakartapost.com/news/2012/05/12/urbanization-and-urban-development-patterns.html
Geletič, J., Lehnert, M., & Dobrovolný, P. (2016). Land Surface Temperature Differences within Local Climate Zones, Based on Two Central European Cities. *Remote Sensing*, *8*(10), 788. https://doi.org/10.3390/rs8100788
Guo, Q., Kelly, M., Gong, P., & Liu, D. (2007). An Object-Based Classification Approach in Mapping Tree Mortality Using High Spatial Resolution Imagery. *GIScience & Remote Sensing*, *44*(1), 24–47. https://doi.org/10.2747/1548-1603.44.1.24
Heiden, U., Heldens, W., Roessner, S., Segl, K., Esch, T., & Mueller, A. (2012). Urban structure type characterization using hyperspectral remote sensing and height information. *Landscape and Urban Planning*, *105*(4), 361–375. https://doi.org/10.1016/j.landurbplan.2012.01.001
Hellström, T. (2008). Transferability and naturalistic generalization: New generalizability concepts for social science or old wine in new bottles? *Quality and Quantity*, *42*(3), 321–337. https://doi.org/10.1007/s11135-006-9048-0
Herold, M., Goldstein, N. C., & Clarke, K. C. (2003). The spatiotemporal form of urban growth: Measurement, analysis and modeling. *Remote Sensing of Environment*, *86*(3), 286–302. https://doi.org/10.1016/S0034-4257(03)00075-0
Hox, J. J., & Boeije, H. R. (2005). Data Collection, Primary vs. Secondary. In *Encyclopedia of Social Measurement* (Vol. 1, pp. 593–599). Elsevier. https://doi.org/10.1016/B0-12-369398-5/00041-4
Hu, Y., & Jia, G. (2010). Influence of land use change on urban heat island derivedfrom multi-sensor data. *International Journal of Climatology*, *30*(9), 1382–1395. https://doi.org/10.1002/joc.1984
Im, J., Beier, C., & Li, M. (2013). Machine learning approaches for forest classification and change analysis using multi-temporal Landsat TM images over Huntington Wildlife Forest. *Giscience & Remote Sensing*, *50*(4), 361–384. https://doi.org/Doi 10.1080/15481603.2013.819161
IPCC. (2014). *Climate Change 2013 - The Physical Science Basis*. (Intergovernmental Panel on Climate Change, Ed.), *Ipcc*. Cambridge: Cambridge University Press. https://doi.org/10.1017/CBO9781107415324
Jin, M., Li, J., Wang, C., & Shang, R. (2015). A Practical Split-Window Algorithm for Retrieving Land Surface Temperature from Landsat-8 Data and a Case Study of an Urban Area in China. *Remote Sensing*, *7*(4), 4371–4390. https://doi.org/10.3390/rs70404371
Kikon, N., Singh, P., Singh, S. K., & Vyas, A. (2016). Assessment of urban heat islands (UHI) of Noida City, India using multi-temporal satellite data. *Sustainable Cities and Society*, *22*, 19–28. https://doi.org/10.1016/j.scs.2016.01.005
Kohli, D., Warwadekar, P., Kerle, N., Sliuzas, R., & Stein, A. (2013). Transferability of object-oriented image analysis methods for slum identification. *Remote Sensing*, *5*(9), 4209–4228. https://doi.org/10.3390/rs5094209
Kuenzer, C., & Dech, S. (2013). *Thermal Infrared Remote Sensing*. (C. Kuenzer & S. Dech, Eds.), *Thermal Infrared Remote Sensing: Sensors, Methods, Applications* (Vol. 17). Dordrecht: Springer Netherlands.

https://doi.org/10.1007/978-94-007-6639-6
Kuffer, M., Barros, J., & Sliuzas, R. V. (2014). The development of a morphological unplanned settlement index using very-high-resolution (VHR) imagery. *Computers, Environment and Urban Systems*, *48*, 138–152. https://doi.org/10.1016/j.compenvurbsys.2014.07.012
Lary, D. J., Alavi, A. H., Gandomi, A. H., & Walker, A. L. (2016). Machine learning in geosciences and remote sensing. *Geoscience Frontiers*, *7*(1), 3–10. https://doi.org/10.1016/j.gsf.2015.07.003
Leconte, F., Bouyer, J., Claverie, R., & Pétrissans, M. (2015). Using Local Climate Zone scheme for UHI assessment: Evaluation of the method using mobile measurements. *Building and Environment*, *83*, 39–49. https://doi.org/10.1016/j.buildenv.2014.05.005
Lelovics, E., Unger, J., Gál, T., & Gál, C. V. (2014). Design of an urban monitoring network based on Local Climate Zone mapping and temperature pattern modelling. *Climate Research*, *60*(1), 51–62. https://doi.org/10.3354/cr01220
Li, Y., Zhang, H., & Kainz, W. (2012). Monitoring patterns of urban heat islands of the fast-growing Shanghai metropolis, China: Using time-series of Landsat TM/ETM+ data. *International Journal of Applied Earth Observation and Geoinformation*, *19*, 127–138. https://doi.org/10.1016/j.jag.2012.05.001
Liu, D., & Xia, F. (2010). Assessing object-based classification: advantages and limitations. *Remote Sensing Letters*, *1*(4), 187–194. https://doi.org/10.1080/01431161003743173
Liu, H., & Weng, Q. H. (2009). Scaling Effect on the Relationship between Landscape Pattern and Land Surface Temperature: A Case Study of Indianapolis, United States. *Photogrammetric Engineering and Remote Sensing*, *75*(3), 291–304.
Liu, Y., Guo, Q., & Kelly, M. (2008). A framework of region-based spatial relations for non-overlapping features and its application in object based image analysis. *ISPRS Journal of Photogrammetry and Remote Sensing*, *63*(4), 461–475. https://doi.org/10.1016/j.isprsjprs.2008.01.007
Luo, Y. M., Huang, D. T., Liu, P. Z., & Feng, H. M. (2016). An novel random forests and its application to the classification of mangroves remote sensing image. *Multimedia Tools and Applications*, *75*(16), 9707–9722. https://doi.org/10.1007/s11042-015-2906-9
McCoy, R. M. (2005). *Field Method in Remote Sensing*.
McGarigal, K., Cushman, S. A., Neel, M. C., & Ene, E. (2002). FRAGSTATS: Spatial Pattern Analysis Program for Categorical Maps. Retrieved January 31, 2017, from http://www.umass.edu/landeco/research/fragstats/fragstats.html
Middel, A., Häb, K., Brazel, A. J., Martin, C. A., & Guhathakurta, S. (2014). Impact of urban form and design on mid-afternoon microclimate in Phoenix Local Climate Zones. *Landscape and Urban Planning*, *122*, 16–28. https://doi.org/10.1016/j.landurbplan.2013.11.004
Mirzaei, P. A. (2015). Recent challenges in modeling of urban heat island. *Sustainable Cities and Society*, *19*, 200–206. https://doi.org/10.1016/j.scs.2015.04.001
Myint, S. W., Gober, P., Brazel, A., Grossman-Clarke, S., & Weng, Q. (2011). Per-pixel vs. object-based classification of urban land cover extraction using high spatial resolution imagery. *Remote Sensing of Environment*, *115*(5), 1145–1161. https://doi.org/10.1016/j.rse.2010.12.017
Orhan, O., Ekercin, S., & Dadaser-Celik, F. (2014). Use of Landsat land surface temperature and vegetation indices for monitoring drought in the Salt Lake Basin Area, Turkey. *The Scientific World Journal*, *2014*(Vci). https://doi.org/10.1155/2014/142939
Pratomo, J., Kuffer, M., Martinez, J., & Kohli, D. (2016). Uncertainties in Analysing the Transferability of the Generic Slum Ontology, (2016).
Ramdani, F., & Setiani, P. (2014). Spatio-temporal analysis of urban temperature in Bandung City, Indonesia. *Urban Ecosystems*, *17*(2), 473–487. https://doi.org/10.1007/s11252-013-0332-1
Roth, M., Oke, T. R., & Emery, W. J. (1989). Satellite-derived urban heat islands from three coastal cities and the utilization of such data in urban climatology. *International Journal of Remote Sensing*, *10*(11), 1699–1720. https://doi.org/10.1080/01431168908904002
Sachindra, D. A., Ng, A. W. M., Muthukumaran, S., & Perera, B. J. C. (2016). Impact of climate change on urban heat island effect and extreme temperatures: a case-study. *Quarterly Journal of the Royal Meteorological Society*, *142*(694), 172–186. https://doi.org/10.1002/qj.2642
Salehi, B., Zhang, Y., Zhong, M., & Dey, V. (2012). Object-based classification of urban areas using VHR imagery and height points ancillary data. *Remote Sensing*, *4*(8), 2256–2276. https://doi.org/10.3390/rs4082256
Schwarz, N., & Manceur, A. M. (2015). Analyzing the Influence of Urban Forms on Surface Urban Heat Islands in Europe. *Journal of Urban Planning and Development*, *141*(3), A4014003. https://doi.org/10.1061/(ASCE)UP.1943-5444.0000263

Schwarz, N., Schlink, U., Franck, U., & Großmann, K. (2012). Relationship of land surface and air temperatures and its implications for quantifying urban heat island indicators - An application for the city of Leipzig (Germany). *Ecological Indicators*, *18*, 693–704. https://doi.org/10.1016/j.ecolind.2012.01.001

Sismanidis, P., Keramitsoglou, I., & Kiranoudis, C. T. (2015). A satellite-based system for continuous monitoring of Surface Urban Heat Islands. *Urban Climate*, *14*, 141–153. https://doi.org/10.1016/j.uclim.2015.06.001

Sobrino, J. A., Jiménez-Muñoz, J. C., & Paolini, L. (2004). Land surface temperature retrieval from LANDSAT TM 5. *Remote Sensing of Environment*, *90*(4), 434–440. https://doi.org/10.1016/j.rse.2004.02.003

Stewart, I. D., & Oke, T. R. (2012). Local climate zones for urban temperature studies. *Bulletin of the American Meteorological Society*, *93*(12), 1879–1900. https://doi.org/10.1175/BAMS-D-11-00019.1

Stewart, I., & Oke, T. (2009). Classifying urban climate field sites by "local climate zones": the case of nagano , japan. *The Seventh International Conference on Urban Climate*, (July), 1–5.

Trimble Germany GmbH. (2016). eCognition ® Developer, 1–267. Retrieved from http://www.ecognition.com/

Tuanmu, M. N., Viña, A., Roloff, G. J., Liu, W., Ouyang, Z., Zhang, H., & Liu, J. (2011). Temporal transferability of wildlife habitat models: Implications for habitat monitoring. *Journal of Biogeography*, *38*(8), 1510–1523. https://doi.org/10.1111/j.1365-2699.2011.02479.x

U.S. Environmental Protection Agency. (2014). Reducing Urban Heat Islands: Compendium of Strategies Urban Heat Island Basics, 1–22. Retrieved from https://www.epa.gov/sites/production/files/2014-06/documents/basicscompendium.pdf

United Nations. (2015). World Urbanization Prospects The 2014 Revision: Final Report. https://doi.org/(ST/ESA/SER.A/366)

Voogt, J. ., & Oke, T. . (2003). Thermal remote sensing of urban climates. *Remote Sensing of Environment*, *86*(3), 370–384. https://doi.org/10.1016/S0034-4257(03)00079-8

Wardana, I. K. (2015). Analysis of Urban Surface Temperature for Green Spaces Planning in Bandung City , Indonesia, (1), 593–605.

Weih, R. C., & Riggan, N. D. (2010). Object-based classification vs. pixel-based classification: Comparitive importance of multi-resolution imagery. *The International Archives of the Photogrammetry, Remote Sensing and Spatial Information Sciences*, *XXXVIII*, 1–6.

Weng, Q. (2009). Thermal infrared remote sensing for urban climate and environmental studies: Methods, applications, and trends. *ISPRS Journal of Photogrammetry and Remote Sensing*, *64*(4), 335–344. https://doi.org/10.1016/j.isprsjprs.2009.03.007

Wieland, M., & Pittore, M. (2014). Performance evaluation of machine learning algorithms for urban pattern recognition from multi-spectral satellite images. *Remote Sensing*, *6*(4), 2912–2939. https://doi.org/10.3390/rs6042912

Wu, H., Ye, L.-P., Shi, W.-Z., & Clarke, K. C. (2014). Assessing the effects of land use spatial structure on urban heat islands using HJ-1B remote sensing imagery in Wuhan, China. *International Journal of Applied Earth Observation and Geoinformation*, *32*, 67–78. https://doi.org/10.1016/j.jag.2014.03.019

Yin, R. K. (2003). *Case study research : design and methods*. Sage Publications.

Yow, D. M. (2007). Urban Heat Islands: Observations, Impacts, and Adaptation. *Geography Compass*, *1*(6), 1227–1251. https://doi.org/10.1111/j.1749-8198.2007.00063.x

Yu, X., Guo, X., & Wu, Z. (2014). Land surface temperature retrieval from landsat 8 TIRS-comparison between radiative transfer equation-based method, split window algorithm and single channel method. *Remote Sensing*, *6*(10), 9829–9852. https://doi.org/10.3390/rs6109829

Zhang, H., Qi, Z., Ye, X., Cai, Y., Ma, W., & Chen, M. (2013). Analysis of land use/land cover change, population shift, and their effects on spatiotemporal patterns of urban heat islands in metropolitan Shanghai, China. *Applied Geography*, *44*, 121–133. https://doi.org/10.1016/j.apgeog.2013.07.021

Zhou, W., Huang, G., & Cadenasso, M. L. (2011). Does spatial configuration matter? Understanding the effects of land cover pattern on land surface temperature in urban landscapes. *Landscape and Urban Planning*, *102*(1), 54–63. https://doi.org/10.1016/j.landurbplan.2011.03.009

APPENDICES

Appendix 1. Questions for Local Experts Interview

Title : Identifying and analysing the behaviour of surface temperature in Bandung, Indonesia
Type : Semi-structured questions

Good afternoon, my name is Royger Maniur Simanjutak. I am currently studying in M.Sc. course in urban planning and management at the University of Twente, in The Netherlands. As part of my research thesis which is analysing the relationship of surface temperature and urban structure types, I would like to ask you several questions regarding the behaviour of surface temperature in Bandung, Indonesia. This interviewed is used for academic research purpose only, therefore all the information you give will remain confidential.

Interviewee information:

1. Name :
2. Gender :
3. Age :
4. Occupation :

Questions:

1. What is your research background?
2. How long have you been doing this research?
3. Can you briefly explain the recent update regarding surface temperature in Bandung?
4. What is the trend of surface temperature in the recent decades (from 1990 up to now)?
5. What are the main factors that influence the behaviour of surface temperature in Bandung?
6. Is there any correlation between surface temperature and urban structure types (built-up and non-built-up)? Yes or No. If yes, can you describe?
7. Do you know about Local Climate Zones (LCZs)? Yes or No. If yes, can you describe the existing LCZs classes in Bandung?
8. Based on your experience, which part is significantly changed in surface temperature across Bandung in the recent decades?
9. Can you please indicate where are the areas that have been changed in surface temperature located in this image?

Appendix 2. Landsat TM 5 & Landsat 8 OLI/TIRS Configuration

Landsat TM 5 band configuration

Band	Wavelength	Resolution
Band 1 - blue	0.45 - 0.52	30
Band 2 - green	0.52 - 0.60	30
Band 3 - red	0.63 - 0.69	30
Band 4 - Near Infrared	0.77 - 0.90	30
Band 5 - Short-wave Infrared	1.55 - 1.75	30
Band 6 - Thermal Infrared	10.40 - 12.50	120 *(30)
Band 7 - Short-wave Infrared	2.09 - 2.35	30

Landsat 8 OLI/TIRS band configuration

Band	Wavelength	Resolution
Band 1 – coastal aerosol	0.43 - 0.45	30
Band 2 – blue	0.45 - 0.51	30
Band 3 - green	0.53 - 0.59	30
Band 4 - red	0.64 - 0.67	30
Band 5 - Near Infrared (NIR)	0.85 - 0.88	30
Band 6 - Short-wave Infrared (SWIR) 1	1.57 - 1.65	30
Band 7 - Short-wave Infrared (SWIR) 2	2.11 - 2.29	30
Band 8 - Panchromatic	0.50 - 0.68	15
Band 9 – Cirrus	1.36 - 1.38	30
Band 10 – TIRS 1	10.60 – 11.19	100 * (30)
Band 11 – TIRS 2	11.5 - 12.51	100 * (30)

Appendix 3. LST Extraction Process Using Model Builder

Step 1:

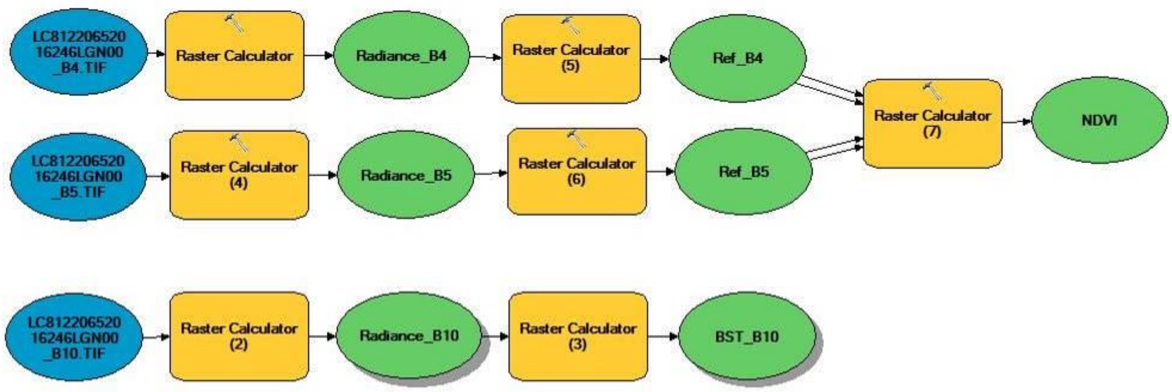

Step 2:

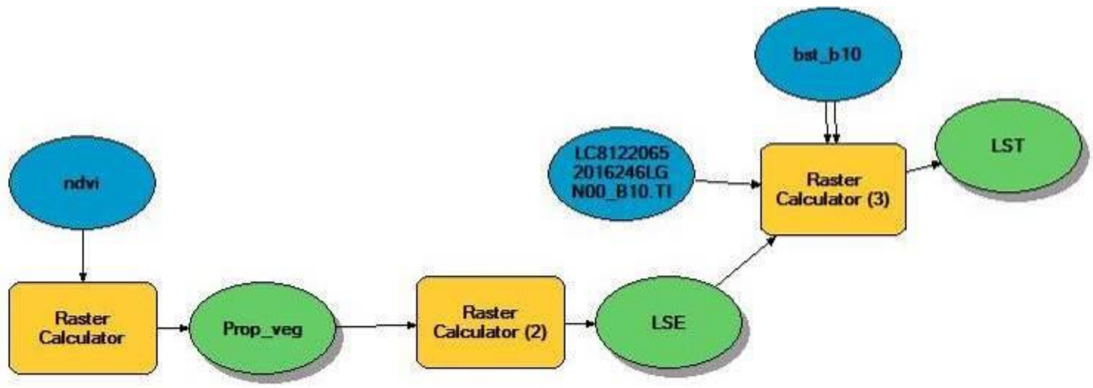

Appendix 4. Value and Parameters of VHR metadata

Band	2016_1(AUG)	2016_2(JULY)	2013_SPOT_ms
Gain Blue	9,09	10,13	8,5175
Bias Blue	0	0	0
Gain Green	9,24	10,18	9,5290
Bias Green	0	0	0
Gain Red	10,32	11,31	10,4416
Bias Red	0	0	0
Gain NIR	15,59	17,38	14,0063
Bias NIR	0	0	0
Gain Panchromatic	-	-	10,4186
Bias Panchromatic	-	-	0

Dataset	Center	
	sun elevation	sine
2016_1 (AUG)	55,4609667898695	0,823740128
2016_2 (JULY)	53,2848616852104	0,801617715
2013	54,5805431025	0,814931032

Appendix 5. LCZs Accuracy Assesment Report From Moderate Resolution Imagery

1. LCZ 2016

Class Name	Reference Data								
	Heavy Industry	Dense Trees	Scattered Trees	Low Plants	Paved	Open Low Rise	Compact Low Rise	Water	Total
Heavy Industry	71	0	0	0	2	0	4	1	78
Dense Trees	0	75	7	11	0	6	0	2	101
Scattered Trees	0	12	41	15	1	11	1	0	81
Low Plants	2	3	21	114	1	15	0	2	158
Paved	0	0	2	4	23	10	12	3	54
Open Low Rise	2	3	16	10	5	52	30	9	127
Compact Low Rise	1	0	3	0	5	27	191	6	233
Water	0	0	0	0	0	1	2	27	30
Total	76	93	90	154	37	122	240	50	862

Class Name	Reference Totals	Classfied Totals	Number Correct	Producers Accuracy	Users Accuracy
Heavy Industry	76	78	71	91.03%	91.03%
Dense Trees	93	101	75	80.65%	74.26%
Scattered Trees	90	81	41	45.56%	50.62%
Low Plants	154	158	114	74.03%	72.15%
Paved	37	54	23	62.16%	42.59%
Open Low Rise	122	127	52	42.62%	40.94%
Compact Low Rise	240	233	191	79.58%	81.97%
Water	50	30	27	54.00%	90.00%
Total	862	862	594		

Overall Classification Accuracy = 69 %
Overall Kappa Statistics = 0.64

2. LCZ 2013

Class Name	Reference Data								
	Heavy Industry	Dense Trees	Scattered Trees	Low Plants	Paved	Open Low Rise	Compact Low Rise	Water	Total
Heavy Industry	53	0	0	0	3	1	8	0	65
Dense Trees	0	69	6	13	0	1	2	6	97
Scattered Trees	0	15	56	14	2	12	0	5	104
Low Plants	13	6	7	110	0	16	1	7	160
Paved	4	0	1	1	21	10	16	3	56
Open Low Rise	4	3	16	11	6	53	29	5	127
Compact Low Rise	2	0	4	3	4	28	183	4	228
Water	0	0	0	2	1	1	1	20	25
Total	76	93	90	154	37	122	240	50	862

Class Name	**Reference Totals**	**Classfied Totals**	**Number Correct**	**Producers Accuracy**	**Users Accuracy**
Heavy Industry	76	65	53	81.54%	81.54%
Dense Trees	93	97	69	74.19%	71.13%
Scattered Trees	90	104	56	62.22%	53.85%
Low Plants	154	160	110	71.43%	68.75%
Paved	37	56	21	56.76%	37.50%
Open Low Rise	122	127	53	43.44%	41.73%
Compact Low Rise	240	228	183	76.25%	80.26%
Water	50	25	20	40.00%	80.00%
Total	862	862	565		

Overall Classification Accuracy = 66 %
Overall Kappa Statistics = 0.61

Appendix 6. Thermal Measurement Report

Point Name : TA 1
LCZ Class : Compact Low Rise

No.	Date	Morning (5.30 - 6.30 AM)		Daylight (10.00 - 10.30 AM)		Night (18.00 - 19.00 PM)	
		Surface	Air	Surface	Air	Surface	Air
1.	7/10/2016	21.5	22.0	38.0	30.0	26.5	29.0

Point Name : TA 2
LCZ Class : Compact Low Rise

No.	Date	Morning (5.30 - 6.30 AM)		Daylight (10.00 - 10.30 AM)		Night (18.00 - 19.00 PM)	
		Surface	Air	Surface	Air	Surface	Air
1.	7/10/2016	21.0	22.0	35.0	30.0	27.5	29.0

Point name : TA 3

LCZ Class : Heavy Industry

No.	Date	Morning (5.30 - 6.30 AM)		Daylight (10.00 - 10.30 AM)		Night (18.00 - 19.00 PM)	
		Surface	Air	Surface	Air	Surface	Air
1.	7/10/2016	21.0	23.0	33.0	30.0	30.0	28.0

Point Name : TA 4

LCZ Class : Heavy Industry

No.	Date	Morning (5.30 - 6.30 AM)		Daylight (10.00 - 10.30 AM)		Night (18.00 - 19.00 PM)	
		Surface	Air	Surface	Air	Surface	Air
1.	7/10/2016	22.0	23.0	35.0	30.0	29.0	28.0

Point Name : TA 5
LCZ Class : Low Plants

No.	Date	Morning (5.30 - 6.30 AM)		Daylight (10.00 - 10.30 AM)		Night (18.00 - 19.00 PM)	
		Surface	Air	Surface	Air	Surface	Air
1.	6/10/2016	19.5	24.0	39.0	35.0	26.0	24.0

Point Name : TA 6
LCZ Class : Paved

No.	Date	Morning (5.30 - 6.30 AM)		Daylight (10.00 - 10.30 AM)		Night (18.00 - 19.00 PM)	
		Surface	Air	Surface	Air	Surface	Air
1.	6/10/2016	21.0	24.0	34.0	37.0	26.0	24.0

Point Name : TA 7
LCZ Class : Low Plants

No.	Date	Morning (5.30 - 6.30 AM)		Daylight (10.00 - 10.30 AM)		Night (18.00 - 19.00 PM)	
		Surface	Air	Surface	Air	Surface	Air
1.	6/10/2016	19.0	24.0	29.5	32.0	24.0	24.0

Point Name : TA 8
LCZ Class : Compact Low Rise

No.	Date	Morning (5.30 - 6.30 AM)		Daylight (10.00 - 10.30 AM)		Night (18.00 - 19.00 PM)	
		Surface	Air	Surface	Air	Surface	Air
1.	6/10/2016	22.5	24.0	33.5	32.0	24.5	25.0

Point Name : TA 9
LCZ Class : Open Low Rise


No.	Date	Morning (5.30 - 6.30 AM)		Daylight (10.00 - 10.30 AM)		Night (18.00 - 19.00 PM)	
		Surface	**Thermo**	**Surface**	**Thermo**	**Surface**	**Thermo**
1.	8/10/2016	21.5	23.0	32.0	32.5	25.0	24.0

Point Name : TA 10
LCZ Class : Open Low Rise


No.	Date	Morning (5.30 - 6.30 AM)		Daylight (10.00 - 10.30 AM)		Night (18.00 - 19.00 PM)	
		Surface	**Thermo**	**Surface**	**Thermo**	**Surface**	**Thermo**
1.	8/10/2016	21.0	23.0	30.0	32.5	24.0	24.0

Point Name : TA 11
LCZ Class : Paved/Bare Soil

No.	Date	Morning (5.30 - 6.30 AM)		Daylight (10.00 - 10.30 AM)		Night (18.00 - 19.00 PM)	
		Surface	Air	Surface	Thermo	Surface	Air
1.	7/10/2016	21.0	22.0	35.5	31.0	27.0	29.0

Point Name : TA 12
LCZ Class : Heavy Industry

No.	Date	Morning (5.30 - 6.30 AM)		Daylight (10.00 - 10.30 AM)		Night (18.00 - 19.00 PM)	
		Surface	Air	Surface	Air	Surface	Air
1.	7/10/2016	21.5	23.0	38.5	31.0	31.5	30.0

Point Name : TA 13
LCZ Class : Compact Low Rise


No.	Date	Morning (5.30 - 6.30 AM)		Daylight (10.00 - 10.30 AM)		Night (18.00 - 19.00 PM)	
		Surface	Air	Surface	Air	Surface	Air
1.	6/10/2016	23.5	22.0	43.0	34.0	28.0	26.0

Point Name : TA 14
LCZ Class : Paved


No.	Date	Morning (5.30 - 6.30 AM)		Daylight (10.00 - 10.30 AM)		Night (18.00 - 19.00 PM)	
		Surface	Air	Surface	Air	Surface	Air
1.	6/10/2016	22.5	22.0	36.5	34.0	28.0	24.0

Point Name : TB 1
LCZ Class : Heavy Industry


No.	Date	Morning (5.30 - 6.30 AM)		Daylight (10.00 - 10.30 AM)		Night (18.00 - 19.00 PM)	
		Surface	Air	Surface	Air	Surface	Air
1.	11/10/2016	22.0	24.0	33.5	32.0	25.5	26.0

Point Name : TB 2
LCZ Class : Heavy Industry


No.	Date	Morning (5.30 - 6.30 AM)		Daylight (10.00 - 10.30 AM)		Night (18.00 - 19.00 PM)	
		Surface	Air	Surface	Air	Surface	Air
1.	11/10/2016	20.5	25.0	33.0	32.0	24.0	27.0

Point Name : TB 3
LCZ Class : Heavy Industry

No.	Date	Morning (5.30 - 6.30 AM)		Daylight (10.00 - 10.30 AM)		Night (18.00 - 19.00 PM)	
		Surface	Air	Surface	Air	Surface	Air
1.	10/10/2016	22.0	24.0	34.5	33.0	29.5	26.0

Point Name : TB 4
LCZ Class : Compact Low rise

No.	Date	Morning (5.30 - 6.30 AM)		Daylight (10.00 - 10.30 AM)		Night (18.00 - 19.00 PM)	
		Surface	Air	Surface	Air	Surface	Air
1.	10/10/2016	22.5	25.0	35.0	33.0	29.0	27.0

Point Name : TB 5
LCZ Class : Heavy Industry


No.	Date	Morning (5.30 - 6.30 AM)		Daylight (10.00 - 10.30 AM)		Night (18.00 - 19.00 PM)	
		Surface	**Air**	**Surface**	**Air**	**Surface**	**Air**
1.	11/10/2016	19.5	24.0	32.0	30.0	25.0	26.0

Point Name : TB 6
LCZ Class : Heavy Industry


No.	Date	Morning (5.30 - 6.30 AM)		Daylight (10.00 - 10.30 AM)		Night (18.00 - 19.00 PM)	
		Surface	**Air**	**Surface**	**Air**	**Surface**	**Air**
1.	11/10/2016	20.0	23.0	31.0	30.0	25.5	26.0

Point Name : TB 7
LCZ Classe : Low Plants

No.	Date	Morning (5.30 - 6.30 AM)		Daylight (10.00 - 10.30 AM)		Night (18.00 - 19.00 PM)	
		Surface	Air	Surface	Air	Surface	Air
1.	10/10/2016	21.0	23.0	33.0	33.0	26.0	27.0

Point Name : TB 8
LCZ Class : Compact Low Rise

No.	Date	Morning (5.30 - 6.30 AM)		Daylight (10.00 - 10.30 AM)		Night (18.00 - 19.00 PM)	
		Surface	Air	Surface	Air	Surface	Air
1.	10/10/2016	22.5	23.0	36.0	34.0	28.0	28.0

Point Name : TB 9
LCZ Class : Heavy Industry

No.	Date	Morning (5.30 - 6.30 AM)		Daylight (10.00 - 10.30 AM)		Night (18.00 - 19.00 PM)	
		Surface	Air	Surface	Air	Surface	Air
1.	11/10/2016	22.0	23.0	34.0	33.0	30.0	28.0

Point Name : TB 10
LCZ Class : Heavy Industry

No.	Date	Morning (5.30 - 6.30 AM)		Daylight (10.00 - 10.30 AM)		Night (18.00 - 19.00 PM)	
		Surface	Air	Surface	Air	Surface	Air
1.	11/10/2016	22.0	23.0	35.0	33.0	31.0	28.0

Point Name : TB 11
LCZ Class : Heavy Industry

No.	Date	Morning (5.30 - 6.30 AM)		Daylight (10.00 - 10.30 AM)		Night (18.00 - 19.00 PM)	
		Surface	Air	Surface	Air	Surface	Air
1.	11/10/2016	22.5	22.0	34.0	33.0	28.5	26.0

Point Name : TB 12
LCZ Class : Compact Low Rise

No.	Date	Morning (5.30 - 6.30 AM)		Daylight (10.00 - 10.30 AM)		Night (18.00 - 19.00 PM)	
		Surface	Air	Surface	Air	Surface	Air
1.	11/10/2016	21.5	22.0	33.0	33.0	26.0	27.0

Point Name : TC 1
LCZ Class : Compact High Rise

No.	Date	Morning (5.30 - 6.30 AM)		Daylight (10.00 - 10.30 AM)		Night (18.00 - 19.00 PM)	
		Surface	Air	Surface	Air	Surface	Air
1.	13/10/2016	20.5	25.0	30.0	28.0	28.0	27.0

Point Name : TC 2
LCZ Class : Compact Low Rise

No.	Date	Morning (5.30 - 6.30 AM)		Daylight (10.00 - 10.30 AM)		Night (18.00 - 19.00 PM)	
		Surface	Air	Surface	Air	Surface	Air
1.	13/10/2016	21.5	25.0	29.0	29.0	27.0	26.0

Point Name : TC 3
LCZ Class : Low Plants/Baresoil


No.	Date	Morning (5.30 - 6.30 AM)		Daylight (10.00 - 10.30 AM)		Night (18.00 - 19.00 PM)	
		Surface	Air	Surface	Air	Surface	Air
1.	13/10/2016	23.5	26.0	33.5	29.0	23.5	27.0

Point Name : TC 4
LCZ Class : Dense Trees


No.	Date	Morning (5.30 - 6.30 AM)		Daylight (10.00 - 10.30 AM)		Night (18.00 - 19.00 PM)	
		Surface	Air	Surface	Air	Surface	Air
1.	13/10/2016	21.0	25.0	22.5	29.0	22.0	26.0

Point Name : TC 5
LCZ Class : Compact Low Rise

No.	Date	Morning (5.30 - 6.30 AM)		Daylight (10.00 - 10.30 AM)		Night (18.00 - 19.00 PM)	
		Surface	Air	Surface	Air	Surface	Air
1.	13/10/2016	23.5	26.0	33.5	29.0	27.5	27.0

Point Name : TC 6
LCZ Class : Scattered Trees

No.	Date	Morning (5.30 - 6.30 AM)		Daylight (10.00 - 10.30 AM)		Night (18.00 - 19.00 PM)	
		Surface	Air	Surface	Air	Surface	Air
1.	13/10/2016	22.0	25.0	29.5	30.0	25.0	28.0

Point Name : TC 7
LCZ Class : Compact Low Rise

No.	Date	Morning (5.30 - 6.30 AM)		Daylight (10.00 - 10.30 AM)		Night (18.00 - 19.00 PM)	
		Surface	Air	Surface	Air	Surface	Air
1.	13/10/2016	24.0	24.0	35.0	31.0	27.0	27.0

Point Name : TC 8
LCZ Class : Dense Trees

No.	Date	Morning (5.30 - 6.30 AM)		Daylight (10.00 - 10.30 AM)		Night (18.00 - 19.00 PM)	
		Surface	Air	Surface	Air	Surface	Air
1.	13/10/2016	21.0	24.0	25.0	29.0	24.0	26.0

Point Name : TC 9
LCZ Class : Open Low Rise

No.	Date	Morning (5.30 - 6.30 AM)		Daylight (10.00 - 10.30 AM)		Night (18.00 - 19.00 PM)	
		Surface	Air	Surface	Air	Surface	Air
1.	13/10/2016	23.5	24.0	29.0	30.0	26.5	26.0

Point Name : TC 10
LCZ Class : Scattered Trees

No.	Date	Morning (5.30 - 6.30 AM)		Daylight (10.00 - 10.30 AM)		Night (18.00 - 19.00 PM)	
		Surface	Air	Surface	Air	Surface	Air
1.	13/10/2016	21.0	24.0	28.0	29.0	26.0	26.0

Point Name : TC 11
LCZ Class : Compact Low Rise


No.	Date	Morning (5.30 - 6.30 AM)		Daylight (10.00 - 10.30 AM)		Night (18.00 - 19.00 PM)	
		Surface	Air	Surface	Air	Surface	Air
1.	13/10/2016	22.0	25.0	33.5	28.0	29.0	27.0

Point Name : TC 12
LCZ Class : Open Low Rise


No.	Date	Morning (5.30 - 6.30 AM)		Daylight (10.00 - 10.30 AM)		Night (18.00 - 19.00 PM)	
		Surface	Air	Surface	Air	Surface	Air
1.	13/10/2016	22.0	25.0	30.5	27.0	28.0	27.0

Point Name : TD 1
LCZ Class : Dense Trees

No.	Date	Morning (5.30 - 6.30 AM)		Daylight (10.00 - 10.30 AM)		Night (18.00 - 19.00 PM)	
		Surface	Air	Surface	Air	Surface	Air
1.	12/10/2016	22.5	25.0	24.5	33.0	23.0	28.0

Point Name : TD 2
LCZ Class : Compact High Rise

No.	Date	Morning (5.30 - 6.30 AM)		Daylight (10.00 - 10.30 AM)		Night (18.00 - 19.00 PM)	
		Surface	Air	Surface	Air	Surface	Air
1.	12/10/2016	24.0	25.0	34.0	33.0	29.0	28.0

Point Name : TD 3

LCZ Class : Compact Low Rise

No.	Date	Morning (5.30 - 6.30 AM)		Daylight (10.00 - 10.30 AM)		Night (18.00 - 19.00 PM)	
		Surface	Air	Surface	Air	Surface	Air
1.	12/10/2016	25.0	25.0	35.5	34.0	29.5	29.0

Point Name : TD 4

LCZ Class : Low Plants/Compact Low Rise

No.	Date	Morning (5.30 - 6.30 AM)		Daylight (10.00 - 10.30 AM)		Night (18.00 - 19.00 PM)	
		Surface	Air	Surface	Air	Surface	Air
1.	12/10/2016	23.0	25.0	30.5	34.0	27.5	28.0

Point Name : TD 5

LCZ Class : Compact Low Rise

No.	Date	Morning (5.30 - 6.30 AM)		Daylight (10.00 - 10.30 AM)		Night (18.00 - 19.00 PM)	
		Surface	Air	Surface	Air	Surface	Air
1.	12/10/2016	23.0	26.0	35.0	34.0	29.5	30.0

Point Name : TD 6

LCZ Class : Compact Low Rise

No.	Date	Morning (5.30 - 6.30 AM)		Daylight (10.00 - 10.30 AM)		Night (18.00 - 19.00 PM)	
		Surface	Air	Surface	Air	Surface	Air
1.	12/10/2016	23.5	27.0	35.5	34.0	29.0	30.0

Point Name : TE 1
LCZ Class : Compact High Rise

 

No.	Date	Morning (5.30 - 6.30 AM)		Daylight (10.00 - 10.30 AM)		Night (18.00 - 19.00 PM)	
		Surface	Air	Surface	Air	Surface	Air
1.	18/10/2016	22.0	23.0	32.5	32.0	29.0	27.0

No.	Date	Morning (5.30 - 6.30 AM)		Daylight (10.00 - 10.30 AM)		Night (18.00 - 19.00 PM)	
		Surface	Air	Surface	Air	Surface	Air
1.	19/10/2016	22.5	23.0	32.0	31.0	28.5	26.0

Appendix 7. Threshold Modification in OBIA Classification

Years	Test Area	SP Level 2	NDVI	GLCM Entropy Red	Visual Brightness
2013	1	300	> =0.2	<= 8 : Open Low Rise > 8 : Compact Low Rise	< 28
	2	250	> = 0.3	<= 8 : Open Low Rise > 8 : Compact Low Rise	< 17
2016	1	500	> = 0	<= 7.61 : Open Low Rise > 7.61 : Compact Low Rise	< 101
	2	300	> = 0	<= 7.78 : Open Low Rise > 7.78 : Compact Low Rise	< 103

Appendix 8. eCognition Rule set Development for LCZ Classification

- LCZ
  - reset
    - delete 'Settlement'
    - delete 'Trees'
    - at New Level: remove classification
  - Level 1 Segmentation
    - Base class segmentation
      - 10 [shape:0.5 compct.:0.5] creating 'New Level'
    - Classification
      - Trees
        - unclassified with NDVI >= 0 and Visual Brightness < 103 at New Level: Trees
        - [Trees at New Level: merge region]
      - Road
        - unclassified with Min overlap [%]: Road > 0 at New Level: Road
        - Road at New Level: merge region
      - Water
        - unclassified with Min overlap [%]: River > 0 or (GLCM Entropy Blue (all dir.) <= 4.1 and Mean NIR <= 28)
        - Water at New Level: merge region
      - Low Plants
        - unclassified with GLCM Entropy Red (all dir.) <= 4 or (NDVI >= 0 and Visual Brightness > 103) at New Lev
        - Low Plants at New Level: merge region
      - Built up
        - unclassified at New Level: Builtup
  - Level 2 Segmentation
    - Tree Segmentation
      - Tree
        - Segmentation
          - Trees at New Level: 300 [shape:0.5 compct.:0.5]
        - Classification
          - Dense Tree
            - Trees with Area >= 5000 Pxl at New Level: Dense Trees
            - Dense Trees at New Level: merge region
          - Scattered Tree
            - Trees with Area < 5000 Pxl at New Level: Scattered Tree
            - Scattered Tree at New Level: merge region
    - Building Segmentation
      - building
        - segmentation
          - Builtup at New Level: 500 [shape:0.5 compct.:0.4]
        - classification
          - Open Low Rise
            - Builtup with GLCM Entropy Red (all dir.) <= 7.78 at New Level: Open Low Rise
            - Open Low Rise at settlement: merge region
          - Compact Low Rise
            - Builtup with GLCM Entropy Red (all dir.) > 7.78 at New Level: Compact Low Rise
            - Compact Low Rise at settlement: merge region
          - Industry
            - Builtup with (Mean Blue >= 80 and Mean Green >= 80 and Brightness >= 80 and Area >= 1.5 ha
            - Industry at New Level: merge region

Appendix 9. LCZs Accuracy Assesment Report From Moderate Resolution Imagery

1. Subset Area 1 (Dago Area)

Class Name	LCZ 2016		LCZ 2013	
	Producer Accuracy	User Accuracy	Producer Accuracy	User Accuracy
Heavy Industry	-	-	-	-
Dense Trees	90.00%	85.71%	80.00%	80.00%
Scattered Trees	80.00%	94.12%	75.00%	78.95%
Low Plants	90.00%	85.71%	75.00%	78.95%
Paved	90.00%	100.00%	85.00%	94.44%
Open Low Rise	73.33%	68.75%	86.67%	72.22%
Compact Low Rise	80.00%	76.19%	85.00%	77.27%
Water	100.00%	93.75%	93.33%	100.00%
Overall Accuracy	**86.15%**		**82.31%**	
Kappa Statistics	**0.84**		**0.79**	

2. Subset Area 2 (Astana Anyar Area)

Class Name	LCZ 2016		LCZ 2013	
	Producer Accuracy	User Accuracy	Producer Accuracy	User Accuracy
Heavy Industry	80.00%	100.00%	80.00%	100.00%
Dense Trees	70.00%	87.50%	40.00%	66.67%
Scattered Trees	80.00%	88.89%	75.00%	68.18%
Low Plants	95.00%	79.17%	60.00%	66.67%
Paved	90.00%	100.00%	90.00%	81.82%
Open Low Rise	95.00%	86.36%	85.00%	68.00%
Compact Low Rise	100.00%	83.33%	80.00%	80.00%
Water	85.00%	100.00%	80.00%	88.89%
Overall Accuracy	**88.89%**		**75.56%**	
Kappa Statistics	**0.87**		**0.72**	

Appendix 10. Boxplots LST and Aggregation Index of Urban Structure Types

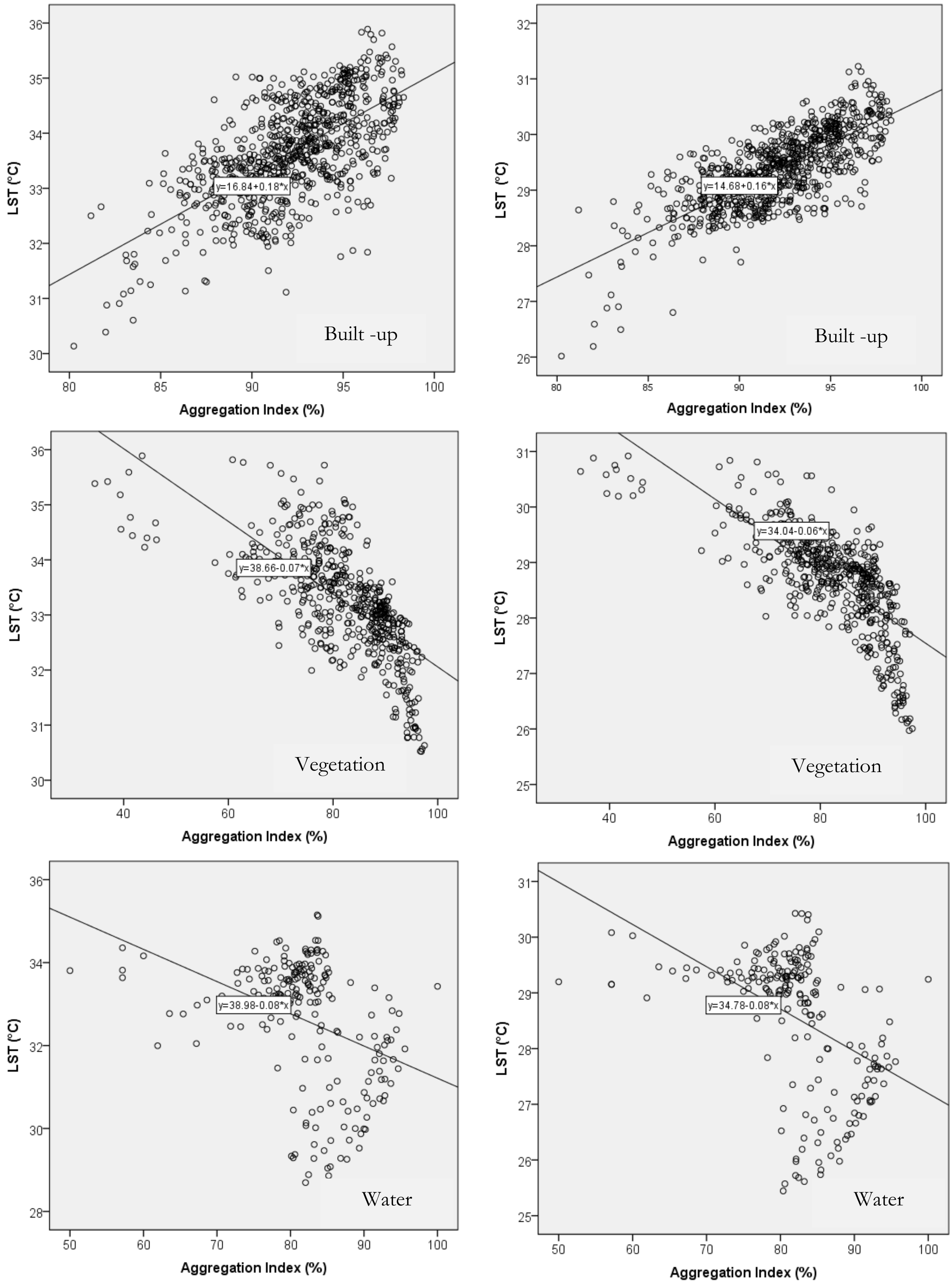

a. 2013

b. 2016

Appendix 11. Boxplots LST and Number of Patches of Urban Structure Types

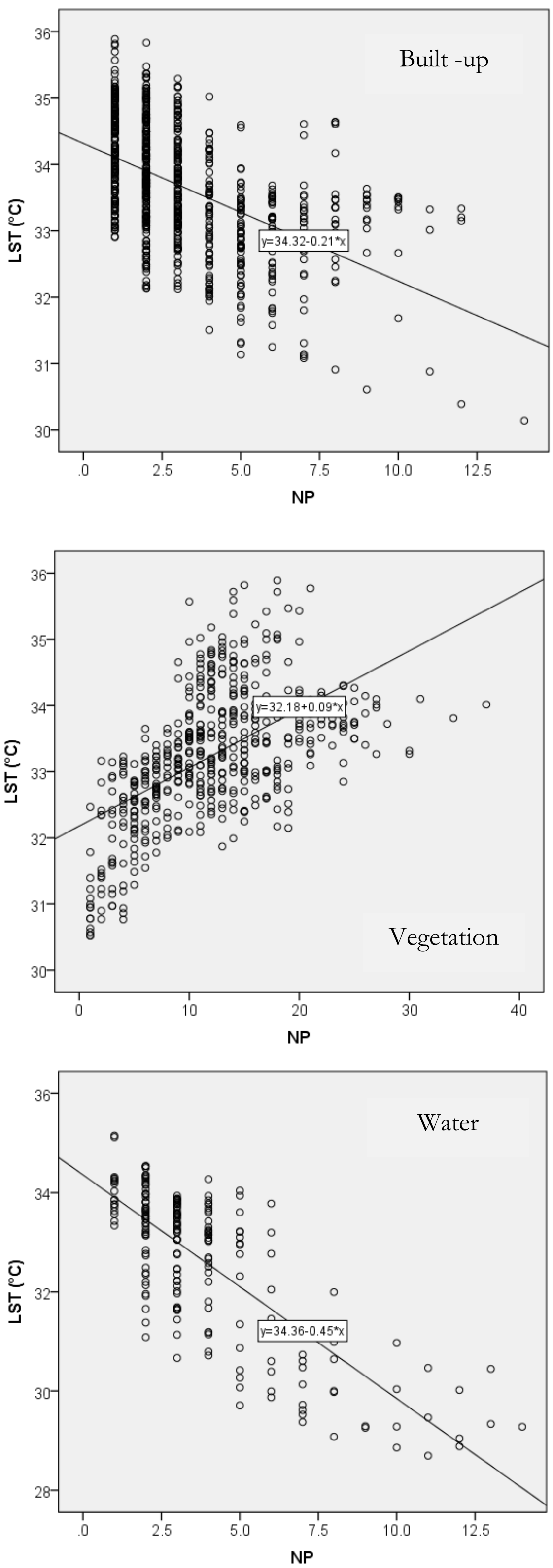

b. 2013

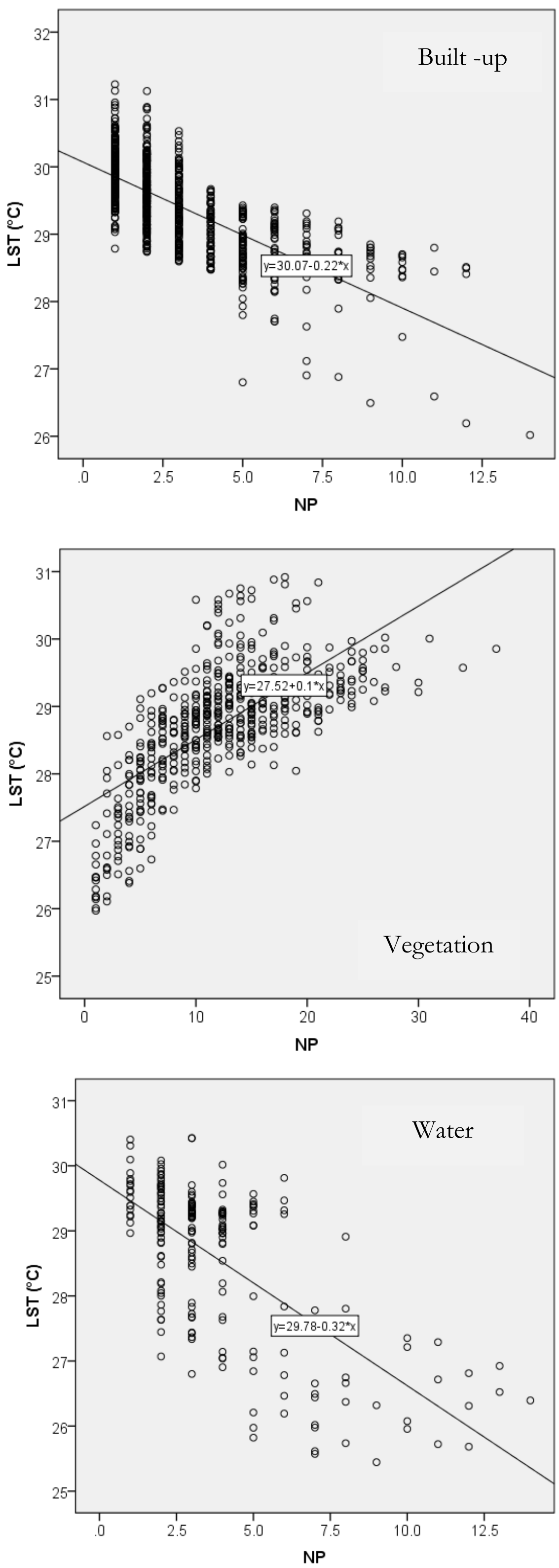

b. 2016